SCUOLA DI DOTTORATO
UNIVERSITÀ DEGLI STUDI DI MILANO-BICOCCA

Department of

Biotecnologie e Bioscienze

PhD program TeCSBi, Converging Technologies for Molecular Biosystems

Cycle XXXIII

Functions and regulation of the MRX complex at DNA double strand breaks

Marsella Antonio

Registration number: 737680

Tutor: Prof. Maria Pia Longhese

Coordinator: Prof. Paola Branduardi

ACADEMIC YEAR 2019/2020

Index

Index

Index....1
Abstract....5
Publications....8
Introduction....11

1. Genome stability and the DNA damage response....12
2. The cellular response to DNA double strand breaks....15
3. DSB Repair by Non-Homologous End Joining....17
4. DSB repair by Homologous Recombination....21

4.1 DNA end resection....22
4.2 Extension of resection by Exo1/EXO1 and Dna2/DNA2....24
4.3 Regulation of DSB resection....26
4.4 Initiation of HR: strand invasion and DNA synthesis....31
4.5 Holliday junctions resolution....35

5. The DNA damage checkpoint....37

5.1 Activation of the DNA damage checkpoint....38
5.2 Propagation of the checkpoint signal....42

6. Structure-function relationships of the MRX complex....44

Results....51

Structurally distinct Mre11 domains mediate MRX functions in resection, end-tethering and DNA damage resistance....52

Identification of *mre11* alleles that suppress the DNA damage hypersensitivity of *sae2*Δ cells....53
Suppression of the CPT hypersensitivity of *sae2Δ* cells correlates with restored DSB resection....55
Mre11-H98Y, Mre11-K292E and Mre11-R389C require Sgs1-Dna2 to suppress the DNA damage hypersensitivity of *sae2*Δ cells....59
Mre11-H98Y, Mre11-K292E and Mre11-R389C relieve Rad9-mediated inhibition of Sgs1-Dna2 activity....61
Mre11-H98Y, Mre11-K292E and Mre11-R389C bind poorly to DSBs and decrease Tel1 association to DSBs....62

Mre11-H98Y affects Mre11 dimer formation....63
R389 mediates the interactions of Mre11 capping domain with both Rad50 and DNA....66
Mre11-R522H bypasses Sae2 function in end-tethering and HR....68
R522 contributes to the stabilization of the Mre11–Rad50 binding domain....71
The ATP-bound conformation of the Mre11–Rad50 complex is essential for Tel1/ATM activation....74
Identification of *mre11* and *rad50* mutations that specifically affect Tel1 activation....75
The *mre11-S499P* and *rad50-A78T* mutations phenocopy *TEL1* deletion with respect to DSB resection and checkpoint signaling....77
The *mre11-S499P* and *rad50-A78T* mutations specifically abolish Tel1-mediated checkpoint activation....79
Mre11-S499P and Rad50-A78T reduce Tel1–MRX interaction and Tel1 association to DNA DSBs....82
The *mre11-S499P* mutation reduces Mre11–Rad50 interaction....84
Structural insights of ATP- and ADP-bound MR subcomplex by molecular dynamics simulations....87
The A78T mutation destabilizes the MR-ATP conformation....92
Sae2 and Rif2 regulate MRX endonuclease activity at DNA double-strand breaks in opposite manners....97
The lack of Rif2 suppresses the DNA damage hypersensitivity of *sae2Δ* cells....98
The lack of Rif2 dampens checkpoint signaling in *sae2Δ* cells by decreasing MRX association to DSBs....100
Rad50-N18S mimics *RIF2* deletion with respect to *sae2Δ* suppression and checkpoint inhibition....104
Rif2 inhibits Mre11-Rad50 endonuclease activity and Mre11-Rad50^{N18S} is refractory to Rif2-mediated inhibition....106
Rif2 binds a Rad50 surface that is essential for Sae2 to stimulate Mre11 nuclease activity....108
Discussion....112
Material and methods....122
Yeast strains and growth conditions....123

Search for *mre11* mutants....123
Search for *mre11* and *rad50* mutants....123
Spot assays....131
DSB resection and ectopic recombination....131
Plasmid religation assay....131
Western blotting and immunoprecipitation....132
ChIP and qPCR....132
Preparation of recombinant proteins....132
ATPase assays....133
Nuclease assays....133
Protein interaction assays....134
Expression and purification of Mre11, Mre11-R522H, Rad50 and Xrs2....134
Affinity pull-down assay....136
ATPase and nuclease assays....136
Structural models....137
Refinement of Homology Modelling (HM) structures....137
MD production....138
Post-production trajectory analysis....138
Homology modeling....139
Molecular dynamics....140
Quantification And Statistical Analysis....141
References....142

Abstract

DNA double strand breaks (DSBs) are among the most severe DNA lesions. If not properly repaired, DSBs could lead to loss of genetic information and genome instability, which is one of the hallmarks of cancer cells.

Eukaryotic cells repair DSBs by non-homologous end joining (NHEJ), which directly re-ligates the DNA broken ends, and homologous recombination (HR), which uses the intact homologous DNA sequence as a template to repair the DSB. HR requires a nucleolytic degradation of the broken DNA ends, in a process called resection. In *Saccharomyces cerevisiae*, the MRX (Mre11, Rad50 and Xrs2) complex, aided by Sae2, initiates resection of the DSB ends by performing an endonucleolytic cleavage on the 5'-ended strands. This cleavage, catalyzed by the Mre11 subunit, allows the access of Exo1 and Dna2 nucleases that elongate the ssDNA ends. In NHEJ, the two broken ends need to be physically connected to allow their correct religation. This function, called end tethering, depends on the Rad50 subunit, which binds and hydrolyses ATP. A transition between an ATP-bound state to a post-hydrolysis cutting state regulates MRX DNA binding and processing activities. The MRX complex is also essential in DNA damage checkpoint activation because it recruits the checkpoint kinase Tel1 at the break site.

In this thesis, we studied functions and regulation of the MRX complex in DSB repair. We found *mre11* alleles that suppress the hypersensitivity of ***sae2Δ*** cells to genotoxic agents. The mutations in the Mre11 N-terminus suppress the resection defect of ***sae2Δ*** cells by lowering MRX and Tel1 association to DSBs. The diminished Tel1 persistence potentiates Dna2 resection activity by decreasing Rad9 association to DSBs. By contrast, the *mre11* mutations localized at the C-terminus bypass Sae2 function in end-tethering but not in DSB resection, possibly by destabilizing the Mre11–Rad50 open conformation. These findings unmask the existence of structurally distinct Mre11 domains that support resistance to genotoxic agents by mediating different processes.

In vitro Tel1 activation by MRX requires ATP binding to Rad50, suggesting a role for the MR subcomplex in Tel1 activation. In this thesis, we describe two separation-of-functions alleles, *mre11-S499P* and *rad50-A78T*, which we show to specifically affect Tel1 activation without impairing MRX functions in DSB repair. Both Mre11-

S499P and Rad50-A78T reduce Tel1–MRX interaction leading to low Tel1 association at DSBs that reduces Tel1 activation. Molecular dynamics simulations show that the wild type MR subcomplex bound to ATP lingers in a tightly 'closed' conformation, while ADP presence leads to the destabilization of Rad50 dimer and of Mre11–Rad50 association, both events being required for MR conformational transition to an open state. By contrast, MR^{A78T} undertakes complex opening even if Rad50 is bound to ATP, indicating that defective Tel1 activation caused by MR^{A78T} results from destabilization of the ATP- bound conformational state.

The lack of Sae2 increases MRX persistence at DSBs and checkpoint activation. In this thesis, we also show that the telomeric protein Rif2, which stimulates ATP hydrolysis by Rad50, inhibits the Mre11 endonuclease activity and is responsible for the increased MRX retention at DSBs in *sae2Δ* cells. We identified a Rad50 residue that is important for Rad50-Rif2 interaction and Rif2-mediated inhibition of Mre11 nuclease. This residue is located nearby a Rad50 surface that binds Sae2 and is important to stabilize the Mre11-Rad50 interaction in the cutting state. We propose that Sae2 stimulates MRX endonuclease activity by stabilizing the cutting state, whereas Rif2 inhibits it by antagonizing Sae2 binding to Rad50 and stabilizing a MR conformation that is not competent for DNA cleavage.

The results described in this PhD thesis contribute to the understanding of the molecular mechanisms supporting functions and regulation of the MRX complex at DSBs.

Publications

- Cassani, C., Gobbini, E., Vertemara, J., Wang, W., **Marsella, A.**, Sung, P., et al. (2018). Structurally distinct Mre11 domains mediate MRX functions in resection, end-tethering and DNA damage resistance. NUCLEIC ACIDS RESEARCH, 46(6), 2990-3008.

- **Marsella, A.**, Cassani, C., Casari, E., Tisi, R., & Longhese, M. (2019). Structure-function relationships of the Mre11 protein in the control of DNA end bridging and processing. CURRENT GENETICS, 65(1), 11-16.

- Cassani, C., Vertemara, J., Bassani, M., **Marsella, A.**, Tisi, R., Zampella, G., et al. (2019). The ATP-bound conformation of the Mre11-Rad50 complex is essential for Tel1/ATM activation. NUCLEIC ACIDS RESEARCH, 47(7), 3550-3567.

- Casari, E., Rinaldi, C., **Marsella, A**., Gnugnoli, M., Colombo, C., Bonetti, D., et al. (2019). Processing of DNA double-strand breaks by the MRX complex in a chromatin context. FRONTIERS IN MOLECULAR BIOSCIENCES, 6(JUN), 43.

In revision

- **Marsella A**., Gobbini E., Cassani C., Tisi R., Cannavo E., Giordano R., et al. (submitted in October 2020, under review). Sae2 and Rif2 regulate MRX endonuclease activity at DNA double-strand breaks in opposite manners. CELL REPORTS.

Introduction

1. Genome stability and the DNA damage response

The maintenance of genome stability is an essential feature of life, and every living organism spends a lot of energy to maintain it. Cells must deal with a high number of DNA lesions every day. It was estimated that the frequency of DNA lesions per day is about 10^4-10^5 [1].

DNA lesions could be due to endogenous or exogenous factors. Endogenous DNA lesions are due to errors during DNA replication, uncontrolled recombination events, spontaneous bases deamination, depyrimidination or depurination of DNA, and oxidation by Reactive Oxygen Species (ROS) generated as side-products of cellular metabolism. Exogenous DNA lesions are due to physical agents, such as Ultraviolet light (UV) or Ionizing Radiation (IR), and to chemical agents, such as intercalating agents, base analogues, hydroxylating agents, alkylating agents, cross-linking agents, and DNA Double Strand Breaks (DSB) or Single Strand Breaks (SSB) inducing agents [2].

To counteract this high number of DNA lesions, cells have evolved a network of cellular pathways, termed DNA damage response (DDR), that allows to sense and repair DNA lesions. Most of these mechanisms are evolutionarily conserved from bacteria to humans, indicating their extreme importance. These DNA repair mechanisms include: Direct reversal, Base Excision Repair (BER), Nucleotide Excision Repair (NER), Mismatch Repair (MMR), Non-Homologous End Joining (NHEJ), and Homologous Recombination (HR) [3][4] (Figure 1).

Failure to repair DNA damage can lead to different types of mutations, such as DNA base mutation, deletions or insertions, and microsatellite expansions or contractions, or changes in chromosome structure, such as inversions, translocations, gross chromosomal rearrangements (GCRs), copy number variants (CNVs) hyper-recombination events and loss of heterozygosity (LOH) [5].

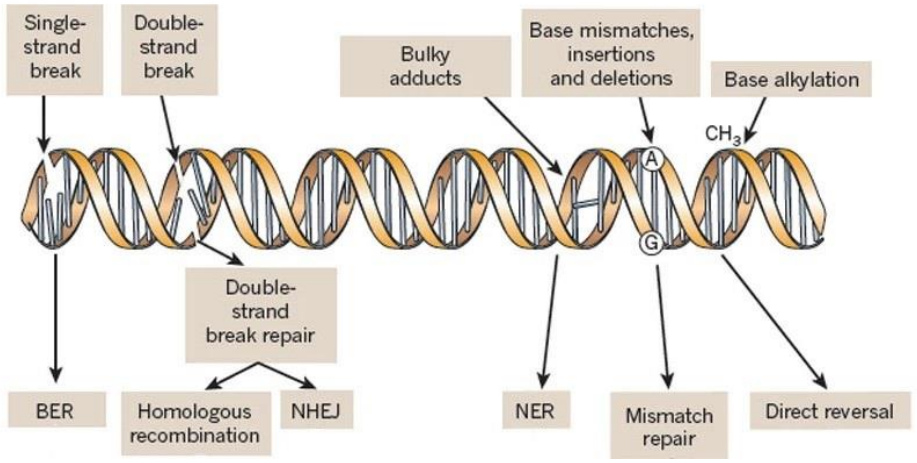

Figure 1 ***Types of DNA lesions and DNA Damage Repair Systems***

Failure of cells to accurately repair damaged DNA manifests in various clinical phenotypes, including neurodegeneration, infertility, immunodeficiencies, and cancer susceptibility. Germline mutations in genes encoding key players in the DNA damage response (DDR), including *BRCA1, BRCA2, BLM, FANCA, TP53, RAD51C,* and *MSH2*, result in cancer susceptibility syndromes, in part because failure to adequately protect the genome against endogenous and exogenous sources of DNA damage results in the accumulation of oncogenic mutations. Genomic instability is, therefore, a recognized hallmark of cancer (Figure 1).

While healthy cells have to deal with a minor amount of damage and take advantage of the full DNA repair capacity, malignant cells are frequently equipped with reduced DNA repair functionality to cope with increased replication stress and elevated endogenous DNA damage levels. Consequently, cancer cells become even more dependent on DNA repair mechanisms to survive and proliferate. For this reason, conventional treatment modalities such as radiation therapy and certain forms of chemotherapy have been built on the premise to force DNA damage-induced cell death in cancer cells.

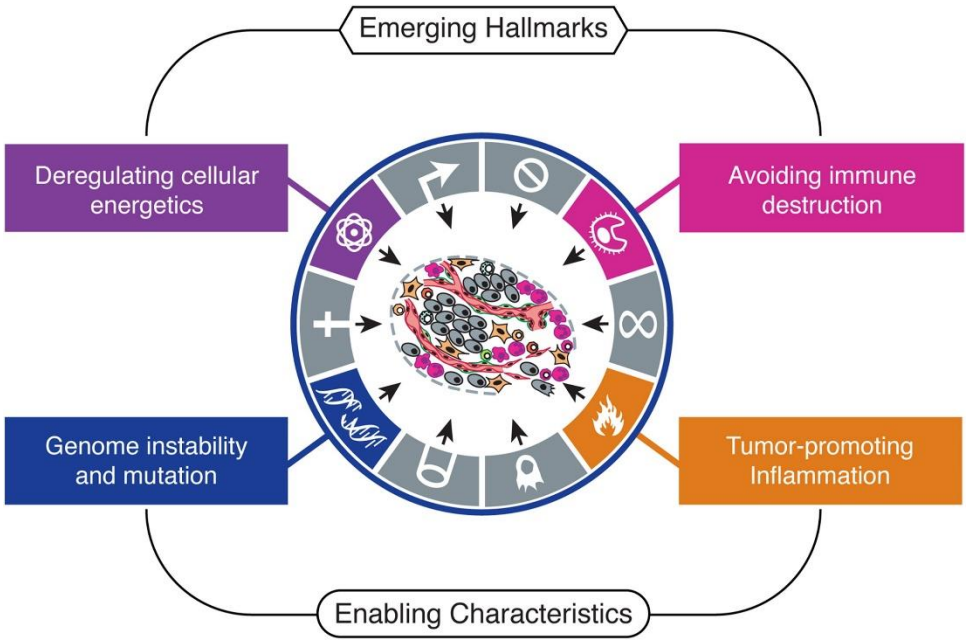

Figure 2 ***Hallmarks of cancer.*** *Scheme showing the hallmarks of cancer.*

2. The cellular response to DNA double strand breaks

DNA double-strand breaks (DSBs) are considered the most lethal DNA lesions, eliciting the majority of the cytotoxic effects induced by ionizing radiation (IR) and certain anti-cancer drugs. These lesions consist of a simultaneous breakage of the complementary DNA strands that involves the physical rupture of the sugar-phosphate backbone of the DNA molecule. DSBs are hazardous events for the cells. If they are not correctly repaired, they can lead to chromosome rearrangements and loss of genetic information. It was observed in eukaryotic cells that the rate of spontaneous DSBs is about 1 in 10^8 base pairs (bp) [1].

Though DSBs threaten genome stability, in some cases, cells deliberately introduce them into their genome to initiate particular cellular processes. An example is the induction of a DSB at the *MAT* locus by the HO endonuclease in *Saccharomyces cerevisiae* that causes the mating-type switch through an intra-chromosomal recombination event. Another example is the DSB that the RAG complex operates in lymphocytes type B and T to trigger the recombination event, known as V(D)J recombination, that is necessary to produce T-cell receptor and antibody-antigen receptors, allowing the recognition of antigens by the immune system. Finally, the evolutionary conserved topoisomerase-like protein Spo11 generates DSBs during meiosis to enable the exchange of the genetic information between homologous chromosomes, which is essential to generate genetic variability in meiotic cells. The generation of meiotic DSBs is also important for correct chromosome segregation in the first meiotic division. In fact, DSBs repair by homologous recombination keeps the homologous chromosomes physically associated through the generation of X-shaped structures known as chiasma [6].

The sources of DSBs can be grouped in exogenous or endogenous factors [7]. Endogenous DSBs can be due to events of oxidation caused by some byproducts of the normal cellular metabolism. For example, during the cellular respiration process, the oxidative phosphorylation that happens in mitochondria could

generate, as oxidative byproducts, a high reactive class of molecules known as Reactive Oxygen Species (ROS). ROS can react with genomic DNA of cells, oxidating it, leading to DSB formation [8].

Exogenous sources include ionizing radiation (IR) that, releasing a high amount of energy, can create breaks in the DNA double helix backbone. Chemical agents represent a wide class of exogenous DSB-inducing agents, many of which are also used in cancer treatment and radiotherapy. An example is camptothecin (CPT), an alkaloid drug that inhibits topoisomerases during DNA replication. CPT generates single strand breaks (SSBs) by creating a topoisomerase-DNA cleavable complex. This complex causes the stalling of the replisome, thus creating SSBs that are converted into DSBs once the replication fork restarts [9]. Another chemical compound that generates DSBs is hydroxyurea (HU), which decreases the nucleotide pool by inhibiting the ribonucleotide reductase enzyme. Therefore, upon hydroxyurea treatment, replication slows down, and this increases the probability of DSB formation. Alkylating agents like methyl methanesulphonate (MMS) transfer a methyl group to nucleotides, causing an arrest of DNA replication. Other chemicals like crosslinking agents can generate DSBs by altering DNA structure. This class of chemicals, like psoralens, mitomycin C or cisplatin, creates a covalent bond between complementary bases (interstrand crosslink) or between adjacent bases of the same DNA strand (intrastrand crosslink). Finally, bleomycin and phleomycin, generates DSBs by mimicking IR action [10].

Cells evolved two main mechanisms to repair DSBs: Non-Homologous End Joining (NHEJ) and Homologous Recombination (HR). During NHEJ, the broken ends of the DSB are re-ligated directly. By contrast, during HR, the DSB ends are processed to generate single stranded DNA ends at both DSB ends, which are used to search and anneal to a complementary intact DNA sequence on the homologous chromosome or a sister chromatid [1], [2].

3. DSB Repair by Non-Homologous End Joining

NHEJ has evolved in prokaryotes and eukaryotes to repair a wide range of broken DNA ends. This capacity is due to the enzymatic flexibility of NHEJ proteins [11]. While HR is errorless – or has an almost negligible probability of errors –, the same is not true for the NHEJ repair mechanism. In fact, by directly re-ligating broken ends together, there is a higher risk of loss of genetic information or insertion of wrong nucleotides at the break site.

The three main steps of DNA repair by NHEJ are: I) recruitment of specific protein complexes to the DSB ends; II) DSB end processing (if required); III) ligation. The highly conserved Ku protein complex plays the first step of NHEJ. This complex is a heterodimer formed by Ku70 and Ku80 subunits that are evolutionary conserved in yeast and mammals. The Ku complex has a specific affinity for DNA ends due to its ring-like shape structure that surrounds dsDNA [12]. The inner part of the ring-like structure of the complex is characterized by the presence of positive charged amino-acid residues. This allows an interaction with the negatively charged phosphate groups of the backbone, ensuring a high affinity but not sequence-specific interaction. In mammals, the Ku complex slides away from the DNA ends, allowing DNA-PK protein recruitment. In yeast, loss of function mutations in *KU70* or *KU80* genes cause growth defects at high temperatures, suggesting that this complex might have other physiological functions. Once the Ku complex is recruited to DSBs, not only it allows the loading of other NHEJ components, but it also protects the DNA ends from degradation. In fact, NHEJ repair of DSBs is not allowed if the two broken DNA ends possess ssDNA longer than few nucleotides.

NHEJ requires that the broken DSB ends are kept in close proximity, in a process called end tethering. This process differs between yeast and mammals. In mammals, the end tethering function is played by a protein, called DNA-PKcs, that is part of the phosphoinositide 3-kinase related protein kinase (PI3KK) family. DNA-PKcs is recruited to DSB ends by the Ku complex to form a complex called DNA-

PK complex. This complex keeps DSB ends close to each other, preventing them to go apart, in order to ligate the DNA ends together. Furthermore, it signals the presence of the DSB through its kinase activity. Differently from mammals, the DNA end tethering process in yeast is played by the MRX complex. This complex is formed by three subunits: Mre11, Rad50 and Xrs2 in *S. cerevisiae* and MRE11, RAD50 and NBS1 in mammals. The end tethering function is due to the Rad50 subunit, whose peculiar structure has globular domains in C- and N- termini, though which it binds DNA, separated by two long coiled-coil domains. At the center of coiled-coil domains there is a zinc-hook domain characterized by a Cys-X-X-Cys (CXXC) motif that is responsible of the tetra-coordination of a Zinc ion [13]. The Zinc positive charge interact with the four cysteine residues – two for each Rad50 [14]. This interaction allows the two Rad50 subunits, each one bound to one DSB end, to physically hold together the DNA ends. In yeast, the protein Sae2 also contributes to the end tethering process, as cells lacking Sae2 show a tethering defect [15].

Once tethered together, the two DSB DNA ends need to be re-joined. If the broken DNA ends are compatible for ligation, they can be ligated directly by the DNA ligase enzyme that catalyzes an ATP-dependent reaction to restore a phosphodiester bond between two DSB ends [16]. In yeast, Xrs2 recruits the DNA ligase 4 (Lig4/Dnl4) by direct interaction with its co-factor protein Lif1. Lif1 nuclear localization is dependent on Nej1 and Lig4-Lif1 recruitment at DSB ends also requires the Ku complex. Once recruited at DSBs, the Lig4 complex religates the DNA broken ends (Figure 3*a*) [17]. In mammalian cells, XRCC4 and XLF cofactors of the DNA ligase IV (DNL4) are recruited to the break by the DNA-PK complex. The XLF cofactor allows the re-joining of mismatched DNA ends by DNL4, while XRCC4 stimulates it phosphodiesterase activity.

If the DNA ends are not perfectly compatible due to the presence of protein adducts, missing nucleotides or mismatching overhangs, they need to be processed. In yeast, the Rad27 nuclease removes mismatching overhangs with the possible contribution of the nuclease activity of Mre11. The Pol4 polymerase, which belongs to the same family of human μ and γ polymerases, gap-fills missing nucleotides (Figure 1*b*) [18]. In mammals, both aprataxin and the polynucleotide kinase (PNKP)

are devoted to the removal of blocks at DSB ends. Removal of mismatching ends is performed by the WRN helicase and by ARTEMIS, APLF, MRN, CtIP, EXO1 and FEN1 nucleases. Gap-filing is performed by the family of X polymerases, such as γ and μ polymerases [17][19].

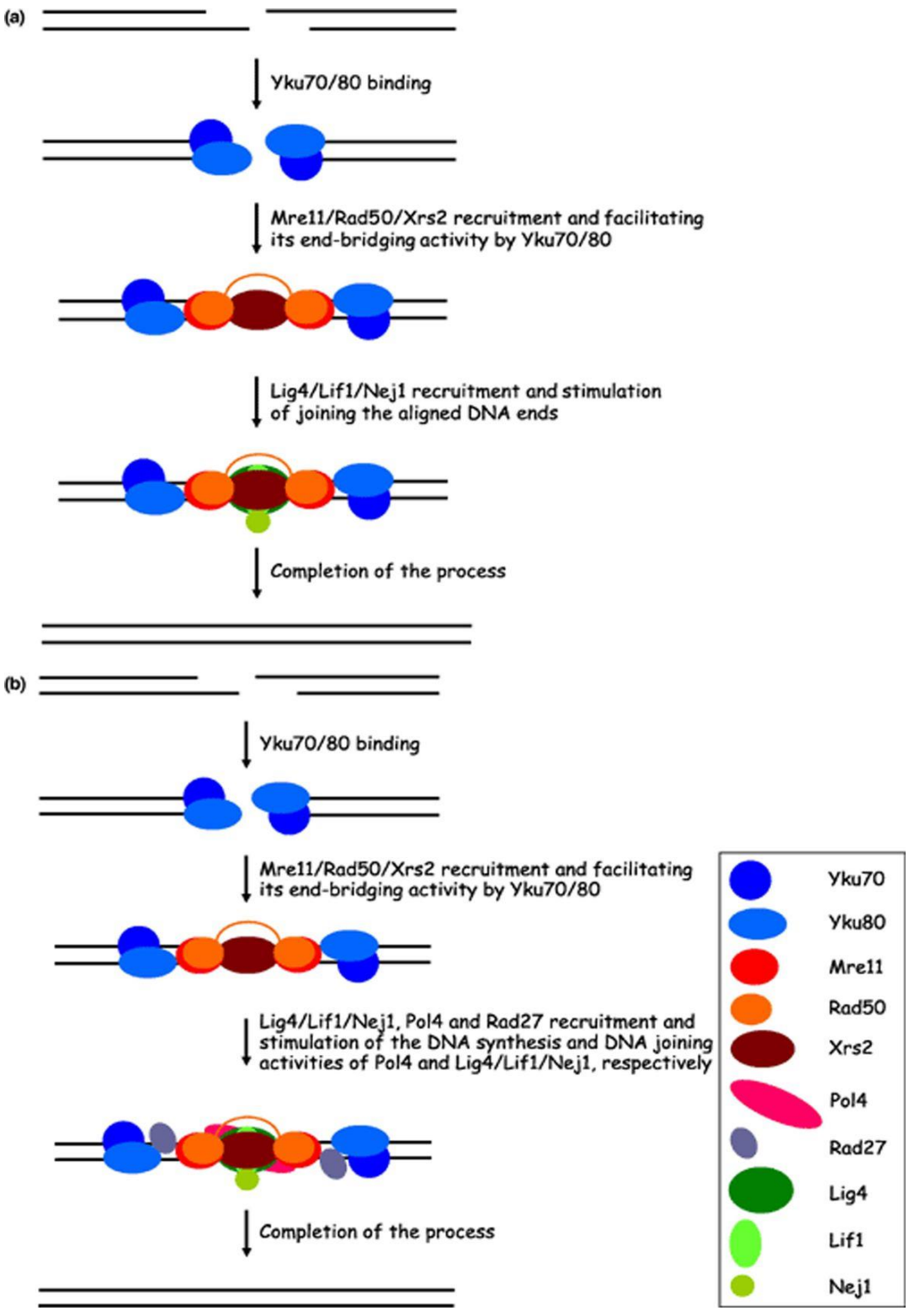
(a)
Yku70/80 binding
Mre11/Rad50/Xrs2 recruitment and facilitating its end-bridging activity by Yku70/80
Lig4/Lif1/Nej1 recruitment and stimulation of joining the aligned DNA ends
Completion of the process
(b)
Yku70/80 binding
Mre11/Rad50/Xrs2 recruitment and facilitating its end-bridging activity by Yku70/80
Lig4/Lif1/Nej1, Pol4 and Rad27 recruitment and stimulation of the DNA synthesis and DNA joining activities of Pol4 and Lig4/Lif1/Nej1, respectively
Completion of the process
Yku70
Yku80
Mre11
Rad50
Xrs2
Pol4
Rad27
Lig4
Lif1
Nej1

Figure 3 ***Current model of the Saccharomyces cerevisiae NHEJ.*** *(a) Simple religation. The Yku70/80 heterodimer is the first NHEJ factor to bind to broken DNA ends. Subsequently, Yku70/80 recruits the MRX complex and facilitates its end-bridging activity. This activity enables Lig4/Lif1/Nej1 complex to join Yku70/80-bound DNA ends. (b) DNA-ends-processing. If broken DNA ends are non-complementary, DNA end-processing reactions, generating ligatable structure and occurring prior simple ligation, are required. These reactions include nucleolytic end-processing and gap-filling mediated by Rad27 and Pol4, respectively* [18]

4. DSB repair by Homologous Recombination

Homologous Recombination (HR) can be considered error free because, unlike NHEJ, uses the homolog chromosome or a sister chromatid as templates to repair the lesion. Due to the availability of template homologous DNA, HR occurrence depends strictly on the phase of the cell cycle [20][21]. In fact, while NHEJ is used mainly in the G1 phase, HR is active in S and G2 when the homolog donor DNA sequence is available. DSB repair channeling into NHEJ or HR depends on the activity of cyclin-dependent kinases (Cdks), whose sequential action determines cell cycle progression. In particular, the low Cdk1 activity in G1-arrested cells prevents DSB processing [22]. This leads to a model in which only NHEJ is permitted in G1 cells, whereas Cdk1 activation in S and G2 phases allows DSB resection and HR. NHEJ is also allowed in S/G2, but it should be completed before resection takes over, thus committing the break to HR.

Distance between the donor and the acceptor sequences, chromatin condensation and nuclear compartmentalization are other factors that influence the availability of the DNA donor sequence as substrate for HR. This repair mechanism, in fact, in mitosis use preferentially sister chromatids, linked by cohesin, as template instead of homologous chromosomes, that are not linked and could be in different part of the nucleus. If chromatin has high condensation, DSB repair by HR is inhibited, and for this reason, many chromatin remodelers are recruited at DSB during the HR process [23]. There is also a topological restriction for HR. In fact, it occurs preferentially in the nucleoplasm, whereas it is inhibited at the nuclear periphery and in the nucleolus. The mechanism of HR can be divided into three main parts:

nucleolytic degradation of DSB ends (resection); strand invasion and DNA synthesis; Holliday junction (HJ) resolution.

4.1 DNA end resection

The first step of HR is the nucleolytic degradation of the DSB ends to generate 3‘-ended single strand DNA (ssDNA). This ssDNA does not allow the binding to the DSB ends of the Ku complex, which is known to promote NHEJ. Thus, initiation of DNA end processing inhibits NHEJ and the repair mechanism is channeled into HR. Generation of ssDNA is also important for the activation of DNA damage checkpoint that provide time to repair the DSB before cells enter the next cell cycle phase [24]. The process of DNA end resection can be divided in two steps: short range resection, which generates ssDNA of 50-200 nucleotides, and long-range resection, that elongates the initial 3’-protruding ssDNA overhangs. Short range resection is essential for the removal of DNA-protein adducts or other proteins covalently bound to the DSB ends that make them “dirty” and, therefore, inaccessible to the downstream nucleases for the extension of resection [25].

Most of the protein complexes involved in resection are evolutionarily conserved. In both yeast and mammals, the MRX/MRN complex is involved in the initiation of resection and its acts in concert with the Sae2/CtIP [26],[25],[27]. In particular, MRX/MRN, aided by Sae2/CtIP, catalyzes an endonucleolytic cleavage of the 5’ strands at both DNA ends [28]. This step is followed by 3′-5′ nucleolytic degradation by Mre11 that proceeds back toward the DNA ends [29], [30]. The MRX-Sae2 ensemble can degrade the 5′-terminated strands up to ~300 nucleotides away from the end and this processing is thus referred to as short-range resection. The resulting nick/gap provides an internal entry site for either Exo1 or the combined activities of the Sgs1 helicase and the Dna2 nuclease [26], [29]–[35].

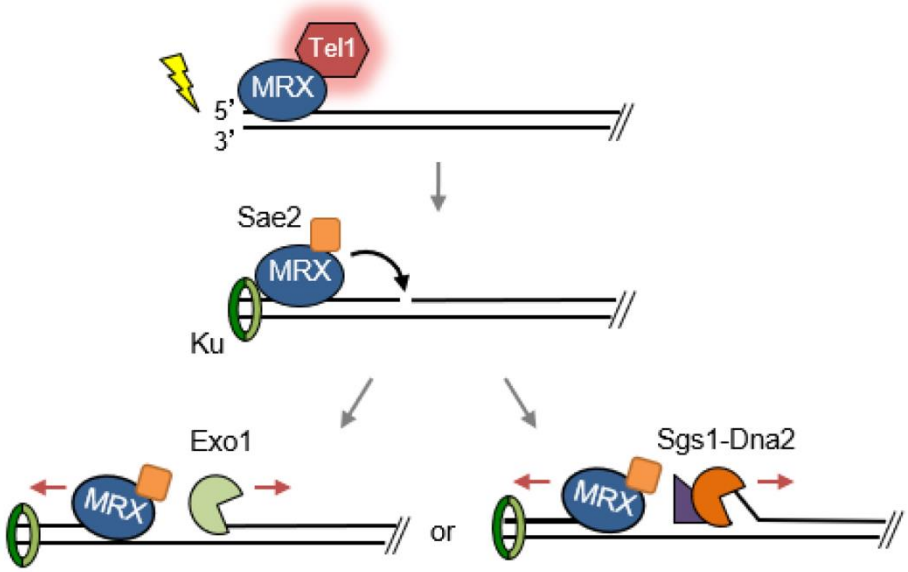

Figure 4 ***DSB end resection****.*
The Mre11-Rad50-Xrs2 (MRX) complex binds the DSB end (only one end is shown). Xrs2 recruits Tel1. Resection follows a two-step, bidirectional mechanism. MRX, together with its cofactor Sae2, initiates resection by endonucleolytic cleavage of the 5′-terminated strand, generating an entry site for long-range resection nucleases Exo1 and Sgs1-Dna2, that proceed in the 5′ to 3′ direction. Meanwhile, the MRX complex proceeds back towards the double-stranded DNA end using its 3′ to 5′ exonuclease activity. Adapded from [181].

Sae2/CtIP phosphorylation is an important event that triggers DSB repair by HR and the confinement of the resection process during the S/G2 phase of cell cycle. Sae2/CtIP is phosphorylated on serines 267 and 134 by cyclin dependent kinases and on multiple serine and threonine residues by the two apical checkpoint kinases Tel1/ATM and Mec1/ATR [36]–[38]. Indeed, it has been shown that Sae2 phosphorylation by Cdk1 is required for Sae2 to interact with Rad50 and to stimulate Mre11 endonuclease activity [28]. Similarly to yeast Sae2, its human CtIP ortholog stimulates the nuclease activity of the MRN complex after its phosphorylation by CDKs [37]. Furthermore, CtIP physically interacts with the NBS1 subunit of the MRN complex that helps CtIP localization at DSB site.

Interestingly, using a reconstituted system, it has been shown that phosphorylated Sae2, or CtIP in humans, promotes the Mre11 nuclease within the MRX/MRN complex to cleave endonucleolytically the 5′-terminated DNA strand ~15–20 nucleotides away from a streptavidin block located at the end of a linear duplex DNA molecule [28], [39], [40]. Phosphorylated Sae2 was shown also to stimulate the MRX

endonuclease activity on linear dsDNA substrates harboring either a streptavidin block or a catalytic inactive EcoRI restriction enzyme located at sites internal to the DSB end [29], [30]. These findings suggest that any stable protein obstacle bound either internally or at the end of a DNA molecule can activate the 5′ DNA strand cleavage activity of MRX-Sae2. As also the Ku complex is as effective as a streptavidin block in stimulating the endonucleolytic cleavage by MRX [29], [30], these data lead to a model, in which Ku bound to DNA ends acts as a protein block to stimulate MRX-Sae2 cleavage. Then, MRX-mediated degradation can proceed by stepwise endonucleolytic incisions, in which one MRX-Sae2 ensemble can act by its own as protein block to stimulate DNA cleavage by another MRX-Sae2 ensemble that is bound at adjacent sites internal to the DSB. The endonucleolytic cuts are followed by 3′-5′ exonucleolytic degradation by Mre11 exonuclease of the short DNA fragments between the incision sites.

Finally, the evidence that *SAE2* deletion in yeast causes a sensitivity to genotoxic agents that is more severe than that of nuclease deficient *mre11* mutants (*mre11-nd*) suggests that Sae2 is involved in other MRX functions besides resection initiation. Accordingly, it is known that Sae2 negatively regulates checkpoint activation by reducing MRX association at DSB and by promoting DNA end tethering [41], [42].

4.2 Extension of resection by Exo1/EXO1 and Dna2/DNA2

Extension of ssDNA during resection is carried out by the nucleases Exo1/EXO1 and Dna2/DNA2. These two nucleases control partially redundant parallel pathways [26], [31], [43]. In fact, deletion of one of them causes a negligible effect on the resection process, whereas their concomitant inactivation decreases the efficiency of DSB resection [38], [44]. Exo1, which is a member of the XPG nuclease family, possesses 5’-3’ exonuclease activity and catalyzes the hydrolysis of the phosphodiester bond on DNA molecules generating mononucleotides starting from a DNA end or a nick on the double helix [45].

Recent studies in *S. cerevisiae* and humans have shown that the MRX complex stimulates Exo1 association at DSBs and its nuclease activity independently of Mre11 nuclease activity [46], [47], [45], [48].. Recently, it was proposed that the MRX complex disentangles the DSB ends, allowing the access of Exo1 and promoting its persistence at the break site [49]. On the other hand, some studies in yeast suggest that Exo1-mediated resection is also possible in the absence of MRX-Sae2, suggesting that other proteins can stimulate Exo1 activity [31]. One key factor that enhances Exo1 nucleolytic activity is the RPA protein complex. RPA binds specifically the protruding ssDNA on the DSB end and seems to stimulate Exo1 activity. In particular, RPA removes Exo1 from DNA and forces its rebinding to the next DNA portion on the same DSB end, thus increasingExo1 processivity [35]. The nuclease activity of Exo1 in yeast does not require any support, whereas in humans EXO1 needs the BLM helicase that increases its persistence on DNA [26], [45].

Interestingly, it was observed that CtIP is a negative regulator of EXO1. This negative regulation is important to limit EXO1 exonuclease activity, preventing an excessive degradation of the DNA strand, which could be dangerous for the cell [48]. Another control on the exonuclease activity of Exo1/EXO1 is played by cyclin-dependent and checkpoint kinases. In fact, in humans, CDK restricts EXO1 action during the S/G2 phase of the cell cycle, while ATR promotes its degradation [50], [51]. In yeast, the checkpoint effector protein Rad53 reduces Exo1-dependent ssDNA production [26].

The other evolutionary conserved nuclease responsible for the long-range resection is Dna2/DNA2. This nuclease also has a role in DNA replication, where it removes the DNA flaps created during lagging DNA synthesis, performing an endonucleolytic cleavage on 5’ or 3’ DNA ends [52]–[56]. Dna2/DNA2 has a bifunctional helicase-nuclease activity, with 5’ - 3’ polarity for the helicase activity and both 5’ - 3’ and 3’ - 5’ polarity for nuclease activity [57]–[60]. In particular, recent studies have shown that the iron-sulfur (FeS) cluster of human DNA2 is essential in its nuclease and ATP-dependent helicase activities [61]. Dna2/DNA2 function in resection requires the helicase activity of the RecQ helicase Sgs1/BLM, which creates a substrate for Dna2/DNA2 nuclease by untwisting dsDNA [32], [35], [62], [63]. It was also shown

that human DNA2 can directly interact with WRN, a helicase belonging to the family of RecQ helicases [64]–[66].

Dna2/DNA2 can also work as ssDNA translocase for the extension of the resection process. The ATP-dependent helicase activity of Dna2/DNA2 promotes its translocation in a 5’ to 3’ direction, and this leads to the formation of degradation products of 12-100 nucleotides length, whereas the length of degradation products in the absence of Dna2 helicase activity is only 5-12 nucleotides long [67], [68]. The RPA protein ensures Dna2 correct polarity during its translocation on DNA. In fact, RPA rapidly binds ssDNA ends to protect them from erosion, and this binding also inhibits Dna2 action on 3’ strands directing its nuclease-helicase activity only on 5’ strands [32], [39], [68]. This RPA-promoted activity of DNA2 is also enhanced in humans by the presence of CtIP [39].

Also Sgs1/BLM helicase is a member of the RecQ helicase family. It has an ATP-dependent translocation activity on DNA that uses to unwind dsDNA, but, differently from Dna2/DNA2, Sgs1/BLM has a 3’ - 5’ polarity [69]–[72]. The helicase activity of Sgs1/BLM supports Dna2/DNA2 activity by providing it a 5’ unwound ssDNA substrate to cleave, while the 3’ protruding DNA strand is rapidly coated by RPA [60], [73], [74]. The MRX/MRN complex is devoted to recruiting Sgs1/BLM at the DSB site by directly interacting with it, both in yeast and human [26], [38]. Sgs1, in yeast, interacts with Top3 and Rmi1 to form the STR complex. This complex is involved in DSB resection and works independently of the Top3 topoisomerase [32], [47], [63]. Similar to Sgs1, BLM also interacts with human TOP3α and RMI1/RMI2 to form a complex that stimulates BLM helicase activity [69], [75], [76].

4.3 Regulation of DSB resection

Since an extensive and uncontrolled nucleolytic degradation of DNA ends are very dangerous events for genome stability, the resection process needs to be finely regulated [77], [78]. One of the most important controls of resection is the one that confines its action to specific cell cycle phases. This regulation is due to CDKs (Cyclin-Dependent Kinases) complexes that limit resection during the S and G2

phases of the cell cycle, where homologous chromosomes are available [22]. Cyclins are a class of proteins, whose expression fluctuates during the cell cycle, and interact with protein kinases to generate CDK complexes that regulate cell cycle transitions [22], [79]. In mammals, four distinct CDKs complexes control the transitions from S to G2 and from G2 to M phases, whereas in yeast this role is played by a single CDK, Cdk1 [22]. Yeast Cdk1 promotes both short range and long range resection by phosphorylating Sae2 and Dna2 [79], [80], [81]. In particular, yeast Cdk1 phosphorylates Sae2 on Serine 267 on the C-terminus of the protein, whereas mammalian CDKs catalyzes phosphorylation of CtIP on threonine 847 in the C-terminal portion of the protein. This control ensures that resection can be executed only in the S/G2 phases of cell cycle [22], [81], [82], [80] when Cdk activity is high. CDK complexes also control long range resection by phosphorylating threonine 4, serine 17 and 237 of Dna2, and these events promote Dna2 persistence at DSBs [81]. Unlike yeast Dna2, human DNA2 seems not to have any consensus site for phosphorylation by CDKs, but EXO1 has four S/TP sites at the C-terminal portion that are recognized and phosphorylated by CDK1 and CDK2. [50]. Other proteins involved in resection have cyclin-CDK consensus sites for phosphorylation (Mre11/MRE11, Xrs2/NBS1, Exo1, Ku and RPA [22], [48]).

The Ku complex is another regulator of resection both in yeast and in humans. This complex is recruited early after DSB formation. If the DSB occurs in the G1 phase of the cell cycle, the presence of the Ku complex promotes its repair by NHEJ, by limiting the formation of ssDNA and preventing the recruitment of resection factors at the DSB site [80], [83], [84]. In particular, the Ku complex exerts this inhibitory function by limiting the resection activity of Exo1/EXO1 and Dna2/DNA2 [85]. During the S/G2 phase of the cell cycle, MRX endonucleolytic activity, stimulated by phosphorylated Sae2, promotes the removal of the Ku complex from DNA ends by forming ssDNA tracts that are less compatible for the Ku binding [46], [86]. Furthermore, the MRX-mediated stimulation of Exo1 nuclease activity during resection also indirectly promotes Ku displacement from the DSB ends [49]. Also the human Ku complex counteracts EXO1 nuclease activity at DSBs, indicating that this negative regulation is evolutionary conserved [87].

Another protein negatively regulating resection is the yeast Rad9 protein, whose functional ortholog is 53BP1 in humans [46], [88], [89]. Rad9 is recruited at the DSB site and creates a physical obstruction to the resection process preventing the action of the nucleases involved. Specifically, Rad9 lowers the association of Sgs1 at the DSB and, therefore, inhibits Sgs1-Dna2 mediated nuclease activity [88], [90], [91].
In humans, 53BP1 during the G1 phase of the cell cycle inhibits BRCA1-CtIP mediated resection through the recruitment at the DSB site of RIF1, a promoter of NHEJ [92]–[94]. Instead, during the S/G2 phase of the cell cycle, BRCA1-CtIP are activated through CDK1-dependent phosphorylation that leads to the removal of 53BP1-RIF1 from the DNA broken ends, allowing the resection process to take place [127].
Rad9 is recruited to DSBs by multiple mechanisms. In fact, it binds methylated lysine 79 residue of H3 histone (H3-K79me) through its Tudor domain, a function that is conserved in humans, as 53BP1 binds H3-K79me but also methylated lysine 20 residue of the H4 histone [92], [95]–[98]. Rad9 through its tandem-BRTC also interacts with histone H2A that has been phosphorylated by Mec1 and Tel1 checkpoint kinases at serine 129 (γH2A) [99]–[103]. Similarly, mammalian 53BP1 interacts with H2A and H2AX histone after their phosphorylation and subsequent ubiquitination by the U3-ubiquitin ligases RNF8 and RNF168 [104]. Rad9 is also recruited to DSBs through an interaction with Dpb11, which is a component of the DNA damage checkpoint and is recruited at DNA lesions in a chromatin independent manner [105], [106].
The recruitment of Rad9 at DSBs is counteracted by the chromatin remodeler protein Fun30, which is the homolog of human SMARCAD1. Consequently, Fun30 has a role in stimulating the nuclease activity of Exo1 and Dna2-Sgs1 needed for the long-range resection [107]–[111]. Also the Slx4-Rtt107 complex negatively regulates Rad9 association at DSB by competing with it for interaction with γH2A and Dpb11 [112], [113].
Other proteins that positively or negatively affect the resection process are the proteins involved in the DNA damage checkpoint. The apical checkpoint kinase Tel1, in yeast, promotes DSB resection by exerting a positive feedback loop on the

MRX complex. Tel1 is loaded by MRX complex at the DSB site through a direct interaction with the Xrs2 subunit. The Tel1 protein kinase in turn stabilizes MRX association at DNA ends independently of its kinase activity [90], [114]. Mec1 has a negative role in regulating the resection process. Mec1 phosphorylates the effector kinase Rad53, which in turn phosphorylates and inhibits Exo1 [115], [116]. Furthermore, Mec1 negatively regulates Exo1 in an indirect manner by promoting Rad9 binding to DSBs through phosphorylation of serine 129 of H2A histone [107], [117], [118]. Interestingly, Mec1 exerts also a positive regulation on the resection process. A phosphorylation target of Mec1 is Slx4, which counteracts Rad9 association at DSB and, thus, its resection inhibition. In fact, Slx4 phosphorylation stimulates the formation on the Dpb11-Slx4-Rtt107 complex, subtracting Dpb11 to Rad9 interaction and impeding its association at DSB site [112], [113], [119], [114]. The same inhibition also happens in humans with the Mec1 ortholog ATR [120]. Mec1 directly phosphorylates Sae2, and this event stimulates the endonucleolytic cleavage by Mre11 that triggers resection [47], [119]. The human ATM and ATR, orthologs of Tel1 and Mec1 in yeast, respectively, control the resection process by phosphorylating CtIP, EXO1 and DNA2 [121]. The 9-1-1 checkpoint complex also has an inhibitory effect on the resection process, both in yeast and mammals. It promotes the recruitment of Rad9/53BP1 at the DSB site, which negatively regulates the resection process, but it also has a positive regulation on resection because it stimulates the nucleolytic processing of the DSB ends performed by Dna2/DNA2 and Exo1/EXO1 nucleases [122], [123]. A schematic representation of the regulation of DSB resection is shown in Figure 5.

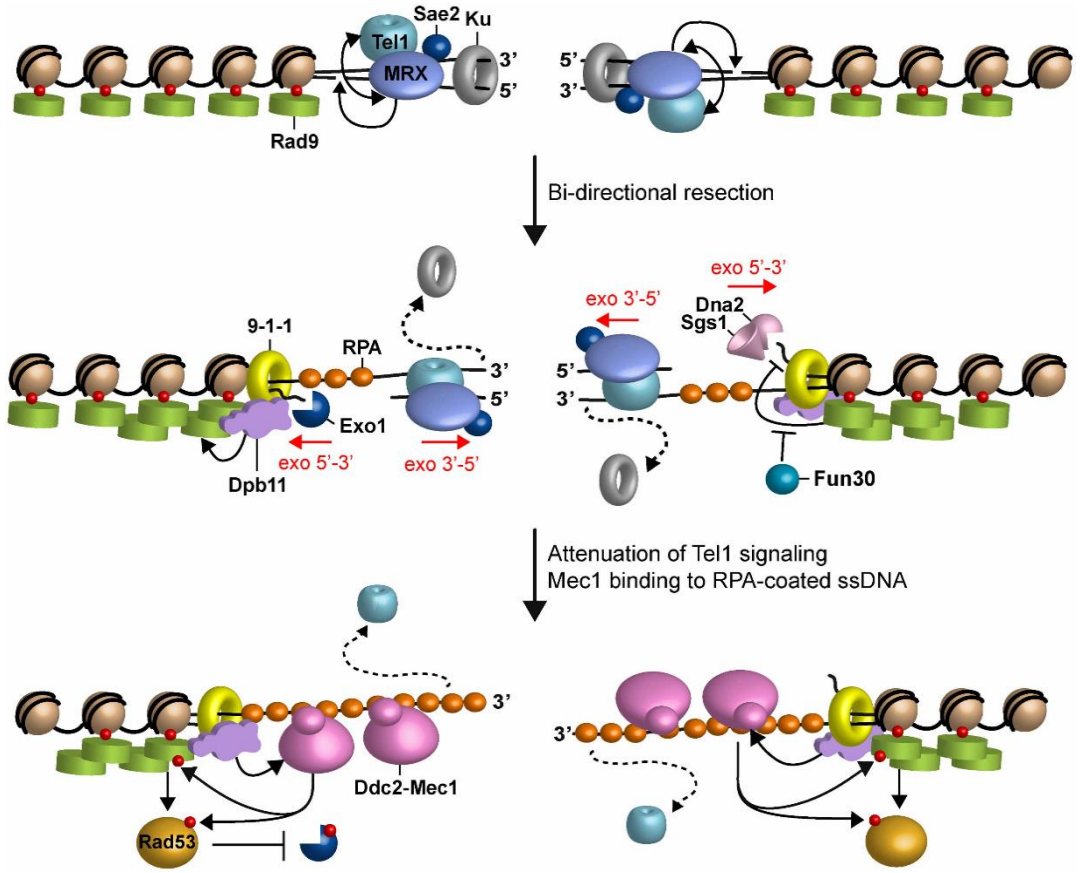

Figure 5 ***Model for sensing and responding to DNA double strand break.***
When a DSB occurs, MRX, Sae2 and Ku are rapidly recruited to the DSB ends. MRX is required for the recruitment at the DSB of Tel1, which in turn stabilizes MRX retention at the DSB (double arrows). Upon ATP hydrolysis by Rad50, Mre11, with the support of Sae2, catalyzes an endonucleolytic cleavage of the 5' strands. This incision allows processing by Exo1 and Sgs1–Dna2 in a 50–30 direction from the nick and by Mre11 in a 30–50 direction toward the DSB ends. The initiation of DSB resection leads to the removal of Ku from the DSB. The resulting 30-ended ssDNA attenuates Tel1 signaling activity and, once coated by RPA, allows the recruitment of Mec1–Ddc2. Initiation of DSB resection also promotes the association to the ssDNA/dsDNA junctions of 9–1–1 and Dpb11, which promote the recruitment of Rad9 at the DSB. Rad9, in turn, transduces the checkpoint signal from Mec1 to Rad53 and limits the resection activity of Dna2–Sgs1. The inhibitory function of Rad9 on Sgs1–Dna2 is counteracted by Fun30. Rad53 activation by Rad9 leads to phosphorylation and inhibition of Exo1. Red dots indicate phosphorylation events. S. cerevisiae proteins are indicated. Adapted from [114].

4.4 Initiation of HR: strand invasion and DNA synthesis

The ssDNA generated at the DSB ends needs to be annealed to a complementary sequence in order to allow DNA synthesis. ssDNA, which is very sensitive to degradation, is rapidly coated by the ssDNA binding protein complex Replication Protein A (RPA), which is a heterotrimeric complex formed by RPA70, RPA32 and RPA14 in humans and Rfa1, Rfa2 and Rfa3 in *S. cerevisiae* [80], [77], [124]. Then, RPA is substituted by the Rad51/RAD51 protein recombinase. This protein is similar to the prokaryotic RecA recombinase and is highly conserved in eukaryotes [32]. The Rad51 recombinase coats the ssDNA to form a multimeric protein-DNA strand hybrid structure, known as nucleoprotein filament, that is made by 6 Rad51 monomers and 18 nucleotides for each helical turn. The resulting nucleoprotein filament, which is also called pre-synaptic filament, with right-handed axial rotation can reach thousands of bases in length and is fundamental for the strand invasion step [80].

The process of RPA removal is supported by many mediators both in yeast and humans. One of the most important mediators is the yeast protein Rad52, which acts as a multimer and is characterized by a ring structure essential for ssDNA binding. Rad52 recruits a high number of Rad51 monomers near RPA-coated ssDNA, and this allows the substitution of RPA with Rad51 by enhancing the probability of Rad51 binding [32], [123]. Rad52 central domain is devoted to the interaction with RPA, while the C-terminus binds ssDNA and Rad51 [123]. Other yeast recombination mediator proteins are Rad55 and Rad57, which are paralogs of Rad51 [123]. Rad51 interacts with the Rad55-Rad57 heterodimer to form a highly stable nucleoprotein filament that is less sensitive to the negative regulation of other factors. One of these negative regulators is the Srs2 helicase that disassembles the Rad51 nucleoprotein filament [123]. There is also a positive regulation operated on Rad51. The Shu complex, formed by the subunits Shu1, Psy3, Shu2 and Csm2, with a still not elucidated mechanism, promotes formation of the Rad51 nucleoprotein filament [123]. In humans, BRCA2 is the most important recombination mediator and has functional homology to yeast Rad52. Human cells

have an ortholog of yeast Rad52, but this protein does not seem to have a crucial role in recombination, contrary to its yeast counterpart [32], [125]. BRCA2 interacts with RPA with domains situated in the N-terminus, while the C-terminal CTRB domain, together with the BRC domain, is devoted to interaction with RAD51. BRCA2 also binds DNA with the 3 OB-fold domains. The BRC and CTRB domains work together to create the nucleoprotein filament. The first RAD51 monomer interacts with the BRC domain, while CTRB cooperates to extend the nucleoprotein filament [32]. Two other proteins act as regulators of BRCA2: PALB2, which binds the BRCA2 N-terminus to ensure its stability in nuclear matrix and chromatin, and DSS1, which probably enhances BRCA2 affinity to ssDNA by directly interacting with its DNA binding domain [32]. Like yeast cells also mammalian cells have RAD51 paralog mediators of recombination, such as RAD51B, RAD51C, RAD51D, XRCC2 and XRCC3, that work for the nucleoprotein filament stabilization [32], [123]. The newly assembled Rad51 nucleoprotein filament is now ready to invade the homolog sequence of the donor DNA to initiate the repair of the DNA molecule. The search for the complementary sequence to invade is a process that is not well known yet, but studies in *Escherichia coli* showed that a stochastic mechanism can be involved. Through a series of random collision with the homologous sequence, the pre-synaptic filament finds the donor compatible DNA sequence, probing different DNA sequences with a reiterative collision process. Once the DNA complementary donor sequence is found, the nucleoprotein filament forms a stable connection with the intact dsDNA sequence [32], [126]. This process leads to the formation of a particular secondary DNA structure, an intermediate three-stranded DNA helix, called D-loop [32], [126]. The yeast Rad54 protein is a member of the Swi2/Snf2 protein family with ATPase, chromatin remodeling and translocase functions. This protein is a positive regulator of the homology search process that stabilizes the D-loop intermediate structure [32], [126]. In fact, it stabilizes the D-loop structure with its chromatin remodeler function. Rad54 interacts directly with Rad51 and promotes the complementary strand separation in the target homolog sequence, by generating DNA supercoiling through its ATP hydrolase function. The Rad54-mediated opening of the dsDNA facilitates the pairing of the resected ssDNA

with the donor DNA sequence [32], [126]. Finally, Rad54, after strand invasion, removes Rad51 monomers from the 3'-OH ends of the ssDNA. This process allows the DNA polymerases to begin DNA synthesis [32], [36], [126]. In humans, RAD54 and Rad54B are the orthologs of yeast Rad54 and, they interact with RAD51, thus promoting homology search and D-loop formation and stabilization [32], [163]. On the other hand, the translocase Mph1 and its human ortholog FANCM act as negative regulators of D-loop formation. They share several activities, including disrupting Rad51-coated D-loops and catalyzing branch migration. Mph1 can also displace the extended primer in D-loop-based DNA synthesis [123]

The strand invasion is the starting process for DNA synthesis. In fact, DNA polymerases use ssDNA as a primer to synthesize a new DNA filament using as a template the intact DNA donor sequence found in homology search. In both yeast and humans, proteins involved in DNA replication, such as PCNA and RFC complexes, Dpb11/TopBP1, and the polymerases δ, η and ζ, are also responsible for the repair DNA synthesis [32], [36], [126], [123].

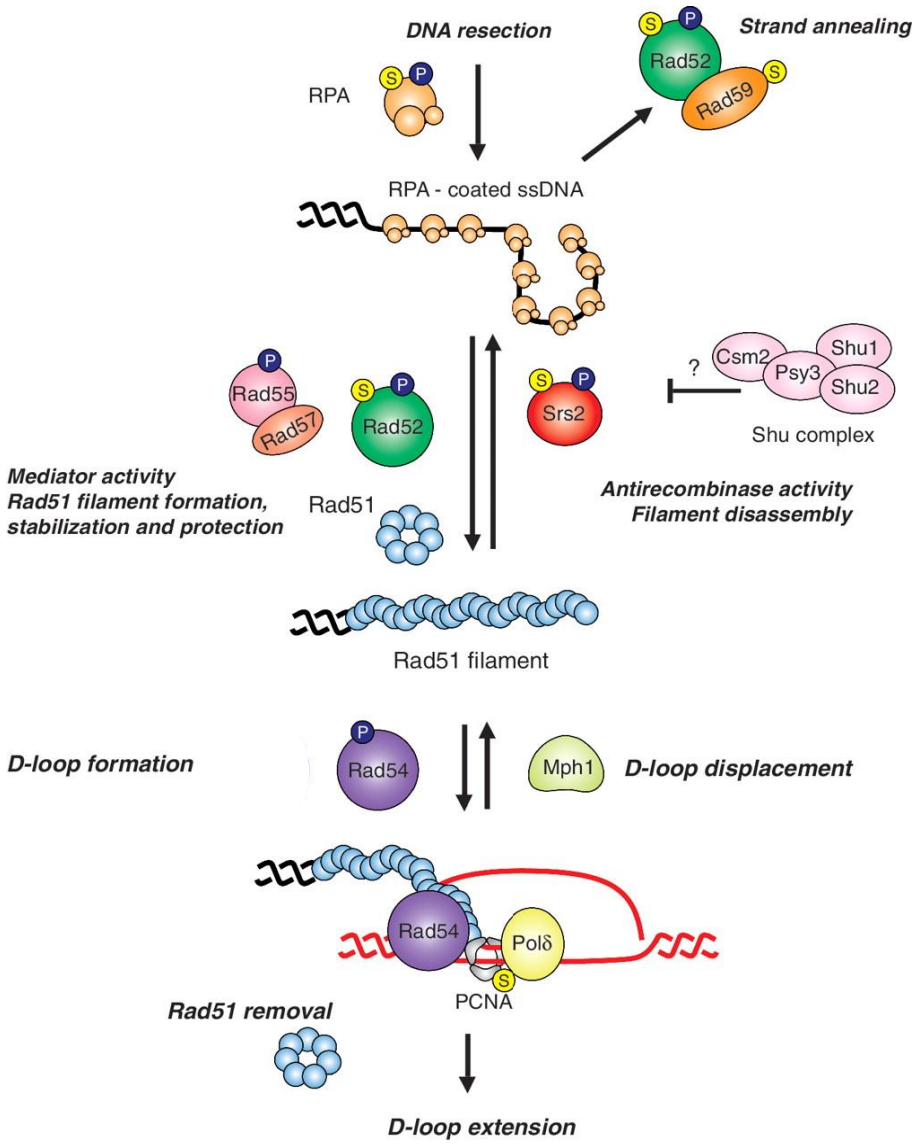

Figure 6 ***Strand invasion and DNA synthesis****. RPA can be replaced by Rad51 from ssDNA with the help of recombination mediators, including Rad52 and Rad55/57. Rad51 presynaptic filaments perform homology search with help from Rad54. Mph1 unwinds D-loop intermediates. Srs2 is capable of dismantling Rad51 filaments in an ATP-dependent manner, leading to the displacement of Rad51 by RPA. This prevents untimely or unwanted recombination. Rad52 and Rad55/57 can antagonize Srs2 activity. The Shu complex promotes Rad51 function during replication-associated repair but may also function by antagonizing Srs2. RPA–ssDNA complex can also lead to Rad51-independent repair wherein Rad52 and Rad59 replace RPA from DNA and anneal complementary strands. Most proteins are modified by phosphorylation (P) and/or SUMOylation (S). Adapted from [121].*

4.5 Holliday junctions resolution

After DNA synthesis starting from the 3'-ended resected strand and using as a template the intact homolog sequence of a donor DNA molecule, HR takes plays by at least three different mechanisms. In the first one, which is called Double Strand Break Repair (DSBR) (Figure 7A), after the formation of the D-loop, the other DSB end, which is also resected to generate a ssDNA 3' protruding filament, anneals with the complementary DNA strand of the D-loop. This process is called "second end capture" and triggers a new DNA synthesis process starting from the 3'-OH of the second DNA end. This event leads to a particular secondary structure with two four-way cross intermediates, known as Holliday Junctions (HJ) [20], [123], [124]. HJs are very important for the correct chromosome segregation during mitosis [127], but they need to be resolved to allow chromosome segregation. The enzymes devoted to the resolution of HJs are a particular class of nucleases called resolvases. They perform nucleolytic cleavage on the branched cruciform structures that result in Cross-Over (CO) or Non-Cross-Over (NCO) structures [24], [164], [128]. In yeast, the resolvases are the Mus81-Mms4 complex and Yen1, while, in mammals, resolution of HJs is made by the orthologs MUS81-EME1 and GEN1 [129], [130]. The resolution of HJs is also possible with the use of helicase-topoisomerase complexes. In yeast, the STR complex, formed by Sgs1, Top3 and Rmi1 and their human orthologs BLM, TOP3α and RMI1/2, resolves the HJs, generating only NCO products [69], [131]. DSBR is also essential during meiosis since it guarantees genetic information exchange between gamete cells and keeps homologous chromosomes linked together through HJs.

The second HR repair pathway is Synthesis Dependent Strand Annealing (SDSA) (Figure 7B). In this process, after the D-loop formation, DNA synthesis takes place, and the ssDNA is displaced from the D-loop. If DNA synthesis is sufficiently long to overcome the break site, the neo-synthetized strand can re-anneal to the other strand of the original DNA molecule. DNA polymerases can fill this ssDNA and the DNA strands can be ligated by DNA ligases [20], [132], [133]. This process generates only NCO products. During mitosis, SDSA is the preferred HR repair

mechanism because it does not allow DNA sequence exchange between homologous chromosomes [24], [171]. During mitosis, the yeast Srs2 helicase, whose role in human is played by RECQ5 FANCJ and BLM, destabilize the D-loop structure promoting SDSA [123], [134].

Lastly, the third homologous recombination repair pathway is Break Induced Replication (BIR), represented in Figure 7C. This process is possible only if the second end of a DSB is lost or degraded. This mechanism requires the conversion of the D-loop into a replicative fork that copies the rest of the chromosome to restore the missing genetic information [24], [164], [127].

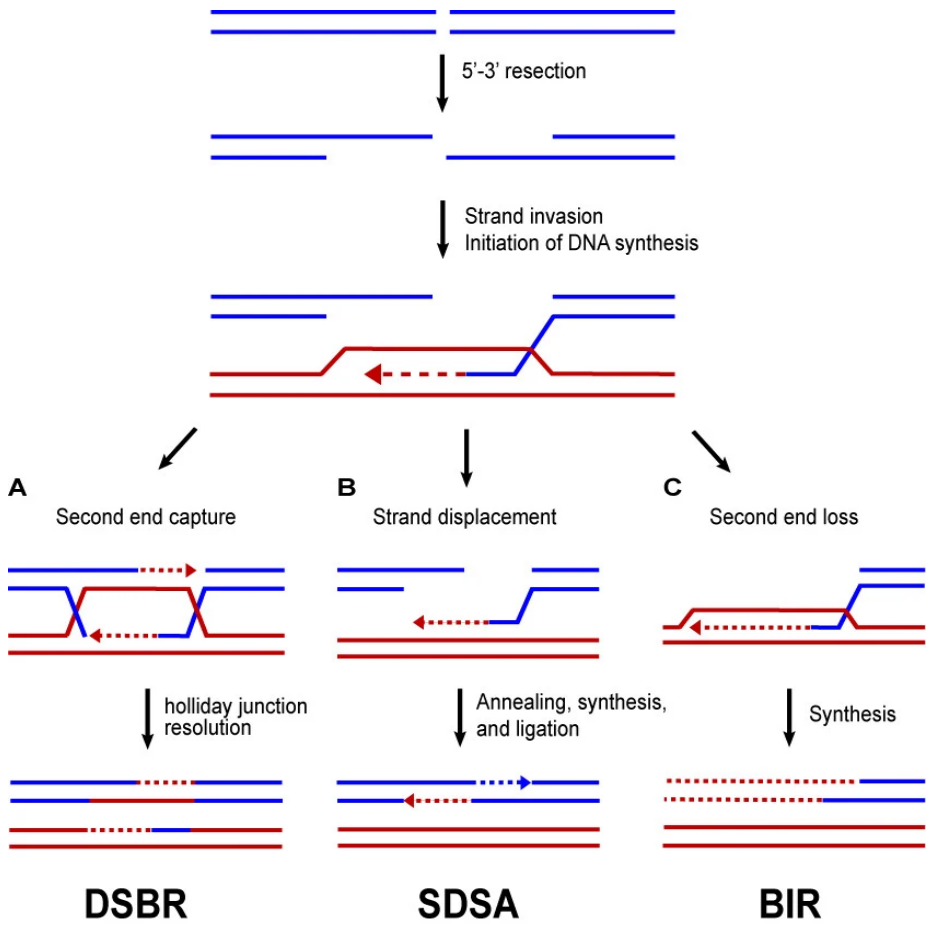

Figure 7 ***Models of homologous recombination.***
The DNA ends are first processed to generate 3' ssDNA tails. These tails invade a homologous template (red) priming new DNA synthesis (dashed line). Three possible outcomes are possible. A) In canonical DSBR, both the initial invading strand and the captured second end anneal to the homologous template and prime new DNA synthesis, resulting in a double Holliday junction that can be resolved by nucleases into crossover or non-crossover products. B) In the Synthesis-dependent strand annealing (SDSA), the invading strand, along with the newly synthesized segment, is unwound by a helicase and anneals with the other resected end. C) In break-induced replication (BIR), one end of the DSB is lost and the remaining end invades the homologous template priming DNA synthesis to the end of the chromosome. Adapted from [127].

5. The DNA damage checkpoint

DNA damage triggers activation of a checkpoint response, known as DNA damage checkpoint (DDC), that slows down cell cycle progression to provide time to repair DNA lesions before entering the next cell cycle phase. The DNA damage checkpoint is a mechanism evolutionary conserved from yeasts to humans. Defects in the checkpoint machinery could result in higher genomic instability for the cells that promotes cancer onset [135]. The DDC machinery senses the presence of DNA lesions and initiates a signal transduction cascade to slow down the cell cycle. DDC protein components and their functions are shown in Table 1.

Saccharomyces cerevisiae	*Schizosaccharomyces pombe*	*Homo sapiens*	Function
Mec1	Rad3	ATR	Checkpoint signaling kinase
Ddc2	Rad26	ATRIP	Mec1/ATR binding partner
Tel1	Tel1	ATM	Checkpoint signaling kinase
Mre11-Rad50-Xrs2	Rad32-Rad50-Nbs1	MRE11-RAD50-NBS1	MRX/MRN complex DSB repair Tel1/ATM activator
Rad53	Cds1	CHK2	Checkpoint effector kinase
Chk1	Chk1	CHK1	Checkpoint effector kinase
Ddc1-Rad17-Mec3	Rad9-Rad1-Hus1	RAD9-RAD1-HUS1	9-1-1 complex Mec1/ATR activator
RFC-Rad24	RFC-Rad17	RFC-RAD17	9-1-1 clamp loader
RFC-Ctf18- Dcc1-Ctf8	RFC-Ctf18- Dcc1-Ctf8	RFC-CTF18-DCC1-CTF8	RFC-Ctf18 complex checkpoint mediator
Dpb11	Rad4	TOPBP1	Replication initiation Mec1/ATR activator
Dna2	Dna2	DNA2	Okazaki fragment processing DSB repair Mec1/ATR activator
Rad9	Crb2	53BP1, BRCA1	Checkpoint mediator Rad53/Dun1 activator
Mrc1	Mrc1	CLASPIN	Checkpoint mediator Rad53 activator
Sgs1	Rqh1	BLM, WRN	Rad53 activator

Table 1 ***Checkpoint factors from yeast to humans.*** *Adapted from* [185].

5.1 Activation of the DNA damage checkpoint

When a DNA lesion occurs, cells must first recognize the lesion. The two apical checkpoint kinases that achieve this task are the checkpoint kinase Tel1 and Mec1 in yeast, orthologs of mammalian ATM (Ataxia-Telangiectasia Mutated) and ATR (Ataxia- Telangiectasia mutated and Rad53-related) [135]. Both Tel1/ATM and Mec1/ATR belong to the family of phosphatidylinositol 3-kinase-related kinase (PIKK), which share common structural features. These kinases are characterized by a HEAT domain at the N terminus responsible for DNA-protein and protein-protein interactions. The kinase domain is located at the C-terminus. Other domains characterize the C terminal part are the FAT (FRAP-ATM-TRRAP) domain, and by PIKK Regulatory Domain (PRD) and FATC (FAT-C-terminal) that are both upstream and downstream, respectively, to the kinase domain. FAT, PRD and FATC domains contribute together to the regulation of the kinase activity of Tel1 [136]–[138], [177]. These two kinases can detect different types of DNA lesions. Tel1/ATM recognizes primarily unprocessed DSB ends, whereas Mec1/ATR recognizes ssDNA intermediates that could arise from the nucleolytic degradation of a DSB or after stalling of the replication forks [129], [140].

The MRX/MRN complex is responsible for Tel1/ATM recruitment at the break site. Once MRX/MRN is recruited onto DNA ends, it recruits Tel1/ATM at the DSB through a physical interaction with the C-terminus of the Xrs2/NBS1 subunit [3], [135], [140], [141]. In humans, there is evidence that the ATM autophosphorylation of serine 1981 causes a transition from inactive ATM homodimers to active monomers [140], [142]. This autophosphorylation requires an initial acetylation of the FATC domain mediated by TIP60 [143]. Moreover, other ATM phosphorylation sites, such as serines 367, 1893 and 2996, are also responsible for ATM activation. MRX/MRX also contributes to Tel1/ATM activation, but the molecular mechanism behind this activation remains unclear. There is evidence that the Rad50/RAD50-ATPase-induced conformational change of MRX/MRN complex contributes to Tel1/ATM activation, as well as Xrs2/NBS1 interaction itself seems to promote this activation [141], [142], [144]. On the contrary, there is no evidence supporting a

Tel1/ATM activation mediated by the MRX/MRN nuclease activity [3], [142], [145]. Once activated, Tel1/ATM initiates the signal transduction cascade that leads to DDC activation and cell cycle arrest through phosphorylation of different targets.

The Mec1/ATR kinase is active principally during the S/G2 phase of the cell cycle when ssDNA is generated. Both in yeast and mammals, Mec1/ATR recognizes ssDNA by binding, with the help of Ddc2/ATRIP cofactor, to RPA-coated ssDNA (41). The evolutionary conserved N-terminal domain of Ddc2/ATRIP is responsible for protein-protein interaction with RPA and Mec1/ATR, thus promoting its recruitment to the DNA damage site [146]–[149]. Mec1/ATR-Ddc2/ATRIP interaction, by contrast, does not affect activation of Mec1 as a kinase [150]. Activation of Mec1/ATR depends primarily on the presence of the 9-1-1 complex, formed by Ddc1, Rad17 and Mec3 in yeast and RAD9, RAD1 and HUS1 in mammals [151]. This heterotrimeric complex, which is conserved in yeast and mammals, has a toroidal structure that allows its binding to DNA at the interface between dsDNA and ssDNA. Its recruitment depends on the RFC-like complex, a clamp-loader, formed by Rad24, Rfc2 and Rfc5 in yeast and RAD17, RFC2 and RFC5 in humans [152]. Mec1, in yeast, directly interacts with the 9-1-1 complex subunit Ddc1. This interaction promotes activation of Mec1 as a kinase (149,167,168). In humans, ATM activation requires the interaction between TOPBP1 and the RAD9 subunit of the 9-1-1 complex after its phosphorylation. TOPBP1 is directly recruited on ssDNA by the MRN complex. After the interaction between TOPBP1 and 9-1-1, TOPBP1 stimulates ATR kinase activity through its ATR-activating domain [140][153], [154]. In yeast, the TOPBP1 ortholog Dpb11 also contributes to the activation of Mec1 [84], [152]. Dpb11 is directly recruited on the DNA damage site by interacting with the Ddc1 subunit of the 9-1-1 complex. The presence of Ddc1 is not essential for Mec1 activation but stimulates its kinase activity, but both Mec1 and Ddc1 needs to be phosphorylated to interact with Dpb11 [155].

The choice between a Tel1/ATM-dependent and a Mec1/ATR-dependent checkpoint activation is not clearly understood. While Tel1/ATM-dependent checkpoint activation seems to be preferred in the presence of blunt or minimally

processed DNA ends, Mec1/ATR activation requires long tracts of ssDNA. Thus, when a DSB occurs, the resection process is crucial for the choice between Tel1/ATM and Mec1/ATR because the nucleolytic processing of DNA ends attenuates Tel1/ATM signaling. On the other hand, resection also generates ssDNA that is coated by RPA, activating Mec1/ATR signaling. Both in yeast and mammals, Tel1/ATM seems to stimulate DNA end processing, thus leading to the transition to the Mec1/ATR signaling [155], [156]. This evidence supports a model where, after the DSB formation, MRX/MRN recruits Tel1/ATM at the lesion, triggering Tel1/ATM-mediated checkpoint activation. Subsequently, MRX/MRN, also stimulated by Tel1/ATM in a feedback loop, initiates the resection process, which causes ssDNA accumulation. Then MRX/MRN is removed, inhibiting Tel1/ATM checkpoint activation and, as the resection process takes over, ssDNA is recognized by Mec1/ATR, which becomes the principal checkpoint activator [196], [152], [84].

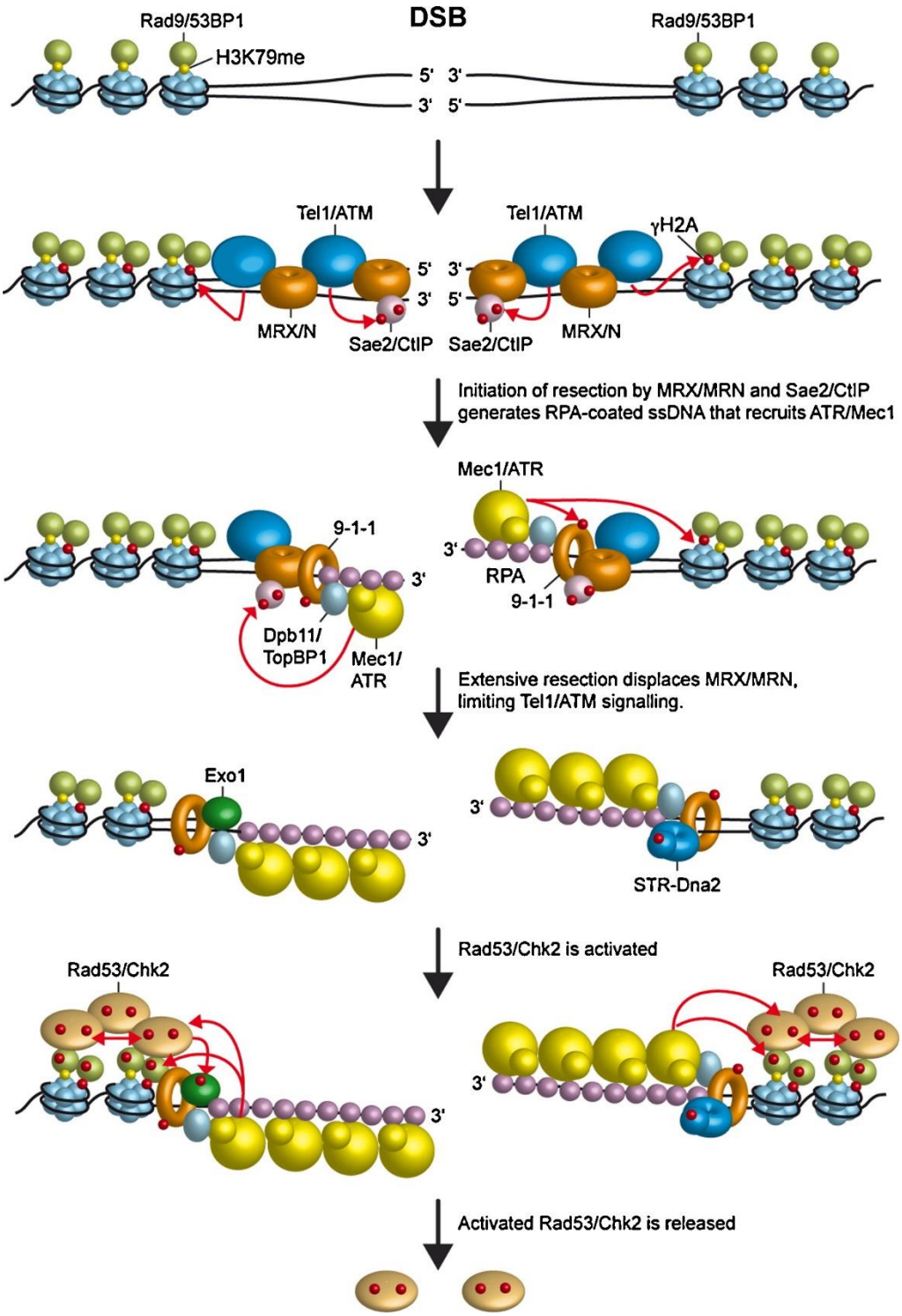
DSB
Rad9/53BP1
H3K79me
Rad9/53BP1
5' 3'
3' 5'
Tel1/ATM
Tel1/ATM
γH2A
MRX/N
Sae2/CtIP
Sae2/CtIP
MRX/N
Initiation of resection by MRX/MRN and Sae2/CtIP generates RPA-coated ssDNA that recruits ATR/Mec1
Mec1/ATR
9-1-1
3'
RPA
9-1-1
Dpb11/ TopBP1
Mec1/ ATR
Extensive resection displaces MRX/MRN, limiting Tel1/ATM signalling.
Exo1
3'
3'
STR-Dna2
Rad53/Chk2 is activated
Rad53/Chk2
Rad53/Chk2
3'
3'
Activated Rad53/Chk2 is released

Figure 8 ***DSB-induced checkpoint activation****.*
Recognition of the DSB by MRX/MRN (MRX/N) leads to recruitment of Tel1/ATM, which phosphorylates Sae2/CtIP and histone H2A (γH2A). MRX/MRN, Sae2/CtIP and other nucleases resect the DSB ends to generate 3'-ended ssDNA tails that, once coated by RPA, allow the loading of the Mec1-Ddc2/ATR-ATRIP complex. Tel1/ATM, possibly by acting on the MRX/MRN complex, promotes DSB resection, which activates Mec1/ATR and concomitantly inhibits Tel1/ATM signaling. Mec1/ATR activation requires Dpb11/TopBP1, the 9-1-1 complex and possibly the MRX/MRN complex itself. Once recruited to the DSB, Mec1/ATR regulates the generation of 3'-ended ssDNA by phosphorylating Sae2/CtIP and histone H2A. Mec1 activates the downstream checkpoint kinase Rad53/Chk2 by phosphorylating Rad9 and Rad53/Chk2 itself. Moreover, phosphorylated Rad9/53BP1 promotes activation of Rad53/Chk2 by allowing its in-trans autophosphorylation. Activated Rad53 is then released from DNA and can regulate both DSB processing by phosphorylating and inhibiting Exo1 and its specific targets in the checkpoint cascade. Adapted from [84].

5.2 Propagation of the checkpoint signal

After detection of DNA lesions, activated Mec1/ATR and Tel1/ATM propagate the checkpoint signal to the effector kinases Rad53/CHK2 and Chk1/CHK1. Rad53 is the most important effector kinase in budding yeast and is part of the Chk2 serine/threonine kinases family. Rad53 shows an SQ/TQ cluster domain (SCD) that is the consensus sequence for Mec1/Tel1 phosphorylation. This modification is needed for Rad53 activation [157], [158]. Near the SCD domain, there is the Forkhead-Associated (FHA) domain that, through binding to phospho-threonine residues, allows protein-protein interaction. Rad53 is the only kinase of the Chk2 kinase family possessing a second FHA domain in the C-terminus [157], [158].

Rad53 activation requires the Rad9 mediator protein. After its phosphorylation by Mec1-/Tel1, Rad9 interacts with Rad53 FHA domains and this interaction drives Rad53 recruitment at the DSB site. This Rad9-dependent recruitment allows Rad53 phosphorylation by Tel1 and Mec1. Furthermore, it promotes the recruitment of Rad53 molecules close to each other that triggers Rad53 *in trans* autophosphorylation on about twenty different phosphorylation sites [159]. These autophosphorylation events lead to full Rad53 activation that is released from Rad9 interaction [160]. The mammalian ortholog of Rad53, CHK2, once recruited at the DNA damage site, is phosphorylated by ATM on threonine 68 and on other residues inside the SCD domain. These phosphorylation events lead to the interaction

between two FHA domains of two CHK2 monomers and full CHK2 by inducing its autophosphorylation, [161].

The other checkpoint effector CHK1 is primarily activated following DNA damage in the G2 phase of cell cycle or after replication stress. CHK1 shows a kinase domain located at the N-terminus, a linker region followed by SQ/TQ domain and, at C-terminus, a domain with a putative regulatory function [162]. Its activation depends on the ATR-mediated phosphorylation of S317 and S345. Even if the mechanism of CHK1 activation is not entirely elucidated, the more likely hypothesis is that phosphorylation induces a conformational change that promotes inhibition of its kinase activity by the C-terminal regulatory domain [162], [163].

Activation of Rad53/CHK2 and Chk1/CHK1 leads to the phosphorylation of different cellular targets that control different functions. The primary purpose of these phosphorylation events is to induce a cellular response aimed to arrest the cell cycle. If the DNA lesion occurs in G1, checkpoint activation depends on Tel1/ATM that phosphorylates Rad53/CHK2. Rad53, in budding yeast, phosphorylates the SBF transcription factor subunit Swi6 leading to SBF inhibition. This event causes transcriptional inhibition of G1 cyclins that prevents degradation of Sic1, a B-type cyclin inhibitor [152], thus leading to a G1 cell cycle arrest. CHK2-mediated phosphorylation of CDC25A in humans leads to its degradation. Thus, the persistence of CDK2 phosphorylation keeps the cell cycle arrested. Also, p53 is a substrate of CHK2, and its phosphorylation leads to the activation of p21, which is a cell cycle inhibitor [161].

If the DNA gets damaged in G2, the presence of ssDNA induces ATR-dependent checkpoint activation. Once phosphorylated by ATR, CHK2 inhibits CDK1 by activating WEE1 kinase, which phosphorylates and inhibits CDK1. CHK2 also phosphorylates CDC25C inhibiting its stimulating effect on CDK1 [162], [163], leading to the arrest of the G2/M transition. In yeast, activated Rad53 and Chk1 phosphorylate the securin Pds1, inhibiting its degradation. This event arrests the G2/M transition by blocking sister chromatid separation [152].

6. Structure-function relationships of the MRX complex

The MRX/MRN complex, as described before, is a crucial regulator of many cellular processes, including DNA damage repair and DNA damage checkpoint activation. In humans, mutations in the *MRE11* gene cause Ataxia Telangiectasia-like disorder (ATLD) [164], while *RAD50* mutations are responsible for the Nijmegen-Breakage Syndrome-like disorder (NBSLD). Both disorders are characterized by increased cancer incidence, cell cycle checkpoint defects, and ionizing radiation sensitivity. Furthermore, *MRE11* and *RAD50* mutations are found in tumor cells, especially related to the large intestine, lung and skin cancers [165]. This supports the importance of the MRX/MRN complex in genomic stability maintenance.

The MRX/MRN complex is composed of two homodimers made by each of the three subunits to form a heterohexameric complex (Figure 9).

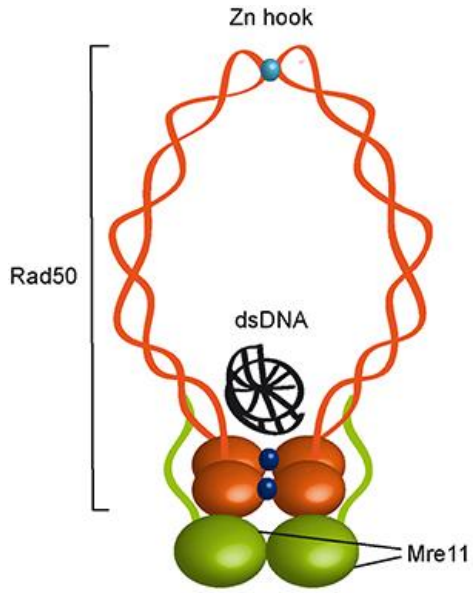

Figure 9 ***MRX complex structure.*** *Schematic structure of MRX (Xrs2 subunit not shown) with dsDNA molecule. The Mre11 dimer (green) is bound to Rad50 dimer (orange) with a double-stranded DNA molecule located on the top surface of Rad50. Adapted from* [13]

The N-terminal part of Mre11/MRE11 is characterized by five phosphodiesterase domains which confer to Mre11/MRE11 its endonuclease and 3'-5' exonuclease activities [166], [167], [168]. The C-terminus is characterized by the Rad50/RAD50 binding domain (RBD) and two DNA binding domains (DBDs)[24], [13], [77], [169]. Two Mre11/MRE11 subunits interact independently with Rad50/RAD50 and Xrs2/NBS1 to form the heterotrimeric complex structure [170]. Mre11/MRE11, with the help of the other two subunits, binds the ends of DSBs, preferring dsDNA and branched DNA as substrate [171], [172].

The Rad50/RAD50 subunit is characterized by a domain organization similar to the Stability Maintenance of Chromosomes (SMC) protein family, which ensures chromatin stability by remodeling chromatin structure. Rad50/RAD50 is also part of the ABC (ATP-binding cassette) ATPase superfamily [173], [174]. Its structure is characterized by two globular domains located at N and C termini, called Walker A and Walker B. These two domains form a bipartite ATPase domain, which is a characteristic of ABC ATPases [174], [169], [175]. The central domain of Rad50/RAD50 that divides the two Walker motifs, as previously described, is constituted by two long symmetrical coiled-coil domains that form the "arms" of the MRN/MRX complex. These coiled-coil domains are separated by a C-X-X-C motif responsible for the coordination of a Zinc atom. The coordination of the Zn atom promoted by two Rad50/RAD50 subunits bridges together two MRX/MRN complexes and, therefore, the two broken DNA ends. There are two main portions where Rad50/RAD50 and Mre11/MRE11 interact to form the complex: one is on the coiled-coil domain of Rad50/RAD50 that interacts with the C-terminal portion of Mre11/MRE11, whereas the other is in the ATPase domain that interacts with the Mre11/MRE11 capping domain [176].

The ATPase domain of Rad50/RAD50 is responsible for changes in MRX/MRN conformation. When Rad50/RAD50 binds ATP, the complex is in the so-called "closed" conformation that is responsible for high affinity binding to DNA. In this "closed" conformation, DNA is not accessible to the nuclease domains of Mre11/MRE11. Thus, the resection process is inhibited. As a consequence, the "closed" conformation promotes NHEJ and checkpoint activation. When the

Rad50/RAD50 ATPase domains hydrolyze ATP, the complex changes its state to an “open” conformation, where the DNA ends are accessible to the nuclease domains of Mre11/MRE11 and resection can take place [177], [178], [179].

The Xrs2/NBS1 subunit is not very evolutionary conserved. In fact, bacteria do not have an ortholog for Xrs2/NBS1 [180]. One of the functions of Xrs2/NBS1 is the nuclear localization of the MRX/MRN complex. There is a Nuclear Localization Sequence (NLS) in the C-terminal portion of the protein. This sequence allows the MRX/MRN complex to translocate into the nucleus once it is assembled in the cytoplasm. The C-terminus of Xrs2/NBS1 is also important because, in this region, there are also the domains that interact with Mre11/MRE11 and with the apical checkpoint kinase Tel1/ATM [181]. The N-terminal domain is characterized by the presence of a Forkhead-Associated (FHA) domain that is responsible for the physical interaction with Lif1/XRCC4 and Sae2/CtIP [182], [183], [184]. In this region, there are other domains. Specifically, there are two tandem repeats of the BRCA1 C-Terminal (BRTC) domain responsible for the binding of MDC1, a checkpoint adaptor that triggers checkpoint signal amplification detecting phosphorylated H2AX histones [185]. Recently it was demonstrated that, despite its importance in Tel1 recruitment at DSB and NHEJ, Xrs2 is dispensable for the resection process. A schematic view of the different domains of the MRX complex is represented in Figure 10 [170].

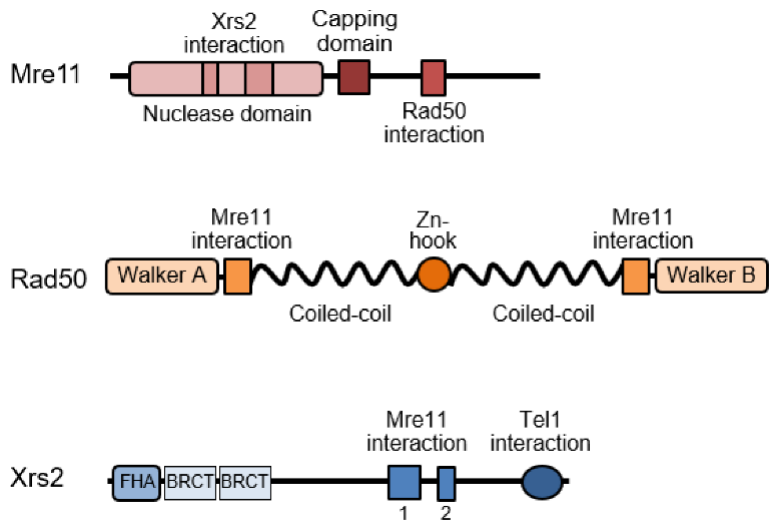

Figure 10 ***Mre11-Rad50-Xrs2 complex domains.*** *Schematic representation of domains localization in Mre11 (red), Rad50 (orange) and Xrs2 (blue) sequence from N-terminus to C-terminus. Adapted from* [170].

An MRX/MRN co-factor is Sae2/CtIP. As previously mentioned, Sae2/CtIP is important to support MRX/MRN functions in resection initiation, end tethering and checkpoint activation. The N-terminus of Sae2/CtIP contains the domain involved in oligomerization, whereas the C-terminal portion is devoted to the regulation and the stimulation of the resection process. The rest of the Sae2/CtIP protein is intrinsically disordered, and there is no a defined crystal structure [186]. Both N- and C-termini of Sae2/CtIP interact with Mre11/MRE11 in order to stimulate its endonucleolytic activity *in vivo* [15], [187], [28].

The current model for resection posits that phosphorylated Sae2 protein activates the Mre11 nuclease activity. Mre11 nuclease activation requires ATPase hydrolysis by Rad50 [81], [82], [28]. Then Mre11 catalyzes an incision of the 5' strand at both DS ends that is followed by Mre11 3′-5′ exonuclease that proceeds back toward the DSB end. Interestingly, degradation proceeds by stepwise endonucleolytic incisions, in which one MRX complex can promote cleavage by another MRX complex bound at an adjacent site. The endonucleolytic cleavage is followed by

Mre11 3′-5′ exonucleolytic degradation of the DNA fragments between the incision sites [13]. The requirement of the endonucleolytic cleavage performed by Mre11 depends on the nature of DSB ends. In yeast, Mre11 endonucleolytic activity seems to be dispensable on the so-called “clean DNA ends” that are not obstructed by adducts. On the other hand, in the presence of the so-called “dirty DNA ends”, the Mre11 endonuclease activity is necessary for giving access to DNA ends to the downstream nucleases Dna2 and Exo1.

Several studies have shown that ATP binding and hydrolysis activities by Rad50 are crucial to regulating DNA binding, tethering and nuclease functions of the MRX complex. Structural studies of Mre11 in complex with Rad50 core domains from bacteria and archaea indicate that, upon ATP binding, Rad50 closes into a rigid conformation that allows the N- and C-terminal domains to interact with each other and to form a central groove that can accommodate dsDNA. This closed the ATP-bound state of Rad50 renders dsDNA inaccessible to the Mre11 nuclease active site [13]. Point mutations that stabilize the ATP-bound conformation of Rad50 increase DNA binding, NHEJ and end-tethering [179], suggesting that MRX exerts these functions when it is present in the ATP-bound state. By contrast, in the ATP-free or hydrolyzed state, the Rad50 ATPase subunits are flexible and relatively open, suggesting that ATP hydrolysis drives the rotation of the two nucleotide-binding domains of Rad50 and the disengagement of the Rad50 dimer that makes DNA accessible to the Mre11 nuclease active sites [138]; [178], Consistent with this hypothesis, biochemical analyses demonstrate that ATP hydrolysis by Rad50 is a prerequisite for Mre11/Rad50-mediated nuclease activity on dsDNA molecules [188], [173], [189], [190]. Altogether, these findings lead to a model whereby these ATP-driven transitions regulate the balance between MRX functions in NHEJ and end-tethering, which require ATP binding, and those in resection and HR, which require ATP hydrolysis (Figure 11).

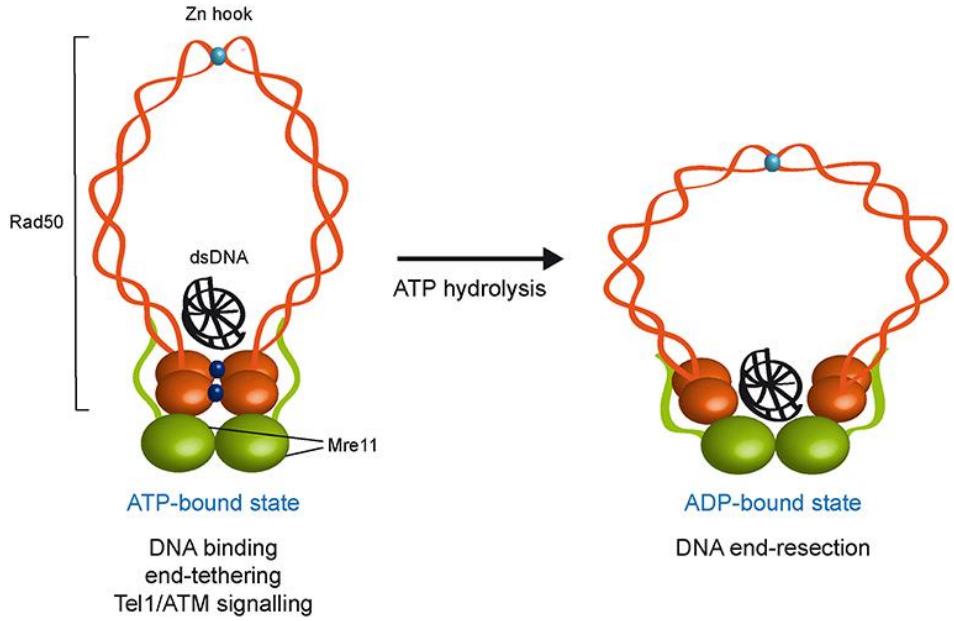

Figure 11 ***ATP- and ADP-bound state of the MRX complex****. The Mre11 dimer (green) is bound to Rad50 dimer (orange) with a double-stranded DNA molecule located on the top surface of Rad50. The ATP-bound state of Rad50 supports DNA binding, end-tethering, and Tel1/ATM signaling, whereas it renders the dsDNA inaccessible to the Mre11 nuclease active sites and therefore negatively regulates Mre11 nuclease activity. ATP hydrolysis by Rad50 opens the complex to allow the Mre11 active sites to access DNA. Whether the ADP-bound state maintains an interlinked assembly is unknown. ATP molecules are indicated as blue dots. Zn2+ atoms are indicated as light blue dots. Xrs2 is not represented.*

The exact mechanism of Tel1/ATM activation by MRX/MRN is mechanistically poorly understood. Indeed, in both yeast and mammals, MRX is required to recruit Tel1/ATM to DSBs. The telomeric protein Rif2 has a role in the regulation of MRX association to DSBs. It was shown that Rif2 stimulates ATP hydrolysis by Rad50 [114]. As the ATP-bound MRX conformation is important for DNA binding, Rif2 can decrease MRX association to DSBs by discharging the ATP-bound state. On the other hand, Rif2 competes with Tel1 for the activation of MRX [114]. Co-immunoprecipitation experiments have shown that the C terminus of Xrs2 interacts with Rif2. As Tel1 also binds this Xrs2 region, Rif2 can limit Tel1 association to DSBs by interfering with MRX-Tel1 interaction [191]. Once Tel1 is recruited to DSBs by MRX, it plays a structural role in stabilizing the association of MRX to the DSB ends in a manner independently of its kinase activity. This Tel1-mediated regulation of

MRX retention on DNA ends is essential to allow proper MRX-DNA binding that is needed for end-tethering and DSB repair [114].

In *S. cerevisiae*, the lack of Sae2 increases MRX and, therefore, Tel1 persistence at DSBs [192]. *mre11-nd* cells also exhibit persistent MRX and Tel1 association at DSB ends [193]. These findings suggest that MRX-Sae2 nuclease activity contributes to eliminating MRX bound to DNA ends, and this MRX displacement limits Tel1 signaling activity. However, *sae2Δ* cells, but not *mre11-nd* cells, exhibit increased accumulation of the Rad9 protein at DSBs and enhanced activity of the Rad53 checkpoint kinase, both of which inhibit the resection activity Dna2-Sgs1 and Exo1 [89], [194]. The lack of Sae2, but not the lack of Mre11 nuclease activity, causes hyperactivation of DNA damage checkpoint signaling caused by Tel1 persistence at DSB [195]. These findings lead to a model whereby Sae2 removes MRX and Tel1 from DNA ends by promoting Mre11 nuclease activity, and it limits Rad9 accumulation to DSBs independently of Mre11 nuclease activity. Both these Sae2 functions contribute to downregulate Rad53 activation, with the control of Rad9 association playing the significant role in supporting DNA damage resistance and checkpoint activation [15].

Results

Nucleic Acids Research
April 2018,
Volume 46, Issue 6,
Pages 2990–3008,
doi: 10.1093/nar/gky086

Nucleic Acids Research

Structurally distinct Mre11 domains mediate MRX functions in resection, end-tethering and DNA damage resistance

Corinne Cassani[1], Elisa Gobbini[1], Jacopo Vertemara[1], Weibin Wang[2], **Antonio Marsella**[1], Patrick Sung[2], Renata Tisi[1], Giuseppe Zampella[1] and Maria Pia Longhese[1],*

[1]Dipartimento di Biotecnologie e Bioscienze, Università di Milano-Bicocca, Milano, Italy and [2]Department of Molecular Biophysics and Biochemistry, Yale University School of Medicine, New Haven, CT 06520, USA.

*To whom correspondence should be addressed. Tel: +39 264483425; Fax: +39 264483565; Email: mariapia.longhese@unimib.it

Identification of *mre11* alleles that suppress the DNA damage hypersensitivity of *sae2Δ* cells

MRX and Sae2 are involved in resection of DSB ends and in maintaining the DSB ends tethered to each other [14]. In order to understand how these diverse Sae2-MRX functions contribute to DNA damage resistance, we used low-fidelity PCR to random mutagenize the *MRE11* gene, and then searched for *mre11* alleles that suppressed the hypersensitivity of *sae2*Δ cells to different DNA damaging agents such as CPT and/or phleomycin. Phleomycin generates chemically complex DNA termini, whereas CPT extends the half-life of topoisomerase 1 (Top1)-DNA cleavable complexes (Top1ccs). Linear *MRE11* PCR products were transformed into *sae2Δ* cells in order to replace the corresponding *MRE11* wild type sequence with the mutagenized DNA fragments (see Materials and Methods for details). Transformant clones showing higher viability than the untransformed strain in the presence of CPT and/or phleomycin were chosen for further characterization. Subsequent sequencing and genetic analysis identified 7 single *mre11* mutations that suppressed the CPT and/or phleomycin sensitivity of *sae2Δ* cells (Figure 12A). Among them, the *mre11-H98Y, mre11-K292E, mre11-R389C* and *mre11-T426I* alleles suppressed the hypersensitivity of *sae2Δ* cells to both CPT and phleomycin, whereas the *mre11-R522H, mre11-N631Y* and *mre11-ΔC41* alleles suppressed only the hypersensitivity of *sae2Δ* cells to phleomycin Figure 12A). No *mre11* alleles able to suppress only the sensitivity of *sae2Δ* cells to CPT have been identified. The inability of the Mre11-R522H, Mre11-N631Y and Mre11-ΔC41 variants to restore CPT resistance of *sae2Δ* cells is not due to hypersensitivity of the corresponding mutant cells to DNA damaging agents, as *mre11-R522H, mre11-N631Y* and *mre11-ΔC41* cells did not show reduced survival to any tested drug in the presence of fully functional Sae2 (Figure 12B).

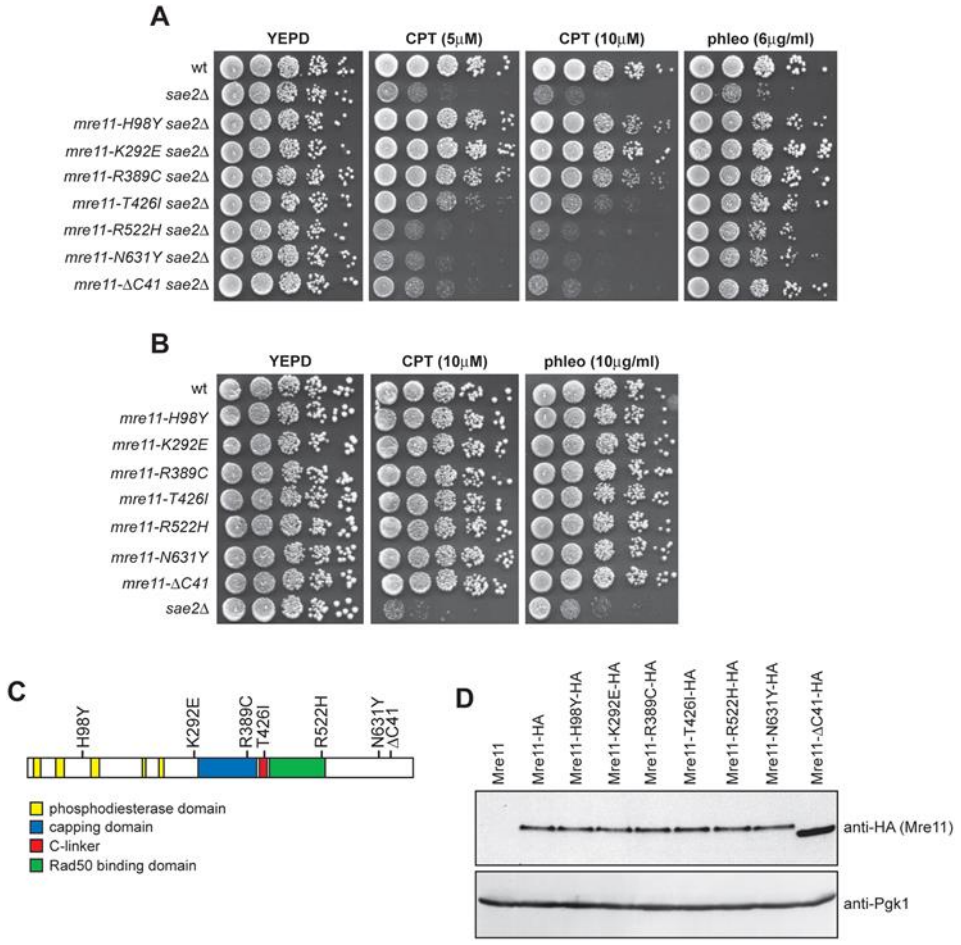

Figure 12 ***mre11 mutations suppress the sensitivity of sae2Δ cells to CPT and/or phleomycin****. (A, B) Exponentially growing cultures were serially diluted (1:10) and each dilution was spotted out onto YEPD plates with or without CPT or phleomycin at the indicated concentrations. (C) Position of the amino acid changes in the Mre11 sequence. (D) Protein extracts prepared from exponentially growing cells were analyzed by western blot using anti-HA antibody. The filter was also hybridized with anti-Pgk1 antibodies as loading control.*

Structural studies have shown that Mre11 can be divided into an N- and a C-terminal domain linked by an extended connecting loop [174], [176], [196] (see Supplementary Figure S2 for a structural alignment of Mre11 orthologs showing the positions of the conserved domains). Interestingly, the mutations restoring both CPT and phleomycin resistance cause amino acid changes in the Mre11 N-terminus, whereas the mutations restoring only phleomycin resistance are located in the Mre11 C-terminus coding region (Figure 12A and C), suggesting that

these two Mre11 domains reflect distinct MRX functions. Consistent with this hypothesis, independent searches for *mre11* mutations that bypass Sae2 function in CPT resistance by two other laboratories identified changes in H37, Q70, T74, L77, L89, E101 and P110 residues, all located in Mre11 N-terminus, as suppressors of the CPT sensitivity of ***sae2Δ*** cells [42], [197]. Curiously, our *mre11* mutations did not come up in these screens, while we did not find the H37, Q70 and P110 substitutions that were identified independently in both the above screens [42], [197].

With the exception of the *mre11-ΔC41* allele, which results in the formation of a stop codon at position 651 leading to a truncated protein lacking 41 amino acids at the C-terminus, all the other Mre11 mutant variants carried single amino acid substitutions due to missense mutations. HA epitope tagging of the mutant proteins followed by western blot analysis revealed that the amount of Mre11-ΔC41 variant was higher than that of wild type Mre11, while the amount of all the other Mre11 mutant proteins were unaltered (Figure 12D).

Suppression of the CPT hypersensitivity of *sae2Δ* cells correlates with restored DSB resection

To investigate whether the above mutations also suppressed the DSB resection defect of ***sae2Δ*** cells, we introduced the mutations in a strain (JKM139), where expression of the HO endonuclease from a galactose-inducible promoter leads to the generation of a single DSB at the *MAT* locus [85]. Due to the lack of the homologous donor sequences *HML* and *HMR*, this DSB cannot be repaired by HR. The extent of suppression in the derivative strains was similar to that observed in W303 background (Supplementary Figure S3). Because ssDNA cannot be cleaved by restriction enzymes, we directly monitored ssDNA formation at the irreparable HO-cut by following the loss of SspI restriction fragments. Southern blot analysis was performed under alkaline conditions, using a single-stranded probe that anneals to the 3′ end at one side of the break. As the *mre11-T426I* mutation suppressed the DNA damage hypersensitivity of ***sae2Δ*** only slightly and the *mre11-*

ΔC41 allele increased the corresponding protein level, only the *mre11-H98Y, mre11-K292E, mre11-R389C, mre11-R522H* and *mre11-N631Y* mutations were examined.

Resection of the HO-induced DSB occurred more efficiently in *sae2Δ mre11-H98Y, sae2Δ mre11-K292E* and *sae2Δ mre11-R389C* cells compared to *sae2Δ* cells (Figure 13A-D), indicating that Mre11-H98Y, Mre11-K292E and Mre11-R389C suppress the resection defect caused by the lack of Sae2. By contrast, the presence of the *mre11-R522H* and *mre11-N631Y* alleles did not suppress the resection defect of *sae2Δ* cells (Figure 14A-C). Rather, *mre11-R522H* and *mre11-N631Y* cells showed a very slight resection defect in the presence of wild type Sae2 (Figure 14A-C). As the Mre11-H98Y, Mre11-K292E and Mre11-R389C mutant proteins also restored CPT resistance in *sae2Δ* cells, whereas Mre11-R522H and Mre11-N631Y did not, suppression of *sae2Δ* CPT sensitivity appears to correlate with restored DSB resection.

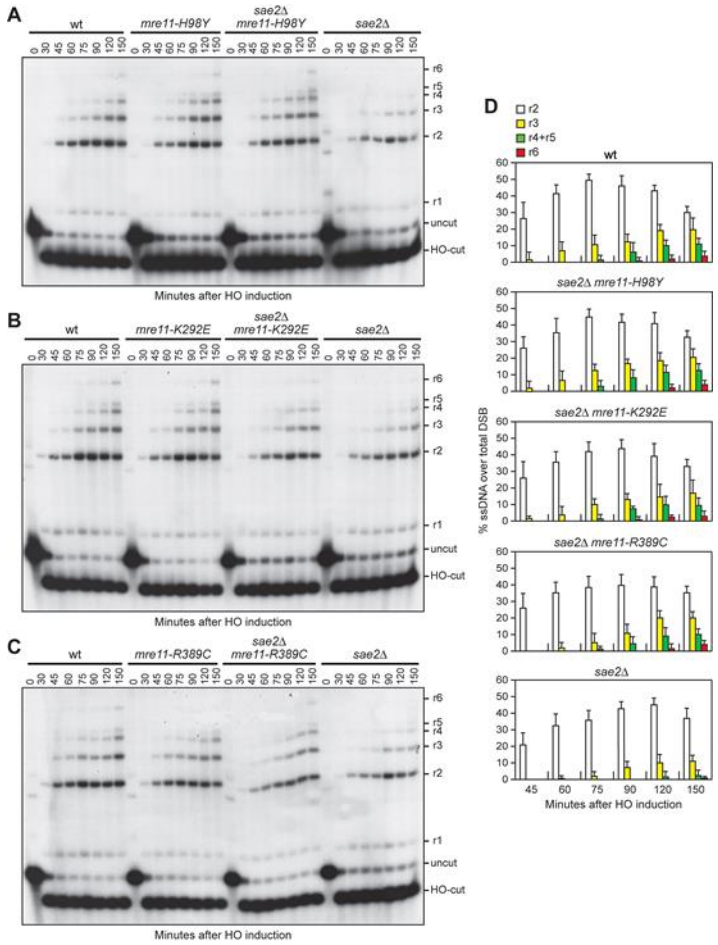

Figure 13 ***Mre11-H98Y, Mre11-K292E and Mre11-R389C suppress the resection defect of sae2Δ cells****.*
(A–C) DSB resection. YEPR exponentially growing cell cultures were transferred to YEPRG at time zero. SspI-digested genomic DNA separated on alkaline agarose gel was hybridized with a single-stranded MAT probe that anneals with the unresected strand. 5'-3' resection progressively eliminates SspI sites, producing larger SspI fragments (r1 through r6) detected by the probe. (D) Densitometric analysis. The experiment as in (A–C) was independently repeated and the mean values are represented with error bars denoting S.D. (n = 3).

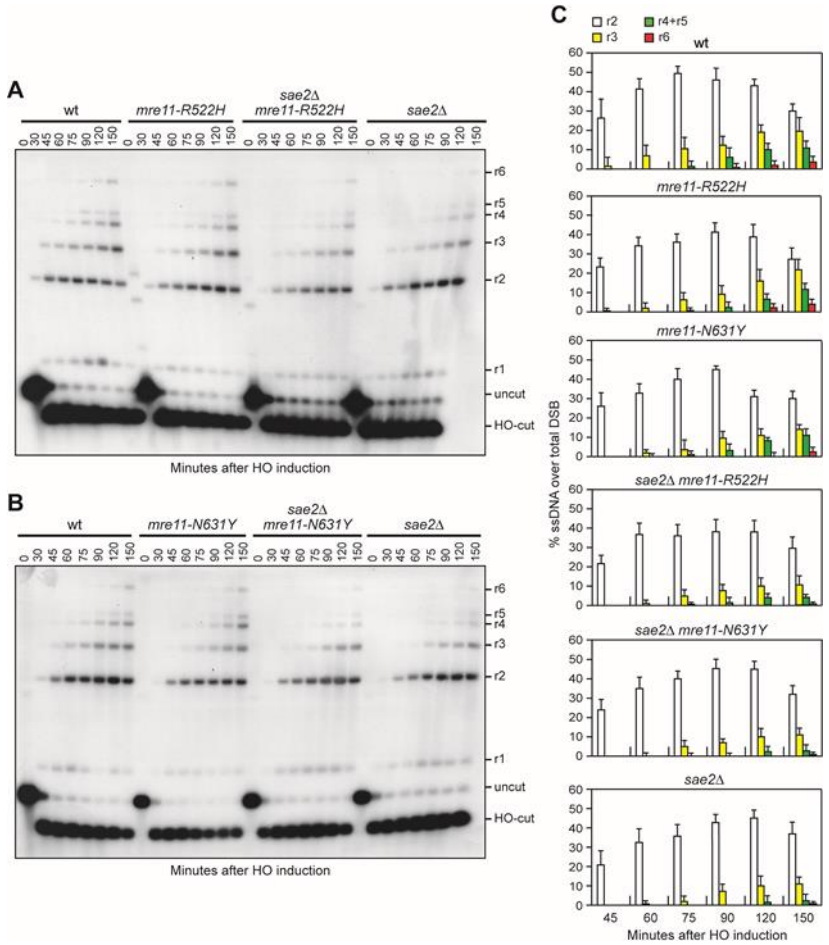

Figure 14 ***Mre11-R522H and Mre11-N631Y do not suppress the resection defect of sae2Δ cells.*** *(A, B) DSB resection. YEPR exponentially growing cell cultures were transferred to YEPRG at time zero. SspI-digested genomic DNA separated on alkaline agarose gel was treated as in Figure 2. (C) Densitometric analysis. The experiment as in (A, B) was independently repeated and the mean values are represented with error bars denoting S.D. (n = 3).*

Mre11-H98Y, Mre11-K292E and Mre11-R389C require Sgs1-Dna2 to suppress the DNA damage hypersensitivity of *sae2Δ* cells

Sae2 activates the Mre11 endonuclease to incise the 5′ strand, followed by resection from the nick by Exo1 and Sgs1-Dna2 in a 5′-3′ direction [28], [31], [44], [174], [176], [178], [179]. In addition, MRX promotes the binding of Exo1 and Sgs1-Dna2 at the DSB ends independently of Mre11 nuclease activity and Sae2 [47]. Thus, Mre11-H98Y, Mre11-K292E and Mre11-R389C could restore DSB resection in *sae2Δ* cells either because they possess a Sae2-independent endonuclease activity or because they potentiate the Exo1 and/or Sgs1-Dna2 downstream nucleases. To distinguish between these possibilities, first we asked whether the suppressor effect of the Mre11 variants was eliminated by abolishing Mre11 nuclease activity through a point mutation changing His125 to Asn in one of the Mre11 phosphoesterase motifs [168]. As shown in Figure 15A, the Mre11-H98Y, Mre11-K292E and Mre11-R389C variants also carrying the H125N amino acid substitution still suppressed the hypersensitivity to genotoxic agents of *sae2Δ* cells, indicating that suppression does not require Mre11 nuclease activity.

The endonucleolytic cleavage catalyzed by MRX-Sae2 is absolutely required to initiate resection at meiotic DSBs, whose 5′-terminated strands are not accessible to exonucleases because they are covalently bound by the topoisomerase-like protein Spo11 [198]–[200]. Consistent with the finding that Mre11-H98Y, Mre11-K292E and Mre11-R389C do not bypass the requirement for Sae2 to activate Mre11 nuclease, the *mre11-H98Y, mre11-K292E* and *mre11-R389C* alleles were unable to suppress the sporulation defect of *sae2Δ/sae2Δ* diploid cells (Figure 15B), suggesting that they fail to remove Spo11 from meiotic DSBs.

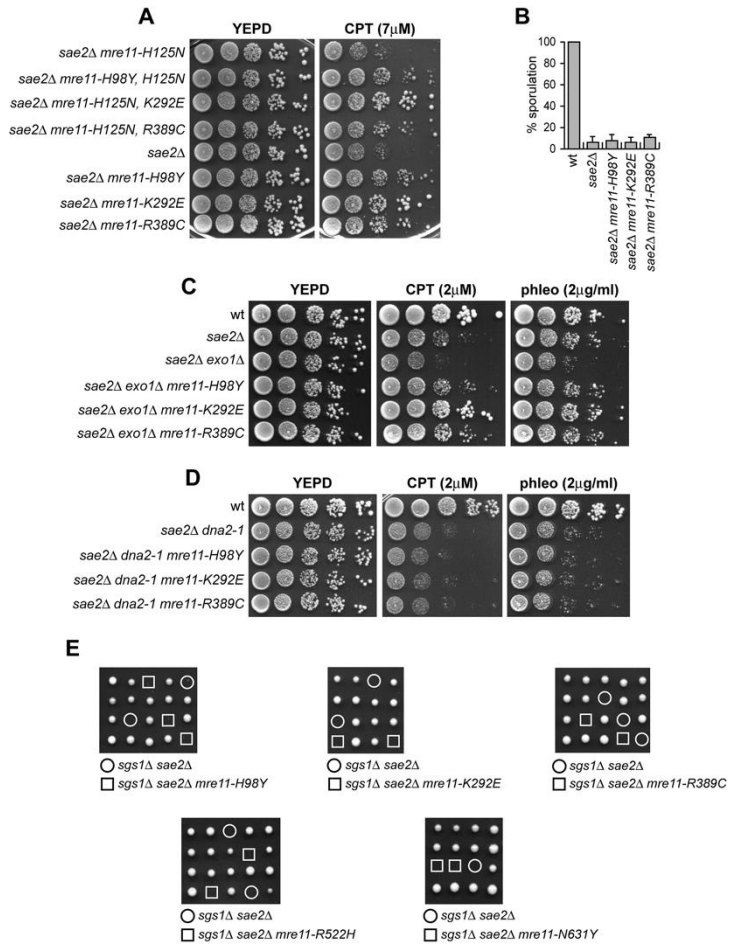

Figure 15 ***Suppression of sae2Δ DNA damage sensitivity by Mre11-H98Y, Mre11-K292E and Mre11-R389C depends on Sgs1-Dna2.***
(A, C, D) Exponentially growing cultures were serially diluted (1:10) and each dilution was spotted out onto YEPD plates with or without CPT or phleomycin at the indicated concentrations. (B) Sporulation efficiency of diploid strains homozygous for the indicated mutations. Data are expressed as percentage of sporulation relative to wild type that was set up at 100%. Plotted values are the mean values with error bars denoting S.D. (n = 3). (E) Meiotic tetrads were dissected on YEPD plates that were incubated at 25°C, followed by spore genotyping.

We then asked whether the *mre11-H98Y, mre11-K292E* and *mre11-R389C* suppression effects might depend on Dna2 and/or Exo1. Although the lack of Exo1 exacerbated the sensitivity to DNA damaging agents of *sae2Δ* cells, *sae2Δ exo1Δ mre11-H98Y, sae2Δ exo1Δ mre11-K292E* and *sae2Δ exo1Δ mre11-R389C* triple mutant cells were more resistant to genotoxic agents than *sae2Δ exo1Δ* double mutant cells (Figure 15C), indicating that the suppressor effect of the analyzed *mre11* alleles is Exo1-independent. By contrast, Mre11-H98Y, Mre11-K292E and

Mre11-R389C failed to suppress the sensitivity to DNA damaging agents of *sae2Δ* cells carrying the hypomorphic *dna2–1* allele (Figure 15D), suggesting that their suppressor effect requires Dna2 activity.

The lack of Sgs1 impairs viability of *sae2Δ* cells even in the absence of genotoxic agents. This synthetic lethality is likely due to defects in DSB resection, as it is suppressed by either *EXO1* overexpression or *KU* deletion [85]. Consistent with a requirement of Sgs1-Dna2 for the bypass of Sae2 function, tetrad dissection of diploids heterozygous for *sae2Δ, sgs1Δ* and the *mre11* mutations under analysis did not allow to find viable *sae2Δ sgs1Δ mre11-H98Y, sae2Δ sgs1Δ mre11-K292E* or *sae2Δ sgs1Δ mre11-R389C* spores (Figure 15E), indicating that Mre11-H98Y, Mre11-K292E and Mre11-R389C do not restore viability of *sae2Δ sgs1Δ* cells. Altogether, these findings indicate that Mre11-H98Y, Mre11-K292E and Mre11-R389C require Sgs1-Dna2 to restore DNA damage resistance in *sae2Δ* cells.

Mre11-H98Y, Mre11-K292E and Mre11-R389C relieve Rad9-mediated inhibition of Sgs1-Dna2 activity

The lack of Sae2 increases Rad9 association to DSBs, which in turn inhibits the resection activity of Sgs1-Dna2 by restricting the access of Sgs1 to the DSB ends [88], [89]. The DNA damage sensitivity and the resection defect of Sae2-deficient cells are suppressed by both the lack of Rad9 and the expression of a hypermorphic Sgs1 variant that escapes Rad9-mediated inhibition [88], [89]. We then asked whether Mre11-H98Y, Mre11-K292E and Mre11-R389C potentiate Sgs1-Dna2 by lowering Rad9 association to DSBs. As expected [19], the decrease in Sgs1 association to DSBs in *sae2Δ* cells was concomitant with an increased Rad9 persistence at DSBs (Figure 16A and B). The *mre11-H98Y, mre11-K292E* and *mre11-R389C* mutations increased Sgs1 association (Figure 16A) and decreased Rad9 association at DSBs (Figure 16B) both in the presence and in the absence of Sae2. Together with the observation that suppression of *sae2Δ* hypersensitivity to genotoxic agents requires Sgs1-Dna2, these findings strongly suggest that Mre11-H98Y, Mre11-K292E and Mre11-R389C restore both DNA damage resistance and

DSB resection in *sae2Δ* cells by decreasing Rad9 association close to the DSB, and therefore by relieving the inhibition of Sgs1-Dna2 resection activity.

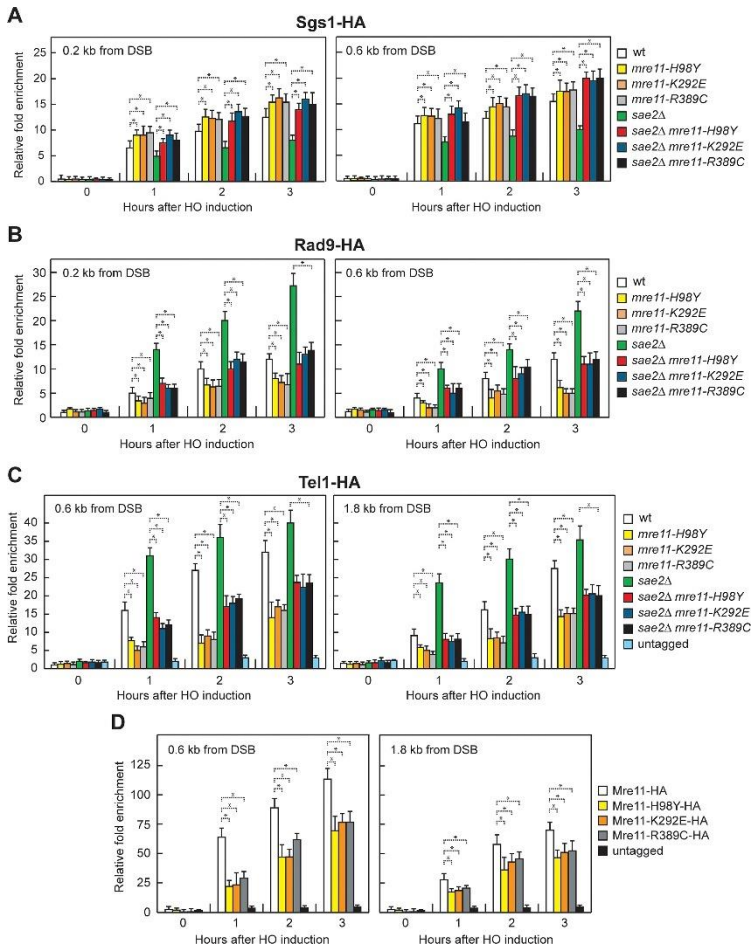

Figure 16 ***Effects of H98Y, K292E and R389C substitutions on Sgs1, Rad9, Tel1 and Mre11 association to DSBs****.*
*(A–D) ChIP analysis. Exponentially growing YEPR cell cultures were transferred to YEPRG at time zero. Relative fold enrichment of the indicated fusion proteins at the indicated distances from the HO cleavage site was determined after ChIP with anti-HA antibody and subsequent qPCR analysis. Plotted values are the mean values with error bars denoting S.D. (n = 3). *P< 0.05 (Student's t-test).*

Mre11-H98Y, Mre11-K292E and Mre11-R389C bind poorly to DSBs and decrease Tel1 association to DSBs

The lack of Sae2 enhances Tel1 signaling activity [41], [194], which is responsible for the increased Rad9 association at DSBs in *sae2Δ* cells [201]. Thus, we asked

whether the low Rad9 association to DNA ends in *mre11-H98Y, mre11-K292E* and *mre11-R389C* cells is due to decreased Tel1 binding to the same DNA ends. Indeed, the *mre11-H98Y, mre11-K292E* and *mre11-R389C* mutations decreased the amount of Tel1 bound at the HO-induced DSB both in the presence and in the absence of Sae2 (Figure 16C), suggesting that Mre11-H98Y, Mre11-K292E and Mre11-R389C reduce Rad9 association/persistence to DSBs by impairing Tel1 recruitment to the same DNA ends.

MRX is required for loading Tel1 to DSBs through a direct interaction between Tel1 and Xrs2 [3], [141], [202]. Thus, the *mre11-H98Y, mre11-K292E* and/or *mre11-R389C* mutations might reduce Tel1 association/persistence to DSBs either because they impair Mre11-Xrs2 interaction or because the corresponding mutant MRX complexes are poorly recruited to DSBs. Similar amount of Xrs2-Myc could be detected in immunoprecipitates of HA-tagged Mre11, Mre11-H98Y, Mre11-K292E and Mre11-R389C (Supplementary Figure S4), strongly suggesting that the reduced Tel1 association at DSBs is not due to defective Mre11-Xrs2 interaction. Rather, the amount of Mre11-H98Y, Mre11-K292E and Mre11-R389C associated to the HO-induced DSB turned out to be lower than that of wild type Mre11 (Figure 16D). Thus, these Mre11 variants appear to reduce Tel1 association at DSBs because they are poorly recruited to DNA ends. As a consequence, the reduced Tel1 binding leads to decreased Rad9 recruitment at the DSB ends, and therefore to the relieve of Rad9-mediated inhibition of Sgs1-Dna2 activity, which can compensate for the lack of Sae2 in DNA damage resistance and resection.

Mre11-H98Y affects Mre11 dimer formation

To map the location of the H98Y, K292E and R389C amino acid substitutions within the Mre11 structure, we used the tertiary structure of the *S. pombe* Mre11 (SpMre11) counterpart [164] as a template to generate a preliminary molecular model of *S. cerevisiae* Mre11 (ScMre11), which was refined further by a molecular dynamic simulation (500ns) (see Materials and Methods for details). Ensuing analyses indicated that the altered residues are located in three different regions that are not in mutual close proximity: H98 is located at the interface of the two

ScMre11 subunits, K292 is situated on the other side of the protein surface respect to H98, and R389 is in the capping domain (Figure 17A). Subsequently, a model for the ScMre11–Rad50 heterotetrameric structure was refined by molecular dynamics (Supplementary File 1), and then the ScMre11 homodimer structure obtained by this simulation was analyzed further by molecular dynamics (Supplementary File 2). These analyses allow to construct a model for the Mre11-Mre11 interface, comprising the latching loops (aa 80–118) together with α1 and α2 helices and the mostly disordered regions spanning residues 130–151 of each monomer, stabilizing the Mre11 dimeric structure and constituting an intermolecular dimerization domain (Figure 17A). This domain was largely uncharacterized due to the lack of structural information on the disordered regions, which are hardly resolved by crystallography. We mapped all the interactions of H98 and K292 residues with the rest of the dimeric ScMre11 protein, monitoring the persistence of hydrogen bonds and salt bridges (Supplementary Figure S5) (Mre11 monomers are indicated as A and B). The two ScMre11 monomers did not show a symmetrical behavior. In particular, both H98 and K292 establish a persistent intra-chain hydrogen bond during the entire simulation, with H98 contacting Y99 and E101 in Mre11-A and Mre11-B, respectively (Supplementary Figurhe S5A), whereas K292 interacting with D284 in both Mre11 monomers (Supplementary Figure S5B). Moreover, H98 is involved in a salt bridge with E101-B (Supplementary Figure S5C) and it also establishes an inter-chain hydrogen bond with L134-A (Supplementary Figure S5A). Altogether, these findings suggest that a complex network of dynamic interactions exists between residues within the dimerization domain and that mutations impairing some

of these interactions would improve the mobility of the disordered regions, likely affecting the stability of the dimerization interface.

While the role of K292 is difficult to envisage, these observations predicted that H98

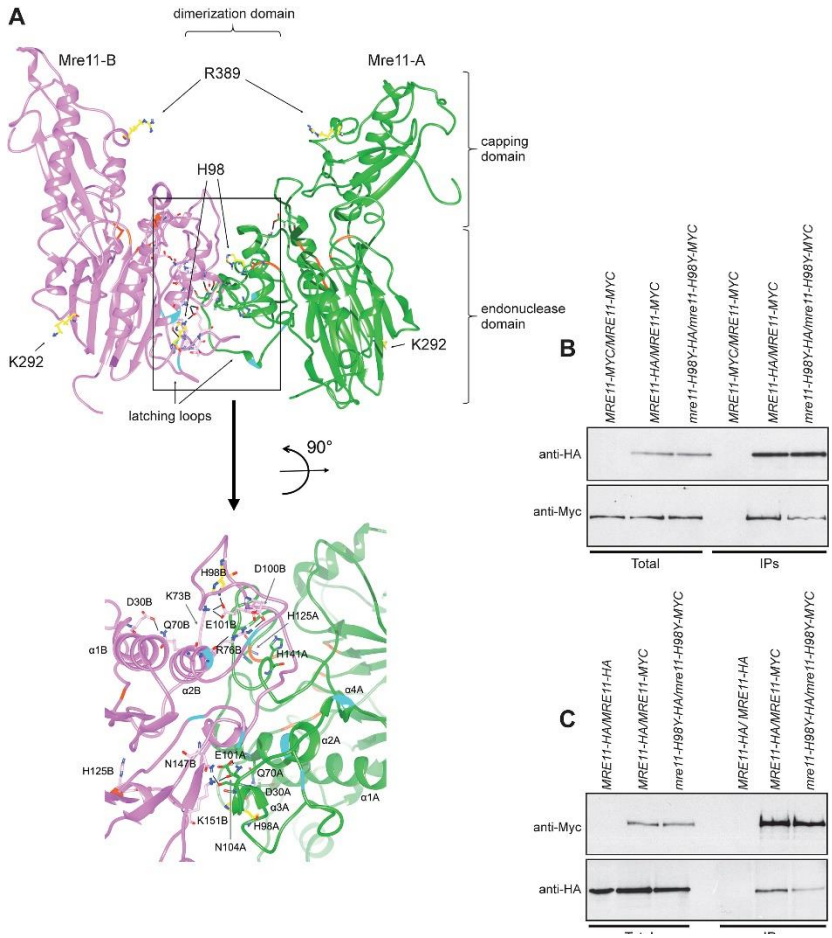

Figure 17 ***Mre11-H98Y alters Mre11 dimer formation. (A) Structural prediction of S. cerevisiae Mre11 dimer, obtained by homology modelling and refined by molecular dynamics***.
The two Mre11 monomers are shown in green (Mre11-A) and pink (Mre11-B). The position of endonuclease, capping and dimerization domains are shown. The lateral chain is shown for the residues (in yellow) whose mutations were described in the text. A close-up view of the dimerization domain is shown at the bottom. On the ribbon, positions involved in direct interaction with Xrs2 are in cyan, while positions constituting the active site are in orange. Black bars represent the hydrogen bonds/salt bridges existing in this particular conformation. (B, C) Mre11 dimer formation. Protein extracts prepared from exponentially growing diploid cells with the indicated genotypes were analyzed by western blotting with anti-HA and anti-Myc antibodies either directly (Total) or after immunoprecipitation (IPs) with anti-HA antibody (B) or anti-Myc antibody (C).

is directly implicated in the stabilization of Mre11 dimerization domain (Figure 17A), and its substitution with Y might lower the affinity between the two Mre11 subunits

by disrupting hydrogen bonds at the dimerization interface. We directly tested this prediction by immunoprecipitating Mre11 with anti-HA or anti-Myc antibody from protein extracts of *MRE11-HA/MRE11-MYC* and *mre11-H98Y-HA/mre11-H98Y-MYC* diploid cells. The amount of Mre11-H98Y-Myc detected by anti-MYC antibodies in immunoprecipitates of Mre11-H98Y-HA was reduced compared to that of wild type Mre11-Myc detected in immunoprecipitates of Mre11-HA (Figure 17B). Furthermore, the amount of Mre11-H98Y-HA detected by anti-HA antibodies in immunoprecipitates of Mre11-H98Y-Myc was reduced compared to that of wild type Mre11-HA detected in immunoprecipitates of Mre11-Myc (Figure 17C). As Mre11 dimer formation is required for MRX association to DSBs [203], this defect in the stabilization of the Mre11 dimer interface could explain the decreased Mre11-H98Y association to DSBs.

R389 mediates the interactions of Mre11 capping domain with both Rad50 and DNA

Residue R389 of Mre11 is localized in the capping domain, facing Rad50 in the ScMre11–Rad50 heterotetramer (Figure 18A). Again, the interaction is not symmetric, involving different residues (E1243 or Q1194) on the different Rad50 subunits. The dynamics of ScMre11 homodimer indicate that R389-A and R389-B do not show any functionally relevant interaction with the rest of the dimeric system (Supplementary Figure S5D and E), although R389-B is involved in a persistent salt bridge (Supplementary Figure S5C). On the other hand, due to the localization of this residue in the capping domain, which has been reported to be involved in the interaction with branched DNA in *Pyrococcus furiosus* Mre11 (PfMre11) crystal structure [203], R389 could also be involved in DNA binding. In fact, R389 is one of a pair of arginine residues (the other being R390) exposed in the correct position to interact with DNA, at least as inferred by superposition with DNA branched bound-PfMre11 structure (PDB: 3DSD) [203]. To test this hypothesis, we performed a MD simulation of 300 ns by including a dsDNA in the model, in order to reconstruct a structure that could reproduce the conformation reached after ATP hydrolysis by

Rad50 but before resection of DNA ends. DNA has been added on the ScMre11 complex using the structure of *Methanococcus jannaschii* Mre11 (MjMre11) dimer bound to a dsDNA end (PDB: 4TUG) [204] as a template. During the simulation, dsDNA binds to residues (such as K62 and N24) that correspond to positions already reported to interact with dsDNA in PfMre11 [203]. Interestingly, R389, which was not previously identified as a possible DNA binding site due to the difficulty in aligning the capping domains of PfMre11 and eukaryotic Mre11 [203], forms hydrogen bonds with the phosphate groups of DNA in both Mre11 subunits, with R389 of subunit B contacting the phosphodiesteric bridge of the 3′ terminus (Figure 18). The R389C substitution, which removes the arginine positive charge, would impair the DNA-binding interface on the capping domain of Mre11 due to the loss of the attractive force between the arginine and the phosphate group.

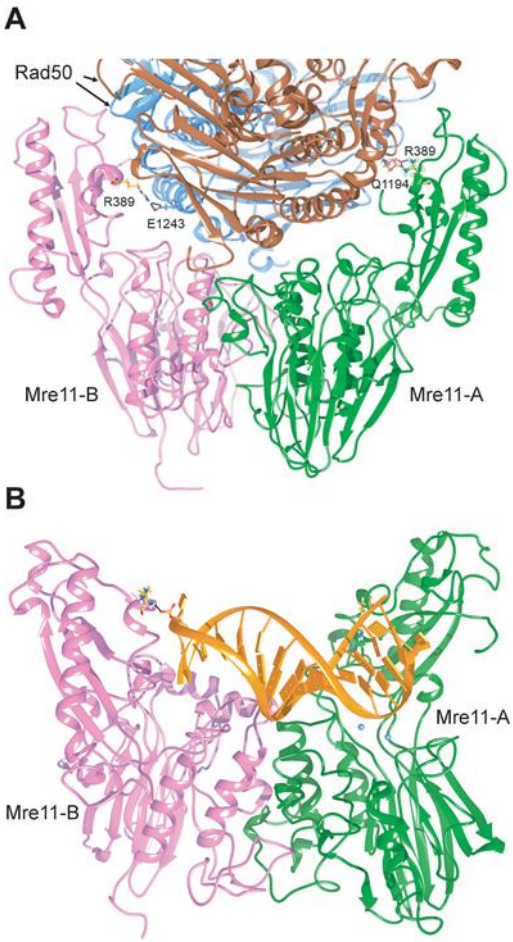

Figure 18 ***R389 at the Mre11–Rad50 and Mre11-DNA interfaces****.*
(A) Residue R389 of Mre11 is localized at the interface between Mre11 and Rad50 in the ScMre11–Rad50 heterotetramer. The position of R389 (in yellow) is shown on each Mre11 monomer constituting a tetramer with Rad50 subunits (in light blue and brown). The interaction is not symmetric, involving different residues (E1243 or Q1194) on the different Rad50 subunits. (B) Interaction of R389 (in yellow) of dimeric ScMre11 (in pink and green) with dsDNA (in orange). Black line indicates the salt bridge between R389 and the phosphodiesterase bridge at the 3' terminus of the dsDNA end. Mg2+ ions in the active site in one monomer are indicated in light blue.

Mre11-R522H bypasses Sae2 function in end-tethering and HR

The *mre11-R522H* and *mre11-N631Y* mutations restore phleomycin resistance of *sae2Δ* cells but neither CPT resistance nor DSB resection (Figure 12A and Figure 14A-C), suggesting that different Sae2 functions are involved in survival to CPT and phleomycin treatment. Consistent with this finding, Mre11-R522H and Mre11-N631Y did not cause a decrease of Rad9 (Supplementary Figure S6A) and Tel1 association to DSBs (Supplementary Figure S6B). Furthermore, they failed to restore viability of *sae2Δ sgs1Δ* cells (Figure 15E), possibly because they did not restore Sae2 function in DSB resection.

In addition to promoting DNA-end resection, MRX and Sae2 are also required to maintain the DSB ends adjacent to each other to facilitate DSB repair by both HR and NHEJ [41], [205]–[207]. Thus, we investigated whether Mre11-R522H and Mre11-N631Y can suppress the DSB end-tethering defect of *sae2Δ* cells. We used a yeast strain where the DNA proximal to an irreparable HO-inducible DSB can be visualized by binding of a LacI-GFP fusion protein to multiple repeats of the LacI repressor binding site that is integrated at a distance of 50 kb on both sides of the HO cut site [206]. HO expression was induced by galactose addition to cell cultures that were arrested in G2 with nocodazole and kept blocked in G2 by nocodazole treatment in order to ensure that all cells would arrest in metaphase. Most wild type cells showed a single LacI-GFP focus after HO induction, indicating their ability to maintain the broken DNA ends together (Figure 19A). Consistent with previous results [41], [205], *sae2Δ* cells showed an increase of cells with two LacI-GFP spots after HO induction compared to wild type cells (Figure 19A). Strikingly, the amounts

of cells showing two LacI-GFP spots after HO induction was decreased in both *sae2Δ mre11-R522H* and *sae2Δ mre11-N631Y* compared to *sae2Δ* cells, with *mre11-R522H* showing the strongest effect (Figure 19A). By contrast, the *mre11-H98Y, mre11-K292E* and *mre11-R389C* alleles did not suppress the end-tethering defect of *sae2Δ* cells (Figure 19A), possibly because of a reduced MRX association to DSBs.

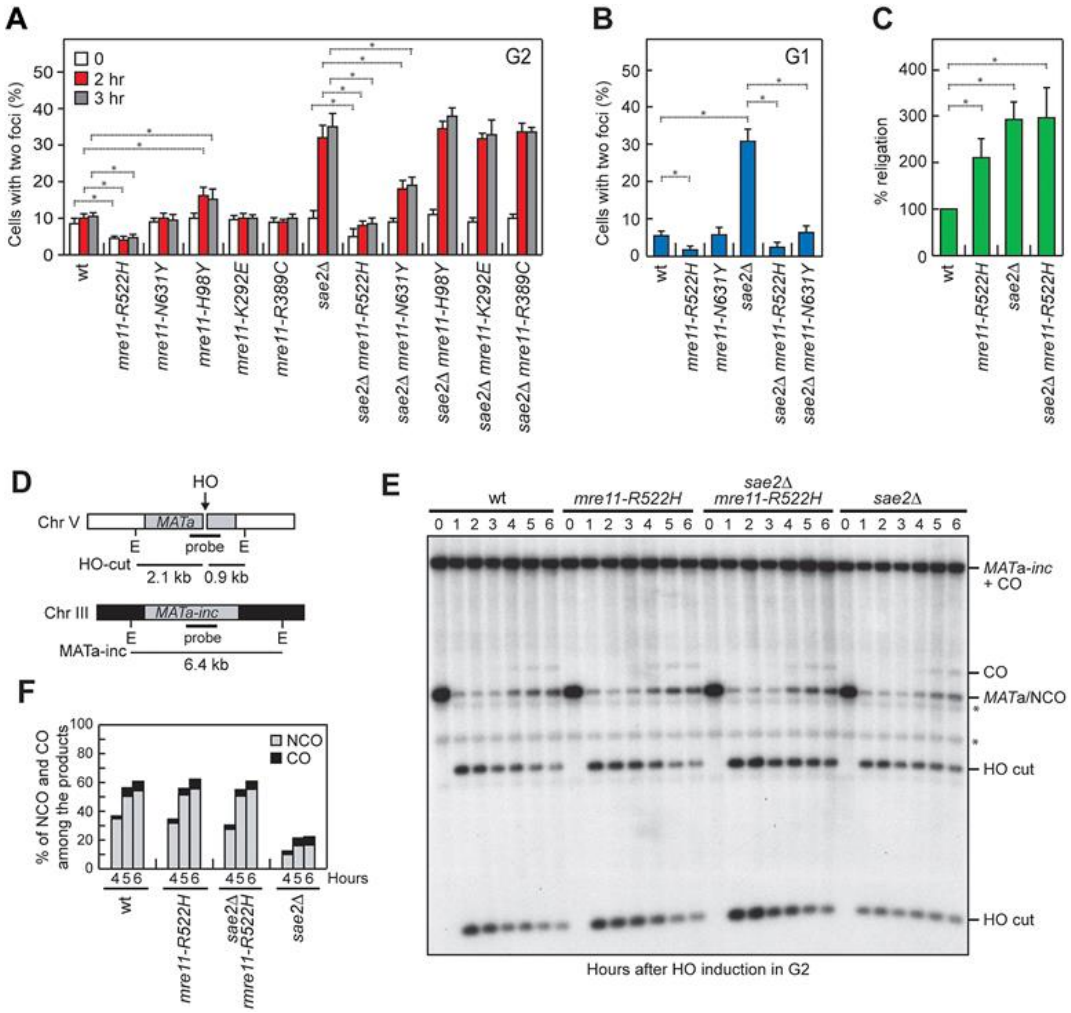

Figure 19 ***Mre11-R522H suppresses the end-tethering and the HR defects of sae2Δ cells.***
*(A, B) DSB end-tethering. Exponentially growing YEPR cell cultures were arrested in G2 with nocodazole (A) or in G1 with α-factor (B) at time zero and transferred to YEPRG in the presence of nocodazole or α-factor, respectively. 200 cells for each strain were analyzed to determine the percentage of cells showing two LacI-GFP foci. Plotted values are the mean values with error bars denoting S.D. (n = 3). *P< 0.05 (Student's t-test). (C) Plasmid re-ligation assay. Cells were transformed with BamH1-linearized or uncut pRS316 plasmid DNA. Data are expressed as percentage of re-ligation relative to wild type that was set up at 100% after normalization to the corresponding transformation efficiency with the uncut plasmid. Plotted values are the mean values with error bars denoting S.D. (n = 3). *P< 0.05 (Student's t-test). (D) System to detect ectopic recombination. HO generates a DSB at a MATa DNA sequence inserted on chromosome V, while the homologous MATa-inc region on chromosome III cannot be cut by HO and is used as a donor for HR-mediated repair. E, EcoRI. (E) YEPR cell cultures arrested in G2 with nocodazole were transferred to YEPRG at time zero in the presence of nocodazole. Southern blot analysis of EcoRI-digested genomic DNA with the MATa probe depicted in D. * indicates cross hybridization signals. (F) Densitometric analysis of CO versus NCO repair bands at the indicated times after HO induction.*

To confirm suppression of the end-tethering defect of *sae2Δ* cells by Mre11-R522H and Mre11-N631Y, we evaluated the frequency of two LacI-GFP foci after HO expression in α-factor-arrested cells that were kept arrested in G1 by α-factor in the presence of galactose. About 30% of G1-arrested *sae2Δ* cells showed two LacI-GFP foci 1 hour after HO induction and this frequency dramatically decreased in *sae2Δ mre11-R522H* and *sae2Δ mre11-N631Y* double mutant cells (Figure 19B).
Interestingly, the percentage of *mre11-R522H* cells showing two LacI-GFP spots was decreased compared to wild type cells even in the presence of functional Sae2 (Figure 19A and B), indicating that the $M^{R522H}RX$ complex possesses increased efficiency of DNA tethering. Consistent with a higher degree of tethering activity, *mre11-R522H* mutant cells were more efficient than wild type cells in re-ligating a plasmid that was linearized before being transformed into the cells (Figure 19C).
The maintenance of the DSB ends tethered to each other is important to repair a DSB by both NHEJ and HR [41], [114], [197], [205]. As both *sae2*Δ and *mre11-R522H sae2*Δ cells exhibit increased NHEJ frequency possibly due to reduced DSB resection (Figure 19C), it is unlikely that the restored end-tethering in *mre11-R522H sae2*Δ and *mre11-N631Y sae2*Δ cells may lead to phleomycin resistance by increasing NHEJ efficiency. Thus, we tested the effect of these mutations on the ability of *sae2*Δ cells to repair a DSB by HR.
In the canonical HR pathway, the 3′-ended ssDNA tail invades an intact duplex homologous, creating a loop structure (D-loop). The displaced ssDNA can then

anneal with the complementary sequence on the other side of the DSB to generate a double Holliday junction, whose random cleavage yield to non-crossover (NCO) and crossover (CO) products [208], [209]. Alternatively, if the ssDNA strand is displaced by the D-loop, its annealing with the 3′ ssDNA end at the other end of the DSB leads to the generation of NCO products in a process called synthesis-dependent strand-annealing (SDSA) [208], [209]. As the end-tethering activity of MRX was shown to be particularly important for SDSA-mediated DSB repair [114], we monitored CO and NCO formation in *sae2*Δ cells. We used a strain that carries a *MAT*a gene on chromosome V that can be cleaved by a galactose-inducible HO endonuclease and repaired by using an uncleavable *MAT*a (*MAT*a-*inc*) gene on chromosome III as template (Figure 19D) [210]. This repair event was shown to generate NCO and CO outcomes, with COs being ~5% among the overall repair events [210]. Galactose was added to induce HO production and then it was maintained in the medium to cleave the HO sites that were eventually reconstituted by NHEJ. Wild type and ***sae2Δ*** cells appeared to have similar percentage of COs Figure 19E and F). By contrast, the 3 kb *MAT*a band resulting from NCO recombination events re-accumulated less efficiently in ***sae2Δ*** cells compared to wild type cells, while the *mre11-R522H* mutation restored wild type levels of NCO products in ***sae2Δ*** cells (Figure 19E and F). As most NCO products are generated by the SDSA mechanism and the end-tethering activity is important to support DSB repair by SDSA [114], this finding suggests that the restored end-tethering conferred by Mre11-R522H can suppress the ***sae2Δ*** phleomycin sensitivity by increasing the efficiency of SDSA-mediated DSB repair.

R522 contributes to the stabilization of the Mre11–Rad50 binding domain

Because Mre11-R522H showed the strongest effect in the bypass of the end-tethering Sae2 function and possessed an increased end-tethering activity by itself, we analyzed the effect of this mutation at biochemical and structural levels. The R522 residue is located in the Rad50 binding domain (RBD) that, together with the

capping domain, mediates the interaction between Mre11 and ATP-bound Rad50 [196]. ATP hydrolysis by Rad50 induces the change from a closed MRX conformation, required for end-tethering, to an open configuration that promotes Mre11 nuclease activity [179]. After ATP hydrolysis, the Mre11 capping domain dissociates from Rad50, leaving the RBD as the only Mre11–Rad50 interface [196]. We then expressed the Mre11-R522H protein in insect cells and purified it to near homogeneity (Supplementary Figure S7A) to test the purified mutant protein for interaction with Rad50 and Xrs2. As shown in Supplementary Figure S7B, Mre11-R522H retained the ability to associate with Rad50 and Xrs2 and, importantly, the $M^{R522H}RX$ complex showed normal ATPase activity (Figure 20A and B) and nuclease activity (Figure 20C and D). These results are consistent with the very minor resection defect of *mre11-R522H* cells (Figure 20A and C).

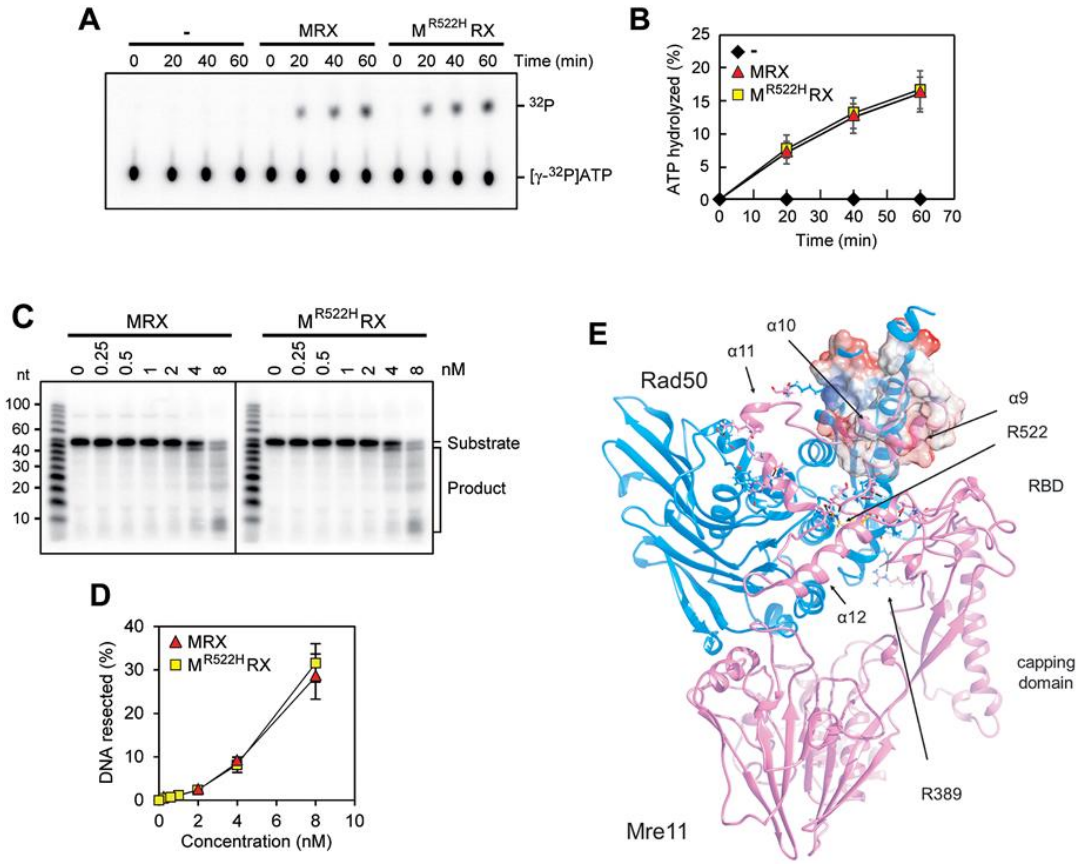

Figure 20 ***Functional and structural characterization of Mre11-R522H****.*
(A, B) ATP hydrolysis by wild type MRX or MR522HRX mutant (100 nM of each) in the presence of 100-bp dsDNA (200 nM) (A). The results from three independent experiments were quantified (B). The mean values are represented with error bars denoting S.D. (n = 3). (C, D) The nuclease activity of wild type MRX or MR522HRX complex was tested on the 5'-labeled 95 bp dsDNA (8 nM) with 5 nt 3' overhangs and a nick 55 nt away from the labeled end. The results were quantified, based on the product at the gel bottom, with error bars denoting S.D. (n = 3). (E) A model for Mre11 comprising Rad50 binding domain (RBD) was optimized by molecular dynamics. The position of residue R522 (in yellow) and of residues involved in Mre11–Rad50 interaction are shown. The Coulomb potential surface (red, negative charge; white, hydrophobic surface; blue, positive charge) is represented for the coiled-coiled region of Rad50 and Mre11 α9 and α10, which mainly share hydrophobic interactions.

As ScMre11 RBD structure was not available, we obtained a model for a heterodimer ScMre11–Rad50 comprising Mre11 RBD by molecular dynamics (Figure 20E) (see Materials and Methods for details). The energetically favored structure for ScMre11 RBD was actually not identical to the Mre11 structure resolved for the thermophilic filamentous fungus *Chaetomium thermophilum* (PDB ID: 5DA9). ScMre11 RBD binds not only to the Rad50 coiled-coiled region but also to the globular domain (Figure 20E). Two helices, α9 and α10, take contact with Rad50 coiled-coil region, mainly via hydrophobic interactions, while a third helix, α11, interacts with the globular region of Rad50. A fourth helix, α12, is involved in stabilization of the structure, mainly by residue R522 indeed, which strongly binds to both E443 (at the beginning of α9 helix) and E494 (at the end of α11 helix). The R522H amino acid substitution would allow maintenance of only a few of these interactions, conferring more mobility to the whole RBD. Consistent with the finding that Mre11-R522H is still capable to associate with Rad50 (Supplementary Figure S7B), the increased RBD mobility is not sufficient to impair the association between Mre11 and ATP-bound Rad50, which in fact depends on both the RBD and the capping domains. However, it could lead to a slight destabilization of the Mre11–Rad50 interaction only after ATP hydrolysis, when the RDB remains the sole Mre11–Rad50 interface. As a consequence, a defect in stabilizing the interaction between Mre11 and ADP-bound Rad50 might lead to increased association at DSBs of MRX in its ATP-bound conformation, and therefore to a more efficient end tethering.

Nucleic Acids Research
April 2019,
Volume 47, Issue 7,
Pages 3550–3567,
doi: 10.1093/nar/gkz038

Nucleic Acids Research

The ATP-bound conformation of the Mre11–Rad50 complex is essential for Tel1/ATM activation

Corinne Cassani†, Jacopo Vertemara†, Matteo Bassani, **Antonio Marsella**, Renata Tisi, Giuseppe Zampella and Maria Pia Longhese*

Dipartimento di Biotecnologie e Bioscienze, Università di Milano-Bicocca, Milano, Italy and

*To whom correspondence should be addressed. Tel: +39 0264483425; Fax: +39 0264483565; Email: mariapia.longhese@unimib.it

†The authors wish it to be known that, in their opinion, the first two authors should be regarded as Joint First Authors.

Identification of *mre11* and *rad50* mutations that specifically affect Tel1 activation

To identify separation of function *mre11* and *rad50* mutations that specifically affect Tel1 activation without impairing MRX functions in DSB repair, we took advantage of the finding that Tel1-deficient cells are hypersensitive to high doses of the type I topoisomerase inhibitor camptothecin (CPT), but not to other genotoxic agents like methyl metansulfonate (MMS) and phleomycin [211](Figure 21A). We used low-fidelity PCR to random mutagenize the *MRE11* and *RAD50* genes, followed by transformation with the linear *MRE11* or *RAD50* PCR products into wild type cells in order to replace the corresponding *MRE11* or *RAD50* wild type sequence with the mutagenized DNA fragments [212]. Transformants were then screened for low viability in the presence of high doses of CPT, while retaining wild type survival to phleomycin and MMS treatment. As the lack of Tel1/ATM causes telomere shortening [213], transformant clones specifically showing CPT hypersensitivity were subsequently analyzed for telomere length by Southern blot. This analysis allowed us to identify the *mre11-S499P* mutation, causing the replacement of the Mre11 Ser499 residue with Pro, and the *rad50-A78T* mutation, causing the replacement of the Rad50 Ala78 residue with Thr. Both *mre11-S499P* and *rad50-A78T* cells lost viability at high doses of CPT, although their CPT hypersensitivity was less severe than that of *tel1*Δ cells (Figure 21A). Furthermore, they did not lose viability in the presence of MMS or phleomycin, differently from *mre11*Δ cells (Figure 21A), indicating that they did not affect MRX functions in DNA damage resistance. Finally, they showed telomere shortening similar to *tel1*Δ cells (Figure 21B).

MRX is essential to repair DSBs by both NHEJ and HR, whereas Tel1 has a very minor role in both processes [114], [214]. We asked whether the *mre11-S499P* and *rad50-A78T* mutations affect MRX function in NHEJ by measuring the ability of *mre11-S499P* and *rad50-A78T* cells to re-ligate a plasmid that was linearized before being transformed into the cells. The efficiency of plasmid re-ligation was similar in wild type, *tel1Δ, mre11-S499P* and *rad50-A78T* cells (Figure 21C), while it was

dramatically decreased in *mre11Δ* cells, indicating that the *mre11-S499P* and *rad50-A78T* mutations do not affect MRX functions in DSB repair by NHEJ.

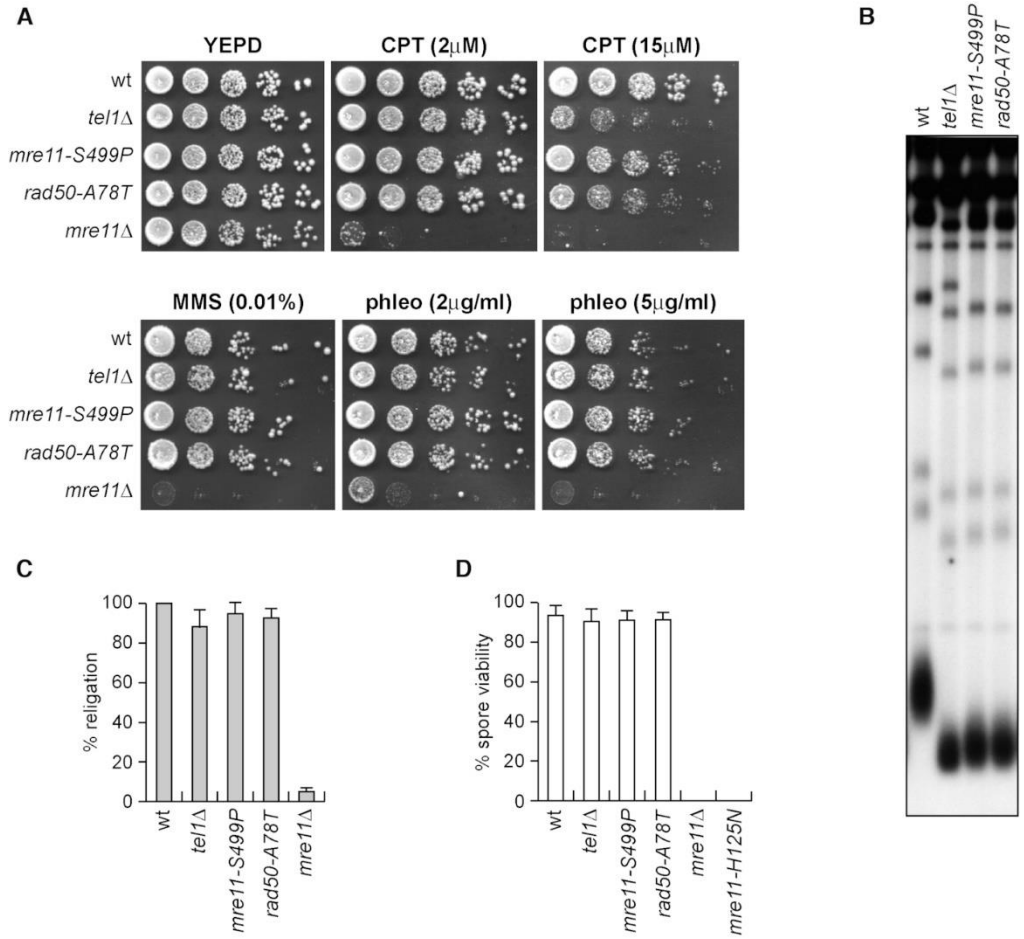

Figure 21 ***The mre11-S499P and rad50-A78T mutations phenocopy TEL1 deletion with respect to CPT hypersensitivity and telomere length****.*
(A) Exponentially growing cells were serially diluted (1:10) and each dilution was spotted out onto YEPD plates with or without CPT, MMS or phleomycin. (B) Telomere length. XhoI-cut genomic DNA from exponentially growing cells was subjected to Southern blot analysis using a poly(GT) telomere-specific probe. (C) Plasmid re-ligation assay. Cells were transformed with the same amounts of BamHI-linearized pRS316 plasmid DNA. Data are expressed as percentage of re-ligation relative to wild type that was set up at 100% after normalization to the corresponding transformation efficiency of the uncut plasmid. (D) Spore viability. Diploid cells homozygous for the indicated mutations were induced to enter in meiosis followed by tetrad dissection on YEPD plates. At least 40 tetrads for each strain have been analyzed. Mean values are represented with error bars denoting S.D. (n = 3).

The MRX complex is essential to generate and resect meiotic DSBs, which are created by the Spo11 transesterase that forms a covalent linkage between a conserved tyrosine residue and the 5′ end of the cleaved strand [215]. Spore viability

is impaired by the lack of either the Mre11 nuclease activity or any MRX subunit [198]. We therefore induced meiosis in wild type, *mre11-S499P*/*mre11-S499P* and *rad50-A78T*/*rad50-A78T* diploid cells, followed by tetrad dissection and spore viability analysis. Spore viability was not reduced by the *tel1Δ, mre11-S499P* and *rad50-A78T* mutations, while it was dramatically decreased in diploid cells either lacking Mre11 (*mre11Δ*/*mre11Δ*) or expressing a nuclease defective *mre11* allele (*mre11-H125N*/*mre11-H125N*) (Figure 21D), indicating that Mre11-S499P and Rad50-A78T variants maintain Mre11 functions in meiosis.

The *mre11-S499P* and *rad50-A78T* mutations phenocopy *TEL1* deletion with respect to DSB resection and checkpoint signaling

During HR, MRX is required to generate 3′-ended RPA-coated ssDNA at the DSB ends that catalyzes strand invasion. This ssDNA also induces activation of a Mec1-dependent checkpoint response [146], [216]. The lack of any MRX subunit severely reduces both ssDNA generation at the DSB ends and Mec1 activation [217], [218]. By contrast, Tel1 has a minor role in DSB signaling compared to Mec1, as *tel1Δ* cells caused only a very slight reduction both in ssDNA generation at the DSB ends and in checkpoint activation in response to a single DSB [214]. To investigate the effect of the *mre11-S499P* and *rad50-A78T* alleles on both processes, we used JKM139 derivative strains, where a single DSB at the *MAT* locus can be generated by expressing the HO endonuclease gene under the control of a galactose-inducible promoter. The *HML* and *HMR* loci were deleted in these strains to prevent DSB repair by gene conversion [218]. Resection of DNA regions flanking the HO-induced DSB renders the DNA sequence resistant to cleavage by restriction enzymes, resulting in the appearance of resection intermediates that can be detected by Southern blot analysis with a probe that anneals to the 3′ end at one side of the break. Both *mre11-S499P* and *rad50-A78T* cells showed only a slight reduction in the efficiency of ssDNA generation at the HO-induced DSB and the extent of this defect was similar to that of *tel1Δ* cells (Figure 22A-C). This resection defect was

not exacerbated in *mre11-S499P tel1Δ* and *rad50-A78T tel1Δ* double mutants (Figure 22A-C), indicating that the *mre11-S499P* and *rad50-A78T* mutations reduce DSB resection by altering the same pathway affected by *TEL1* deletion.

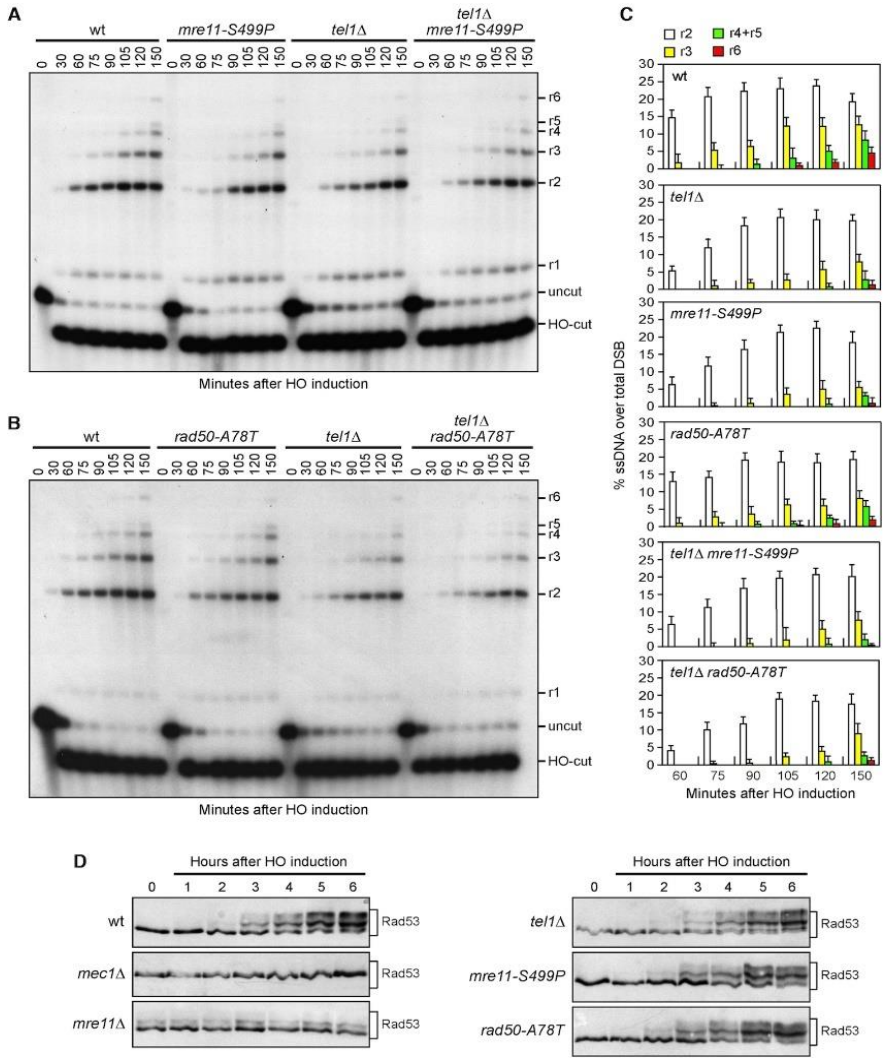

Figure 22 ***The mre11-S499P and rad50-A78T mutations phenocopy TEL1 deletion with respect to DSB resection and checkpoint activation****.*
(A, B) DSB resection. YEPR exponentially growing cell cultures were arrested in nocodazole and then transferred to YEPRG at time zero to induce HO expression. SspI-digested genomic DNA was separated and hybridized with a single-stranded MAT probe that anneals to the unresected 3' end at one side of the break. 5'-3' resection progressively eliminates SspI sites, producing larger SspI fragments (r1 through r6) that can be detected by the probe. (C) Densitometric analysis. The experiment as in (A, B) was independently repeated and the mean values are represented with error bars denoting S.D. (n = 3). (D) Rad53 phosphorylation. Exponentially growing YEPR cultures were transferred to YEPRG (time zero) to induce HO, followed by western blot analysis with anti-Rad53 antibodies.

To monitor checkpoint activation, we followed Rad53 phosphorylation, which is required for Rad53 activation and is detectable as a decrease of Rad53 electrophoretic mobility. As previously reported [214], phosphorylated Rad53 was not detectable in galactose-induced JKM139 *mec1Δ* cells. Furthermore, HO induction did not cause Rad53 phosphorylation in *mre11*Δ cells, where a basal level of Rad53 phosphorylation was detectable even in the absence of DSB formation possibly due to DNA replication defects (Figure 22D). By contrast, *mre11-S499P, rad50-A78T* and *tel1Δ* cells phosphorylated Rad53 with kinetics similar to that of wild type cells (Figure 22D). Altogether, these data indicate that both Mre11-S499P and Rad50-A78T mutant variants behave like *TEL1* deletion with respect to DSB resection and checkpoint activation.

The *mre11-S499P* and *rad50-A78T* mutations specifically abolish Tel1-mediated checkpoint activation

The checkpoint response triggered by a single unrepairable DSB can be eventually turned off, allowing cells to resume cell cycle progression through a process that is called adaptation [216], [219]. In the absence of Sae2, cells display heightened Tel1 activation, which is associated with persistent Rad53 phosphorylation that prevents cells from adapting to an unrepaired DSB [41], [117], [194]. If the *mre11-S499P* and *rad50-A78T* mutations affect Tel1 activation, they would be expected to suppress the adaptation defect of *sae2Δ* cells by reducing Tel1-dependent Rad53 phosphorylation. As shown in Figure 23A, Rad53 phosphorylated forms were detectable with similar kinetics ~2–4 h after galactose addition in wild type, *sae2Δ, tel1Δ sae2Δ, mre11-S499P sae2Δ* and *rad50-A78T sae2Δ* cells. Consistent with DSB-induced checkpoint activation, when cells arrested in G1 with α-factor were spotted on galactose-containing plates to induce *HO*, all the above cell cultures accumulated large budded cells within 4 h (Figure 23B). However, *sae2Δ* cells showed persistent Rad53 phosphorylation (Figure 23A) and most of them remained arrested as large budded cells for at least 24 h (Figure 23B). By contrast, the amounts of phosphorylated Rad53 decreased in *sae2Δ mre11-S499P* and *sae2Δ*

rad50-A78T cells (Figure 23A), which formed microcolonies with more than two cells ~12–16 h after HO induction with kinetics similar to those observed in ***sae2Δ tel1Δ*** cells (Figure 23B). Therefore, both Mre11-S499P and Rad50-A78T rescue the Tel1-mediated ***sae2Δ*** adaptation defect, indicating that they impair Tel1 signaling. The unscheduled Tel1 activation in ***sae2Δ*** cells was shown to suppress the hypersensitivity to hydroxyurea (HU) and MMS caused by the lack of Mec1 [194] (Figure 23C). In fact, *SAE2* deletion suppressed the MMS and HU hypersensitivity of ***mec1Δ*** cells, but not that of ***mec1Δ tel1Δ*** cells (Figure 23C). Consistent with the inability of Mre11-S499P and Rad50-A78T to activate Tel1, the lack of Sae2 failed to restore resistance to HU and MMS of *mre11-S499P* ***mec1Δ*** and *rad50-A78T* ***mec1Δ*** cells. In fact, *mre11-S499P* ***sae2Δ mec1Δ*** and *rad50-A78T* ***sae2Δ mec1Δ*** cells lost viability in the presence of HU or MMS to the same extent as *mre11-S499P* ***mec1Δ*** and *rad50-A78T* ***mec1Δ*** cells (Figure 23D). By contrast, due to the requirement of Sae2 in repairing CPT-induced DNA lesions [14], [220], *SAE2* deletion did not restore CPT resistance not only in ***mec1Δ tel1Δ,*** *mre11-S499P* ***mec1Δ*** and *rad50-A78T* ***mec1Δ*** cells, but also in ***mec1Δ*** cells (Figure 23D). Finally, consistent with an increased CPT sensitivity caused by the *mre11-S499P* and *rad50-A78T* mutations, *mre11-S499P* ***mec1Δ*** and *rad50-A78T* ***mec1Δ*** cells were more sensitive to CPT compared to ***mec1Δ*** cells (Figure 23D).

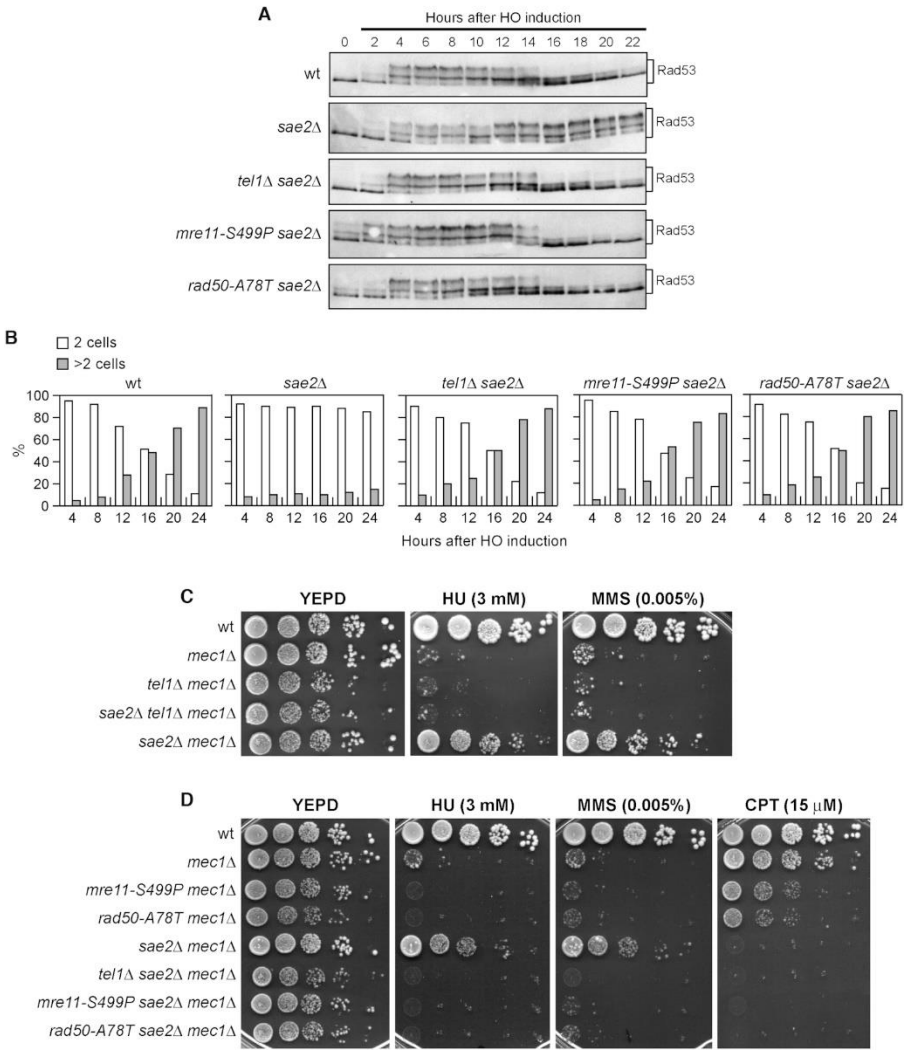

Figure 23 ***The mre11-S499P and rad50-A78T mutations suppress the adaptation defect of sae2Δ cells****.*
(A) Rad53 phosphorylation during adaptation. Exponentially growing YEPR cultures were transferred to YEPRG (time zero), followed by western blot analysis with anti-Rad53 antibodies. (B) Adaptation assay. YEPR G1-arrested cell cultures of the strains in (A) were plated on galactose-containing plates (time zero). At the indicated time points, 200 cells for each strain were analyzed to determine the frequency of large budded cells (two cells) and of cells forming microcolonies of more than two cells. (C, D) Drop test. Exponentially growing cells were serially diluted (1:10) and each dilution was spotted out onto YEPD plates with or without HU, MMS and CPT at the indicated concentrations. All strains carried SML1 deletion to keep mec1Δ cells viable.

Mre11-S499P and Rad50-A78T reduce Tel1–MRX interaction and Tel1 association to DNA DSBs

To investigate whether the defective Tel1 signaling activity in *mre11-S499P* and *rad50-A78T* cells was due to decreased Tel1 persistence to DSBs, we measured Tel1 association at DSBs by chromatin immunoprecipitation (ChIP) and quantitative real time PCR (qPCR). Although similar amount of Tel1 were detected in protein extracts from wild type, *mre11-S499P* and *rad50-A78T* cells (Figure 24A), the amount of Tel1 bound at the HO-induced DSB was dramatically lower in both *mre11-S499P* and *rad50-A78T* cells than in wild type cells (Figure 24B). This finding indicates that Mre11-S499P and Rad50-A78T reduce Tel1 association to DNA DSBs.

Indeed, when Tel1 is recruited by MRX at DSBs [3], [141], [202], it promotes MRX association/persistence in a positive feedback loop [114]. Thus, we measured Mre11 association at DSBs in both *mre11-S499P* and *rad50-A78T* cells either in the presence or in the absence of Tel1. We found that the *tel1Δ, mre11-S499P* and *rad50-A78T* alleles decreased the amount of Mre11 bound at DSBs, with *tel1Δ* cells showing the strongest effect (Figure 24C). If the decrease in Mre11 association to DSBs caused by the *mre11-S499P* and *rad50-A78T* mutations were due to defective MRX–DNA interaction rather than to failure of Tel1 in promoting MRX persistence at DSBs, *tel1Δ mre11-S499P* and/or *tel1Δ rad50-A78T* cells would be expected to show a further decrease of the amount of MRX bound at DSBs compared to *tel1Δ* cells. However, the amount of Mre11 bound at DSBs in both *mre11-S499P tel1Δ* and *rad50-A78T tel1Δ* double mutants was similar to that of *tel1Δ* single mutant (Figure 24C), suggesting that the poor Mre11 persistence to DSBs in both *mre11-S499P* and *rad50-A78T* cells is a consequence of the decreased Tel1 association at DSBs.

Next, we analyzed the ability of $M^{S499P}RX$ and $MR^{A78T}X$ to interact with Tel1 by coimmunoprecipitation. When Tel1 was immunoprecipitated with anti-HA antibodies, a reduced amount of Mre11-S499P-Myc (Figure 24D) or Rad50-A78T-Myc (Figure 24E) could be detected in HA-tagged Tel1 immunoprecipitates compared to wild type Mre11-Myc and Rad50-Myc, respectively. Altogether, these data indicate that the *mre11-S499P* and *rad50-A78T* mutations reduce Tel1 association to DSBs by impairing MRX–Tel1 interaction.

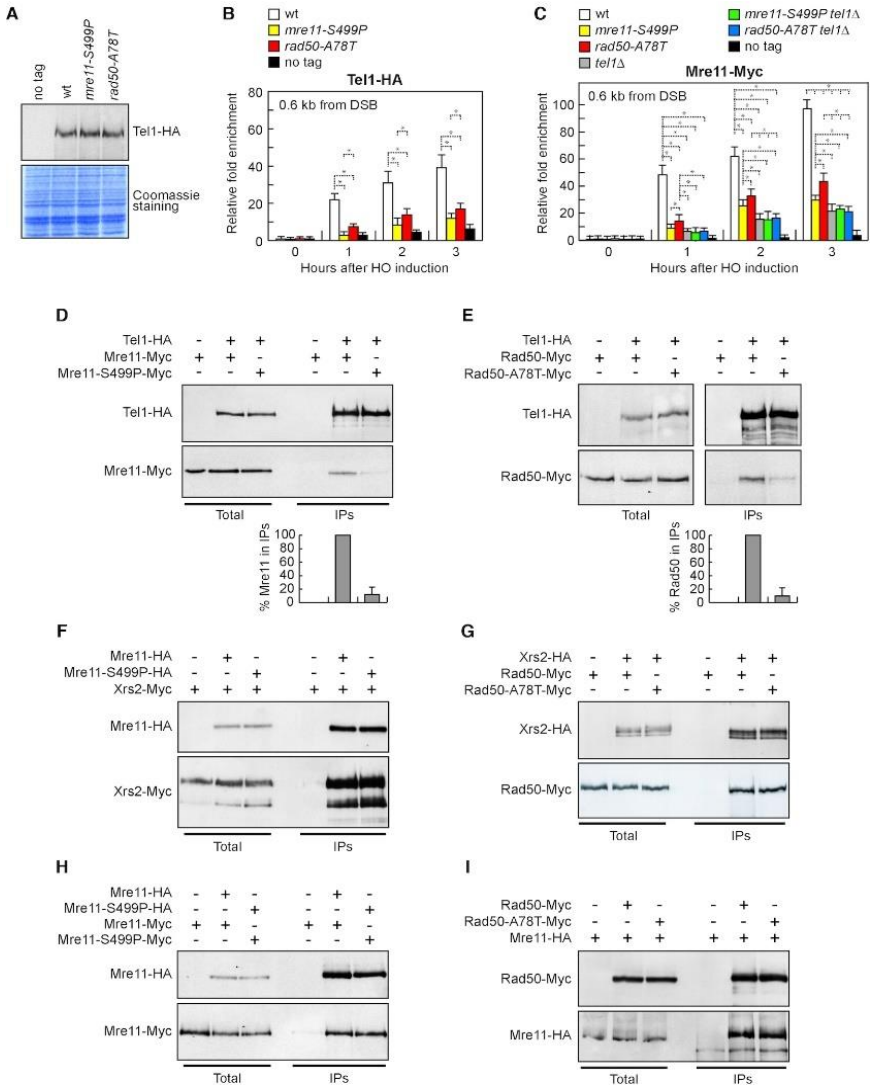

Figure 24 ***Tel1 association to DSBs and Tel1–MRX interactions.***
*(A) Western blot analysis with anti-HA antibodies of protein extracts prepared from exponentially growing cells. The same amounts of extracts were separated by SDS-PAGE and stained with Coomassie Blue as loading control. (B, C) ChIP analysis. Exponentially growing YEPR cell cultures were transferred to YEPRG at time zero. Relative fold enrichment of Tel1-HA (B) and Mre11-Myc (C) proteins at the indicated distances from the HO cleavage site was determined after ChIP and qPCR analysis. Plotted values are the mean values with error bars denoting S.D. (n = 3). *P < 0.05 (Student's t-test). (D, E) Protein extracts from exponentially growing cells that were treated with phleomycin (15 μg/ml) for 1 hour were analyzed by western blotting with anti-HA and anti-Myc antibodies either directly (total) or after immunoprecipitation (IPs) with anti-HA antibody. Graphs represent the amount of Mre11-S499P-Myc (D) and Rad50-A78T-Myc (E) in IPs relative to Mre11-Myc and Rad50-Myc, respectively, which were set up to 100%. Plotted values are the mean values with error bars denoting S.D. (n = 3). An immunoblot from one of these experiments is shown. (F–H) Protein extracts prepared from exponentially growing cells were analyzed by western blotting with anti-HA and anti-Myc antibodies either directly (Total) or after immunoprecipitation (IPs) with anti-HA antibody. (I) As in F-H, but after immunoprecipitation with anti-Myc antibody.*

The *mre11-S499P* mutation reduces Mre11–Rad50 interaction

MRX was shown to recruit Tel1 to DSBs through a direct interaction between Tel1 and Xrs2 [3], prompting us to test whether the defective MRX–Tel1 interaction in *mre11-S499P* and/or *rad50-A78T* cells was due to reduced ability of Xrs2 to interact with $M^{S499P}R$ or MR^{A78T}. However, similar amounts of Xrs2-Myc could be detected in immunoprecipitates of HA-tagged Mre11 and Mre11-S499P (Figure 24F). Furthermore, similar amounts of Rad50-Myc and Rad50-A78T-Myc could be detected in immunoprecipitates of Xrs2-HA (Figure 24G). Thus, the reduced MRX–Tel1 interaction in both *mre11-S499P* and *rad50-A78T* cells is not due to a poor Xrs2 ability to interact with $M^{S499P}R$ or MR^{A78T}.

Mre11-S499P turned out to be proficient also in Mre11 dimer formation. In fact, when Mre11 was immunoprecipitated with anti-HA antibodies from protein extracts of *MRE11-MYC/MRE11-HA* and *mre11-S499P-MYC/mre11-S499P-HA* diploid cells, the amount of Mre11-S499P-Myc detected by anti-Myc antibodies in immunoprecipitates of Mre11-S499P-HA was similar to that of wild type Mre11-Myc detected in immunoprecipitates of Mre11-HA (Figure 24H). Furthermore, the *rad50-A78T* mutation does not impair the ability of Rad50 to interact with Mre11, as similar amount of Mre11-HA could be detected in immunoprecipitates of Rad50-Myc and Rad50-A78T-Myc (Figure 24I).

The structure of the Rad50 binding domain (RDB) is still unknown in eukaryotic MR complexes, although the only structure available from *C. thermophilum* [138] suggests the presence of a helix-loop-helix motif spanning three hydrophobic helices clanging to Rad50 coiled coil region and stabilized by a fourth helix. We have previously proposed a computational model for ScMre11 Rad50 RDB [212], where the helix-loop-helix motif (H5 and H6 in Figure 25A and B) is flanked by an additional helix (H7 in Figure 25A and B) that contacts the globular domain of Rad50. The S499 residue is localized on the flexible loop leading to the fourth helix (H8 in Figure 25A and B), which proved to be relevant for the stability of the RBD [212]. The Ser499 substitution with the more rigid proline residue would impinge on this connector flexibility that is required to accommodate the necessary mobility of the RBD-Rad50 interface during the large-scale conformational changes occurring upon ATP hydrolysis by Rad50. This analysis raises the possibility that the *mre11-S499P* mutation could affect Mre11–Rad50 interaction. We directly tested this prediction by immunoprecipitating Rad50 with anti-HA antibodies from protein extracts of *MRE11-MYC RAD50-HA* and *mre11-S499P-MYC RAD50-HA* cells. A reduced amount of Mre11-S499P-Myc compared to Mre11-Myc could be detected in immunoprecipitates of HA-tagged Rad50 (Figure 25C), indicating that the S499P amino acid substitution affects Mre11–Rad50 interaction. In any case, the amount of Rad50 bound to Mre11 appears to be sufficient to support MRX function in DSB

repair, as *mre11-S499P* cells did not show major defects in DSB resection and NHEJ.

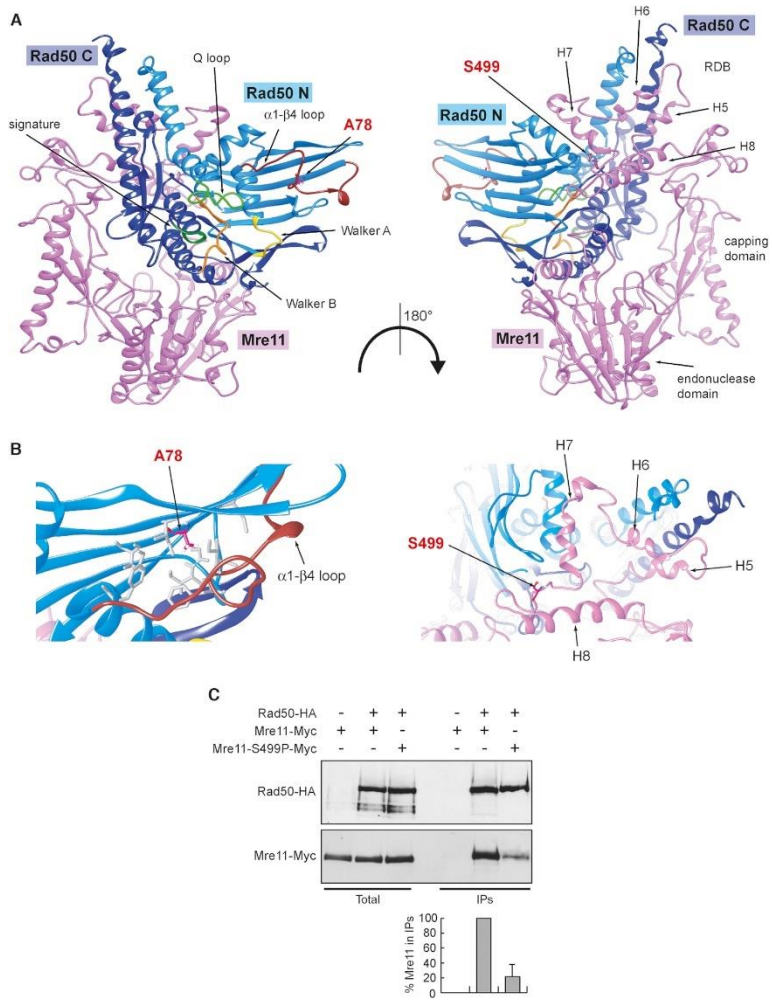

Figure 25 ***The mre11-S499P mutation is localized at the Mre11–Rad50 interface and reduces Mre11–Rad50 interaction****.*
(A) Structural prediction of S. cerevisiae Mre11–Rad50 heterodimer, obtained as previously described (38), showing the localization of S499 residue in the Rad50-binding domain (RBD) of Mre11 and of A78 residue in the N-terminal of Rad50. Pink, Mre11. Light blue, N-terminal lobe of Rad50 (Rad50 N). Dark blue, C-terminal lobe of Rad50 (Rad50 C). (B) Detailed view of the molecular surroundings of the residues affected by the mutations. The hydrophobic residues surrounding A78 in Rad50 are shown as gray sticks. (C) Mre11–Rad50 interaction. Protein extracts prepared from exponentially growing cells were analyzed by western blotting with anti-HA and anti-Myc antibodies either directly (Total) or after immunoprecipitation (IPs) with anti-HA antibody. Graph represents the amount of Mre11-S499P-Myc relative to Mre11-Myc that was set up to 100%. Plotted values are the mean values with error bars denoting S.D. (n = 3). An immunoblot from one of these experiments is shown.

Structural insights of ATP- and ADP-bound MR subcomplex by molecular dynamics simulations

In vitro activation of human ATM by MRN requires ATP but not Mre11 nuclease activity [221], suggesting that MRX/MRN activates Tel1/ATM when it is present in the ATP-bound state. To investigate further this hypothesis, we analyzed the conformations of the MR subcomplex bound to either ATP (MR-ATP) or ADP (MR-ADP) by molecular dynamics (MD). Ten replicas of 200 ns were carried out on the two aforementioned systems in order to obtain a total 2 μs trajectory for each set of simulations. All replicas immediately reached a stable value of backbone root-mean-square deviation (RMSD), thus ensuring that the calculated parameters reflect the real behavior of the investigated systems (Supplementary Figure S1A and B). Principal Component Analysis (PCA) was used to identify globally correlated motions from MD trajectories. PCA analysis was performed on the protein backbone and ATP/ADP atoms trajectories to inspect the functional motions collected during the simulations. This method calculates eigenvectors (PC) and eigenvalues, which describe the direction and the magnitude of concerted motions, respectively. The first two eigenvectors (PC1 and PC2) calculated from the MD trajectories account for most of the total variance (Supplementary Figure S2, top). Interestingly, while they reveal only minor motions for the MR-ATP system (Supplementary Figure S3A), they show the separation of two Rad50 subunits from each other and the disengagement of Mre11 endonuclease site from Rad50 in the MR-ADP system (Supplementary Figure S3B). These two movements combined together describe the initial steps of MR complex opening, an event that occurs after ATP hydrolysis by Rad50 at the resection onset.

Movements along PC1 and PC2 were used as reaction coordinates to build 3D histograms of the percentage of existence in each molecular conformation, from which free energy landscape (FEL) graphs were calculated (Figure 26A and B). All FELs show a good overlap among replicas, which highlights that the transitions

among all basins are predicted to occur at the simulation temperature (300 K) (Supplementary Figure S4, top). FELs allow the identification of free energy basins, which correspond to the energetically favored protein conformations. Since the projection of a multidimensional trajectory in a two-dimensional space (PC1 and PC2) involves a large reduction in dimensionality, FEL plots might show only a partial picture of the protein conformational scenario. For this reason, we confirmed FEL results with cluster analysis derived from the concatenated trajectory, in order to retrieve all conformational variance stored in the entire simulation that allows estimating which conformations are more favorable for each system with respect to energy content. The results of the cluster analysis were in agreement with the FELs (data not shown).

All basins, progressively numbered with roman numbers from the lowest to the highest energy, in MR-ATP FELs (Figure 26A) correspond to MR conformations in which the two Rad50 subunits are tightly bound to each other and bury the ATP molecules in their interface (Figure 26C) (Supplementary Dataset S1). This is consistent with ATP requirement for the MR complex to assemble in a 'closed' conformation [174], [176], [196], [222]. By contrast, basins in the MR-ADP FELs (Figure 26B) correspond to different MR conformations, suggesting a higher flexibility of the complex. In particular, the first basin (I) represents MR complexes in which the two Rad50 subunits have drifted apart (Figure 26D) (Supplementary Dataset S2), whereas the second basin (II) represents a conformation where, although the two Rad50 subunits are closer than in basin I, they are not tightly bound as in MR-ATP (Supplementary Figure S5A), suggesting that the Rad50 dimer interface in MR-ADP is different from that in MR-ATP complex. The third and fourth basins (III and IV) describe a transition state between the previous conformations (Supplementary Figure S5B for basin III).

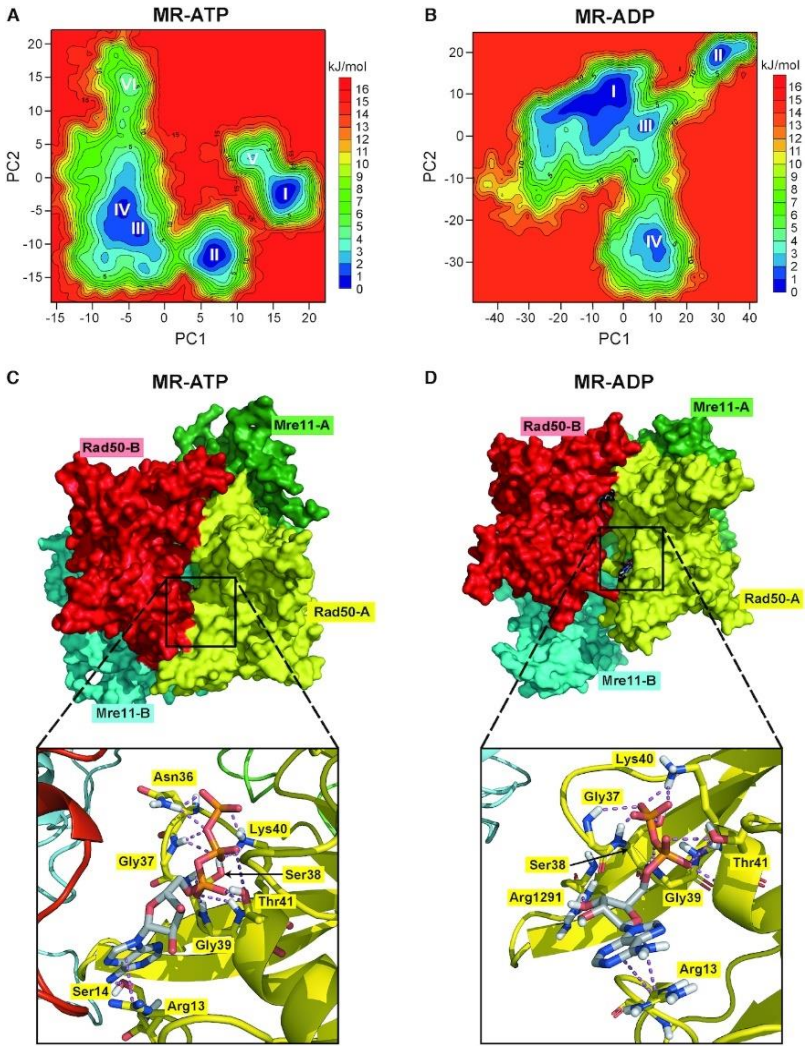

Figure 26 ***MD simulations to identify stable MR-ATP and MR-ADP conformations****.*
(A, B) FELs were evaluated for MR-ATP (A) and MR-ADP (B). Analyses have been carried out using the projection of concatenated trajectories along the first and the second principal components (PC1 and PC2) as reaction coordinates. Basins are progressively numbered according to their energetic stability. Energy values are reported in kJ/mol. (C, D) The most energetically favoured conformations shown are derived from the FELs and cluster analysis for MR-ATP (C) (corresponding to basin I in panel A) and MR-ADP (D) (corresponding to basin I in panel B). Rad50 subunits are in red and yellow; Mre11 subunits are in cyan and green. Close-up views of one of the nucleotide binding sites are shown at the bottom. Nucleotides and residues interacting with ATP/ADP are shown as sticks; each residue is colored according to the chain it belongs to.

These motions can be monitored by measuring the distance between the centers of mass (COM) of the different MR complex subunits (Figure 27A) (Mre11 and Rad50 monomers are indicated as A and B). In particular, we monitored the distances over the interfaces between each Mre11–Rad50 dimer (Mre11-A chain A versus Rad50-A chain D in Figure 27B; Mre11-B chain B versus Rad50-B chain F in Figure 27C) and those between Rad50-Rad50 dimers, corresponding to the two nucleotide binding sites (ATP binding site 1, between Rad50-A chain C and Rad50-B chain F, in Figure 27D; ATP binding site 2, between Rad50-A chain D and Rad50-B chain E, in Figure 27E). MR bound to ADP undergoes dissociation of Mre11-B chain B from Rad50-B chain F (Figure 27C) and opening of the ATP binding site 1 (Figure 27D). By contrast, the ATP binding site 2 is permanently less tight in the MR-ADP compared to the MR-ATP system (Figure 27E), further suggesting that the two Rad50 subunits have lower affinity for each other in presence of ADP than in the presence of ATP. The observation of an asymmetric opening of Rad50 dimer was expected, due to the ATP-driven cooperativity and allosteric control typical of ABC-ATPases superfamily to which Rad50 belongs with [173]. The cooperativity implies that the opening of the two ATP binding sites does not occur simultaneously, but the opening of the first site induces the opening of the second one. However, changes in the quaternary structure and/or allosteric transitions are very slow and occur at ms/s time scale, still unachievable in MD simulations for large molecular systems [223], [224].

The observed variations of COM distances represent a genuine interchain movement and it is not due to an internal rearrangement of the center of gravity of subunits. In fact, the overall folding of each subunit is not changing significantly over the simulation, as demonstrated by the lack of variation in the radius of gyration (R_g) (Supplementary Figure S6).

Altogether, these analyses indicate that the MR subcomplex, in the presence of ATP, lingers in a tightly closed conformation with the two ATP molecules deeply buried at the interface between the Rad50 subunits (Supplementary Movie S1). By contrast, the presence of ADP leads to the loosening of the Rad50 homodimer,

which exposes the ADP molecules, and to a destabilization of Mre11–Rad50 association (Supplementary Movie S2).

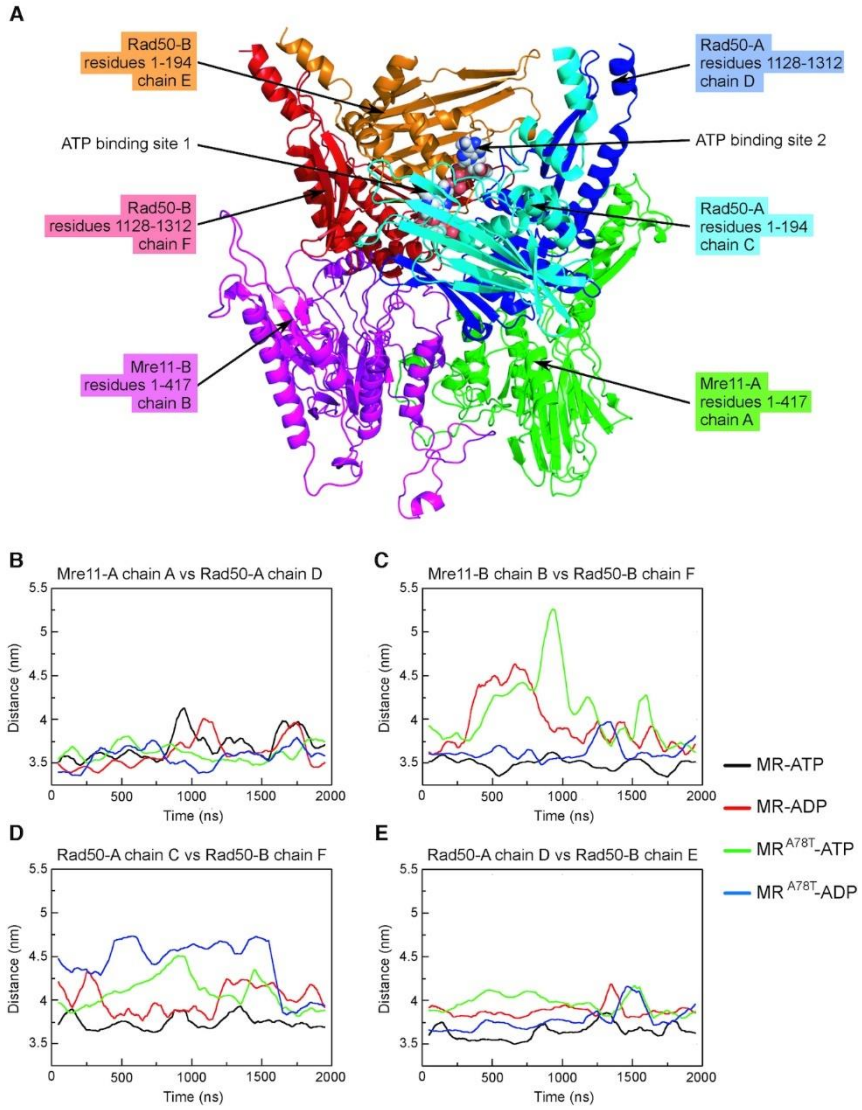

Figure 27 ***Distance between the centers of mass (COM) of the MR complex subunits***.
(A) Labeling of the different chains in the model used for simulations. Mre11 and Rad50 monomers are indicated as A and B. Mre11-A and Mre11-B monomers are in green and purple, respectively; N-terminal and C-terminal parts of Rad50-A monomer are in light blue and dark blue, respectively; N-terminal and C-terminal parts of Rad50-B monomer are in orange and red, respectively. (B–E) Graphs show distances among centers of mass of the indicated chains as monitored along the concatenated trajectory of the MD simulations.

Structural studies describing the conformational transitions occurring on thermophilic Archaean Rad50 upon binding to ATP analogues showed that the main difference is a rotation of the C-terminal lobe with respect to the N-terminal lobe (Figure 28A and B) [174], [196], which reduces the affinity of Rad50 subunits for each other [174]. The Q loop release from Mg^{2+} coordination upon ATP hydrolysis allows the switch in the hinge helix and the release of the region spanning from residue 50 to 65, named α1-β4 loop; interestingly, the same movements have been observed by NMR also in the *P. furiosus* Rad50-R805E mutant protein [225]. Indeed, we found that the α1-β4 loop shows higher mobility in MR-ADP than in MR-ATP simulations (Supplementary Figure S7A). All of these events can be visualized when the most stable conformations of Rad50 subunit along the MD simulations for MR-ATP and MR-ADP systems are superimposed by structural alignment on the N-terminal lobe (Figure 28C), which shows that the Rad50 subunit undergoes the typical conformation changes observed in MR crystals in the presence or not of ATP analogues (compare Figure 28B and C). Moreover, our results suggest that ADP presence loosens not only the association of Rad50 monomers, allowing the initial opening of Rad50 dimer, but also the Rad50–Mre11 association, both events being required to open the MR complex for its engagement in DSB resection.

The A78T mutation destabilizes the MR-ATP conformation

The A78 residue is located within a hydrophobic region of Rad50, facing the α1-β4 loop residues (Figure 28B). To investigate the structural impact of the A78T mutation, ATP- and ADP-bound MR^{A78T} complexes have been subjected to MD analyses. Again, ten replicas of 200 ns immediately reached a stable value of backbone root-mean-square deviation (RMSD) (Supplementary Figure S1C and D). As for MR simulations, the first two eigenvectors (PC1 and PC2) calculated from the MD trajectories account for most of the total variance (Supplementary Figure S2, bottom) and describe the initial steps of MR^{A78T} complex opening (Supplementary Figure S3C and D).

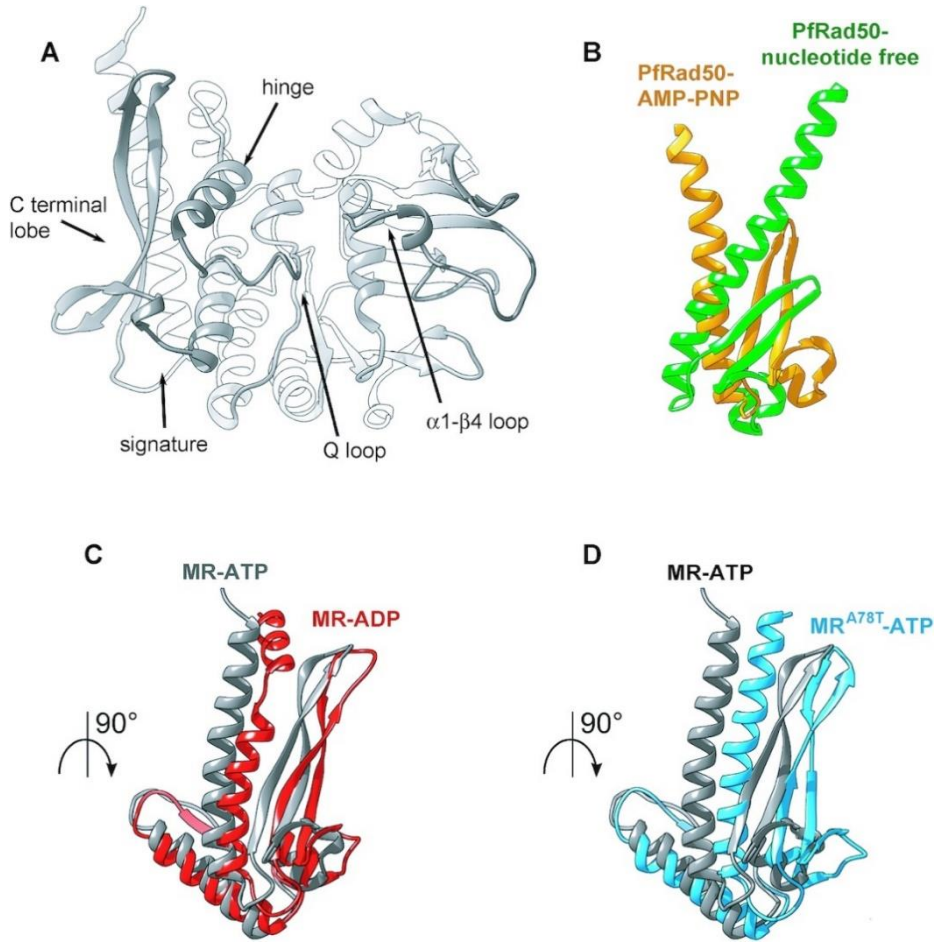

Figure 28 ***The rad50-A78T mutation induces similar conformational changes in Rad50 as ATP hydrolysis****.*
(A) Cartoon of the centroid structures of one Rad50 subunit (chains C and D) from the absolute minimum corresponding clusters from MR-ATP showing the main features involved in the conformational change upon ADP versus ATP binding. (B) View of the C-terminal lobes of the structure of P. furiosus Rad50 bound to AMP-PNP (PDB:3qku; orange) superimposed to nucleotide-free Rad50 (PDB:3qks; green). (C, D) View of the C-terminal lobes of centroid structures of the energetic absolute minimum of Rad50 subunit from MR-ATP MD simulations (gray) superimposed by structural alignment to the N-terminal region of MR-ADP (C) and MRA78T-ATP (D) energetically favorite Rad50 structures

Movements along PC1 and PC2 were used as reaction coordinates to build 3D histograms of the percentage of existence in each molecular conformation, from which FELs graphs were calculated (Figure 29A and B). Again, all FELs show a good overlap among replicas (Supplementary Figure S4, bottom) and the energy

basins, identified in the FELs and progressively numbered from the lowest to the highest, were consistent with the results of cluster analysis (data not shown).

The A78T substitution in Rad50 completely changes the behavior of the MR subcomplex in the presence of ATP (Supplementary Movie S3). In fact, the most stable structures for MR^{A78T}-ATP show a less tight conformation compared to MR-ATP, i.e. one of the nucleotide binding pockets is accessible to the solvent in the most stable conformation (basin I in Supplementary Figure S5C), while both are exposed in all the other energetically similar conformations (basins II and III) (Figure 29C for basin II) (Supplementary Dataset S3). Moreover, the structure associated with basin V also shows the disengagement of Rad50 from the endonucleolytic site of Mre11 (Supplementary Figure S5D). The open conformation is stabilized further in MR^{A78T}-ADP, as shown by the higher existence probability of basin I (Figure 29B and D) (Supplementary Movie S4) (Supplementary Dataset S4). The other structures are less stable and have low probability of being sampled, suggesting they are not relevant.

We found that the increment in COM distances in MR^{A78T} is accentuated compared to that of wild type MR (Figure 29). In fact, the variations that were characteristic of the MR-ADP system (see in particular Figure 29C and D) can be detected with enhanced intensity in the MR^{A78T} system, albeit in the presence of ATP. Furthermore, MR^{A78T}-ADP shows the maximum distance between the two Rad50 subunits (Figure 29D). These findings indicate that the A78T substitution in Rad50 causes the MR complex to undergo conformational motions similar to those observed for wild type MR-ADP, even when MR^{A78T} is bound to ATP.

All of these events can be visualized when the most stable conformations of Rad50 subunit along the MD simulations for MR-ATP and MR^{A78T}-ATP systems are superimposed (Figure 29D). The conformational changes occurring in the *P. furiosus* Rad50 protein upon binding to ATP [174], described as a rotation of the C-terminal lobe with respect to the N-terminal lobe (Figure 29B), are also observed when the most energetically stable conformation of wild type Rad50 bound to ATP is superimposed to Rad50-A78T, notwithstanding the presence of ATP (Figure

29D), with the mutant protein showing a more dramatic effect on the hinge helix switch than the Rad50-ADP itself.

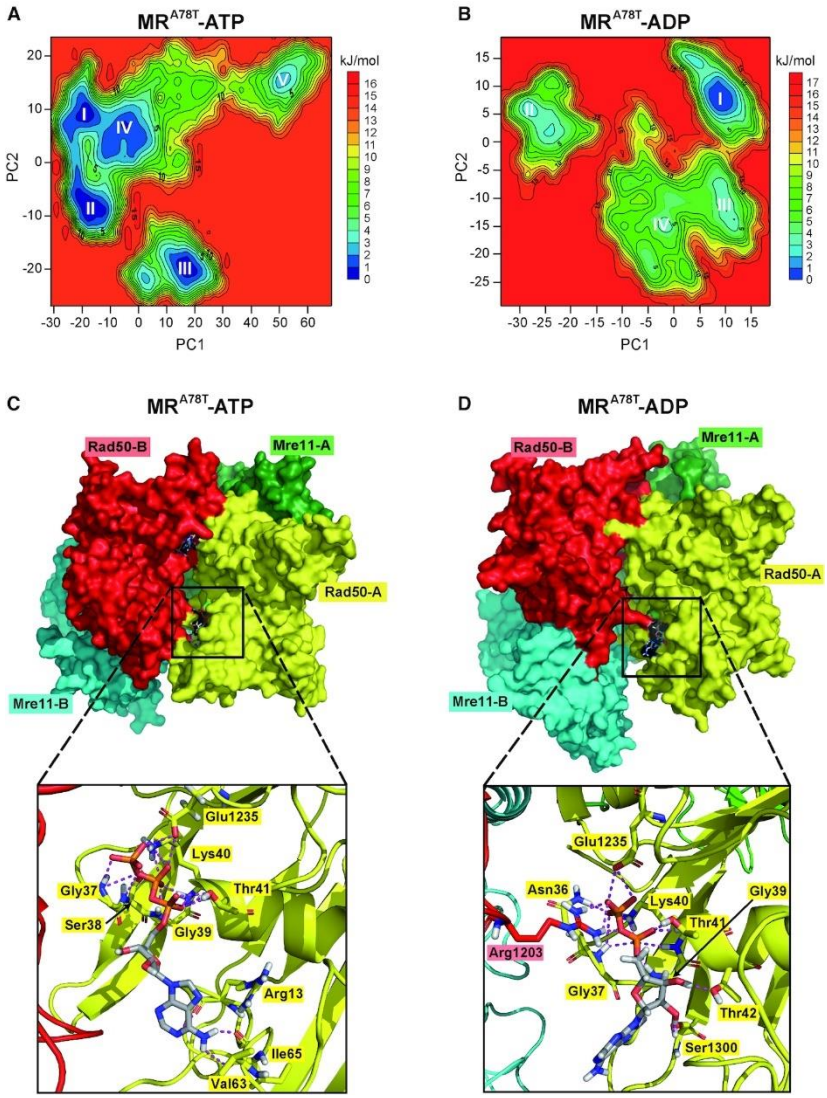

Figure 29 ***MD simulations to identify stable MRA78T-ATP and MRA78T-ADP conformations****. (A, B) FELs were evaluated for MRA78T-ATP (A) and MRA78T-ADP (B). Analyses have been carried out using the projection of concatenated trajectories along the first and the second principal components (PC1 and PC2) as reaction coordinates. Basins are progressively numbered according to their energetic stability. Energy values are reported in kJ/mol. (C, D) The most energetically favored conformations shown are derived from the FELs and cluster analysis for MRA78T-ATP (C) (corresponding to basin II in panel A), and MRA78T-ADP (D) (corresponding to basin I in panel B). Rad50 subunits are in red and yellow; Mre11 subunits are in cyan and green. Close-up views of the nucleotide binding site are shown at the bottom. Nucleotides and residues interacting with ATP/ADP are shown as sticks; each residue is colored according to the chain it belongs to.*

As aforementioned, comparison between Rad50 Root-Mean-Square Fluctuation (RMSF) profiles of MR-ATP and MR-ADP complexes shows an increased mobility within the region spanning from residue 50 to 65 (α1–β4 loop) (Supplementary Figure S7A). The same is observed for Rad50-A78T RMSF profiles in MR^{A78T}-ATP MD simulations (Supplementary Figure S7B). Interestingly, as already described, the A78 residue is opposite to the α1–β4 loop residues and is located within a hydrophobic region of Rad50 (Figure 29B). Hence, its substitution with the polar threonine residue can easily destabilize this hydrophobic region, thus increasing its mobility. This event would be sufficient to induce conformational rearrangements in MR^{A78T} bound to ATP similar to those observed when wild type MR is bound to ADP. Consistent with this hypothesis, the high mobility of the α1-β4 loop has been previously described as one of the events in the conformational transition occurring in Rad50 upon ATP hydrolysis [174], [196], [225].

Cell Reports
Submitted October 2020,
Under revision

Sae2 and Rif2 regulate MRX endonuclease activity at DNA double-strand breaks in opposite manners

Antonio Marsella[1], Elisa Gobbini[1], Corinne Cassani[1], Renata Tisi[1], Elda Cannavo[2], Giordano Reginato[2,3], Petr Cejka[2,3] and Maria Pia Longhese[1,*]

[1]Dipartimento di Biotecnologie e Bioscienze, Università degli Studi di Milano-Bicocca, Milano, 20126, Italy
[2]Institute for Research in Biomedicine, Faculty of Biomedical Sciences, Università della Svizzera italiana (USI), Bellinzona, Switzerland.
[3]Department of Biology, Institute of Biochemistry, Eidgenössische Technische Hochschule (ETH) Zürich, Switzerland.

*Correspondence: mariapia.longhese@unimib.it (M.P.L.)

The lack of Rif2 suppresses the DNA damage hypersensitivity of *sae2Δ* cells

Phosphorylated Sae2 stimulates the endonuclease activity of Mre11 within the MRX complex [28]. Although Sae2 does not appear to influence the overall Rad50 ATP hydrolysis rate, stimulation of Mre11 nuclease by Sae2 requires ATP hydrolysis by Rad50, suggesting that Sae2 helps coupling ATP hydrolysis by Rad50 with productive endonucleolytic DNA cleavage by Mre11 [226].

As Rif2 has been shown to stimulate the Rad50 ATPase activity [114], [227], to better understand the interplay between Sae2 and Rif2 in MRX regulation, we analyzed the effect of deleting *RIF2* in *sae2Δ* cells. *sae2*Δ *rif2Δ* double mutant cells were more resistant to camptothecin (CPT) and methyl methansulphonate (MMS) compared to *sae2Δ* cells (Figure 30A), indicating that the lack of Rif2 partially suppresses the DNA damage sensitivity of *sae2*Δ cells.

The Sae2-induced Mre11-Rad50 endonuclease activity not only incises the 5'-terminated strands at both DNA ends, but it also opens DNA hairpin structures [189], [228]. Inverted Alu elements inserted in the *LYS2* gene on chromosome II stimulate ectopic recombination with a truncated *lys2* copy (*lys2-Δ5'*) located on chromosome III to generate Lys+ prototrophs (Figure 30B), and this recombination is largely dependent on Mre11 endonuclease and Sae2 [228]. The inverted Alu repeats are thought to extrude to form a hairpin or cruciform structure that is cleaved by an unknown nuclease to form a hairpin-capped DNA end, or to form a foldback structure following resection of a nearby DSB, which is then cleaved by MRX-Sae2 and subsequently repaired by HR to generate Lys^+ cells [228]. *RIF2* deletion failed to suppress the hairpin resolution defect conferred by either *sae2*Δ or *mre11-H125N* (*mre11-nd*) cells, which are specifically defective in Mre11 nuclease activity (Figure 30C), indicating that *RIF2* deletion does not suppress *sae2*Δ DNA damage sensitivity by activating the Mre11 nuclease independently of Sae2 (Figure 30C). Consistent with this conclusion, *RIF2* deletion failed to suppress the DNA damage hypersensitivity of *mre11-nd* cells (Figure 30D).

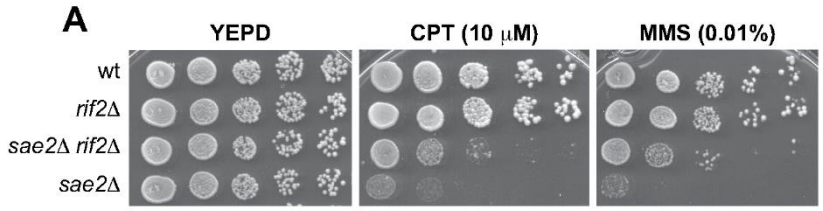

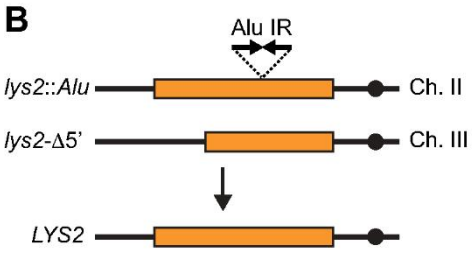

C

	Recombination rate (10^{-7})
wt	1,680 (±180)
rif2Δ	1,540 (±223)
sae2Δ	17 (±7)
mre11-nd	21 (±8)
sae2Δ rif2Δ	23 (±8)
mre11-nd rif2Δ	19 (±6)

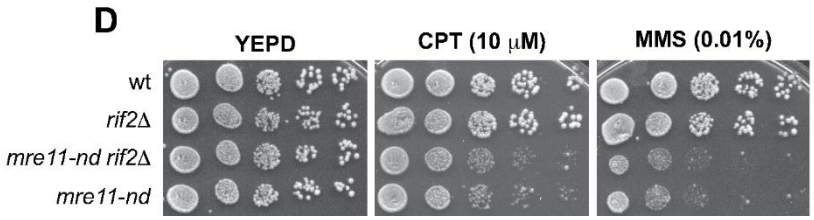

Figure 30 ***The lack of Rif2 partially restores DNA damage resistance of sae2Δ cells by decreasing checkpoint activation****.*
(A, D) Exponentially growing cultures were serially diluted (1:10) and each dilution was spotted out onto YEPD plates with or without CPT or MMS. (B) Schematic representation of the lys2-AluIR and lys2-Δ5' ectopic recombination reporter. (C) Recombination frequency of strains with the lys2-AluIR and lys2-Δ5' ectopic recombination reporter system. The rate of Lys+ recombinants was derived from the median recombination frequency. The reported values are the mean values of 3 independent experiments with s.d. indicated in brackets. of strains with the lys2-AluIR and lys2-Δ5' ectopic recombination reporter system. The rate of Lys+ recombinants was derived from the median recombination frequency. The reported values are the mean values of 3 independent experiments with s.d. indicated in brackets.

The lack of Rif2 dampens checkpoint signaling in *sae2Δ* cells by decreasing MRX association to DSBs

Previous studies demonstrated that the increased DNA damage sensitivity of *sae2*Δ cells is in part due to increased retention of MRX, Tel1 and Rad9 at DSBs, which leads to a persistent Rad53 phosphorylation and activation [194], [193], [192]. Thus, we asked whether the *RIF2* deletion can partially suppress the DNA damage sensitivity of *sae2*Δ cells by decreasing checkpoint activation. A checkpoint response triggered by a single unrepairable DSB can be eventually turned off, allowing cells to resume cell cycle progression through a process that is called adaptation [192]–[194]. The increased Tel1-mediated Rad53 activation in *sae2Δ* cells prevents cells from adapting to an unrepaired DSB [192], prompting us to investigate the effect of *RIF2* deletion on the adaptation defect of *sae2Δ* cells.

To measure adaptation to a checkpoint response triggered by an unrepaired DSB, we used a haploid strain carrying the *HO* gene under the control of a galactose-inducible promoter [218]b. In this strain, induction of HO by galactose addition leads to the generation at the *MAT* locus of a single DSB that cannot be repaired by HR due to the lack of the homologous donor loci *HML* and *HMR*. *HO* expression was induced by transferring to galactose wild type, *sae2Δ*, *rif2Δ* and *sae2Δ rif2Δ* cells exponentially growing in raffinose. Checkpoint activation was monitored by following Rad53 phosphorylation, which is required for Rad53 activation and is detectable as a decrease of its electrophoretic mobility. When galactose was added to exponentially growing cells, Rad53 phosphorylation was detectable about 3-4 h after HO induction in wild type, *rif2*Δ, *sae2*Δ and *sae2*Δ *rif2*Δ cells (Figure 31B). Furthermore, when cells arrested in G1 with α-factor were spotted on galactose-containing plates to induce HO, all the above cell cultures accumulated as large budded cells within 4 h from HO induction caused by checkpoint activation (Figure 31B). Then, Rad53 decreased in wild-type cells and *rif2*Δ cells 12-14 h after galactose addition, when cells resumed cell cycle progression, whereas it persisted longer in *sae2*Δ cells that remained arrested as large budded cells for at least 24 h (Figure 31D). Interestingly, the amount of phosphorylated Rad53 decreased 12-14

h after galactose addition in *sae2*Δ *rif2*Δ cells (Figure 31A), which formed microcolonies with more than two cells with wild type kinetics (Figure 31B). Thus, we can conclude that *RIF2* deletion suppresses the adaptation defect of *sae2*Δ cells by decreasing Tel1-mediated checkpoint activation.

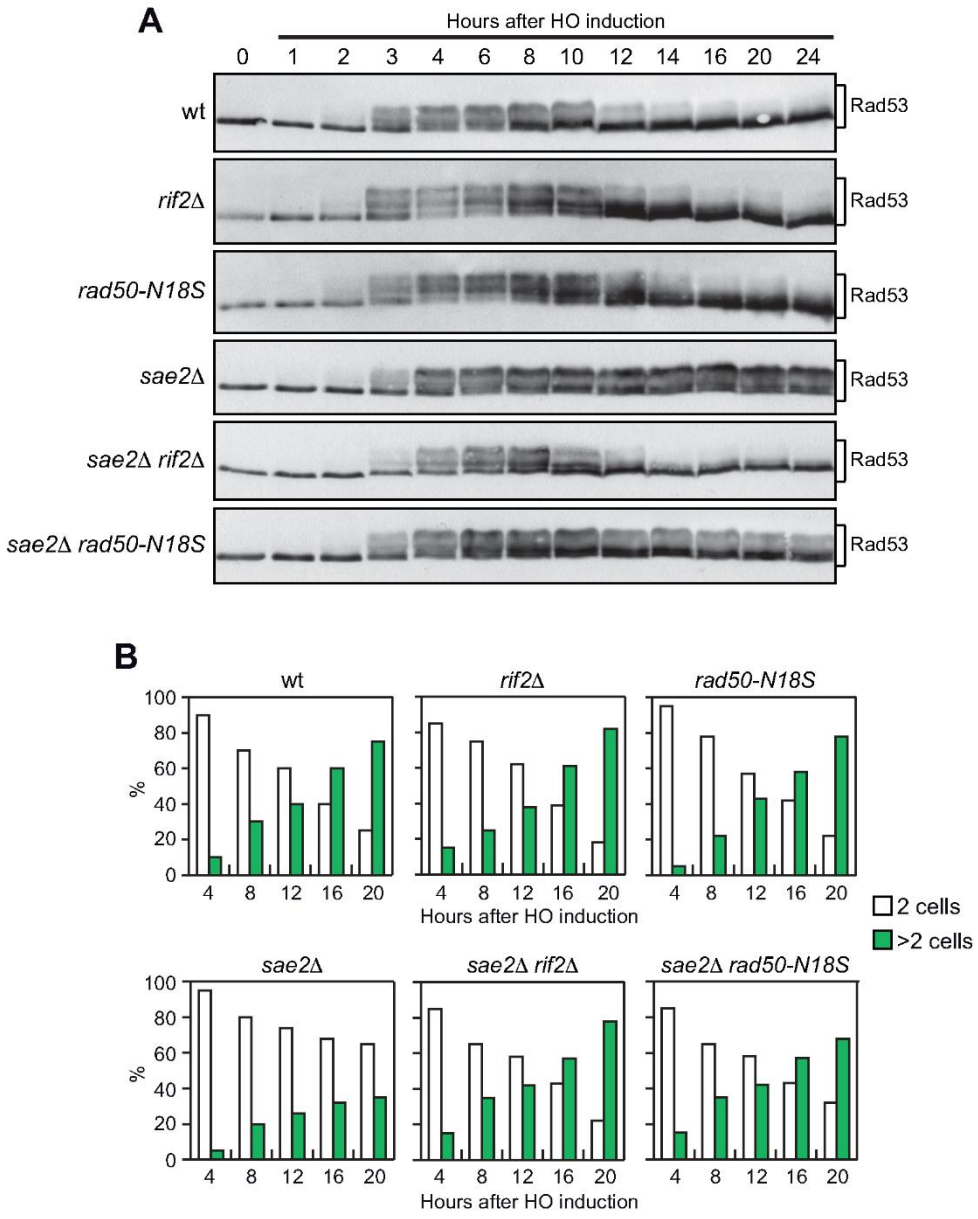

Figure 31 ***The rif2△ and rad50-N18S alleles suppress the adaptation defect of sae2△ cells by decreasing checkpoint persistence****.*
(A) Rad53 phosphorylation during adaptation. Exponentially growing YEPR cultures were transferred to YEPRG (time zero), followed by western blot analysis with anti-Rad53 antibodies. (B) Adaptation assay. YEPR G1-arrested cell cultures were plated on galactose-containing plates (time zero). At the indicated time points, 200 cells for each strain were analyzed to determine the frequency of large budded cells (two cells) and of cells forming microcolonies of more than two cells.

MRX is required to recruit and activate Tel1, which in turn transduces the checkpoint signals to Rad53 through the Rad9 protein [159], [160], [194], [229]. Previous works have established that *mre11* alleles that reduce MRX binding to DSBs restore DNA damage resistance of *sae2*Δ cells by decreasing Tel1-dependent Rad53 activation [42], [197], [212]. Thus, we measured Mre11, Tel1 and Rad9 association at the HO-induced DSB by chromatin immunoprecipitation (ChIP) and quantitative PCR (qPCR). The lack of Rif2 decreased the amount of Mre11, Tel1 and Rad9 bound to DSBs in *sae2*Δ cells (Figure 32A), thus explaining the diminished Rad53 activation in *sae2Δ rif2Δ* cells compared to *sae2*Δ cells. The decreased Mre11 association at DSBs in *sae2Δ rif2Δ* cells compared to *sae2*Δ cells was not due to a diminished Mre11 levels, as all the mutants contained similar amount of Mre11 (Figure 32B). This finding indicates that Rif2 is responsible for the stabilization of the MRX complex at DSBs in *sae2Δ* cells, which in turn leads to unscheduled checkpoint activation.

The increased MRX retention at DSBs in *sae2Δ* cells has been proposed to be due to defective MRX nuclease, as the amount of the nuclease defective $M^{H125N}RX$ complex bound at DSBs is also increased compared to wild type MRX [193], [195]. To assess whether MRX stabilization at DSBs by Rif2 is specific for *sae2Δ* cells, we asked whether *RIF2* deletion decreases the association to DSBs also of the nuclease defective Mre11-H125N mutant variant. While Mre11 association at the HO-induced DSB was increased in *mre11-nd* cells compared to wild type cells, *mre11-nd rif2Δ* cells decreased Mre11 binding to the DSB to wild type levels (Figure 32C). Altogether, these finding indicates that Rif2 is responsible for the increased retention at DSBs of MRX that is nuclease defective either because is catalytically inactive or because of the lack of Sae2.

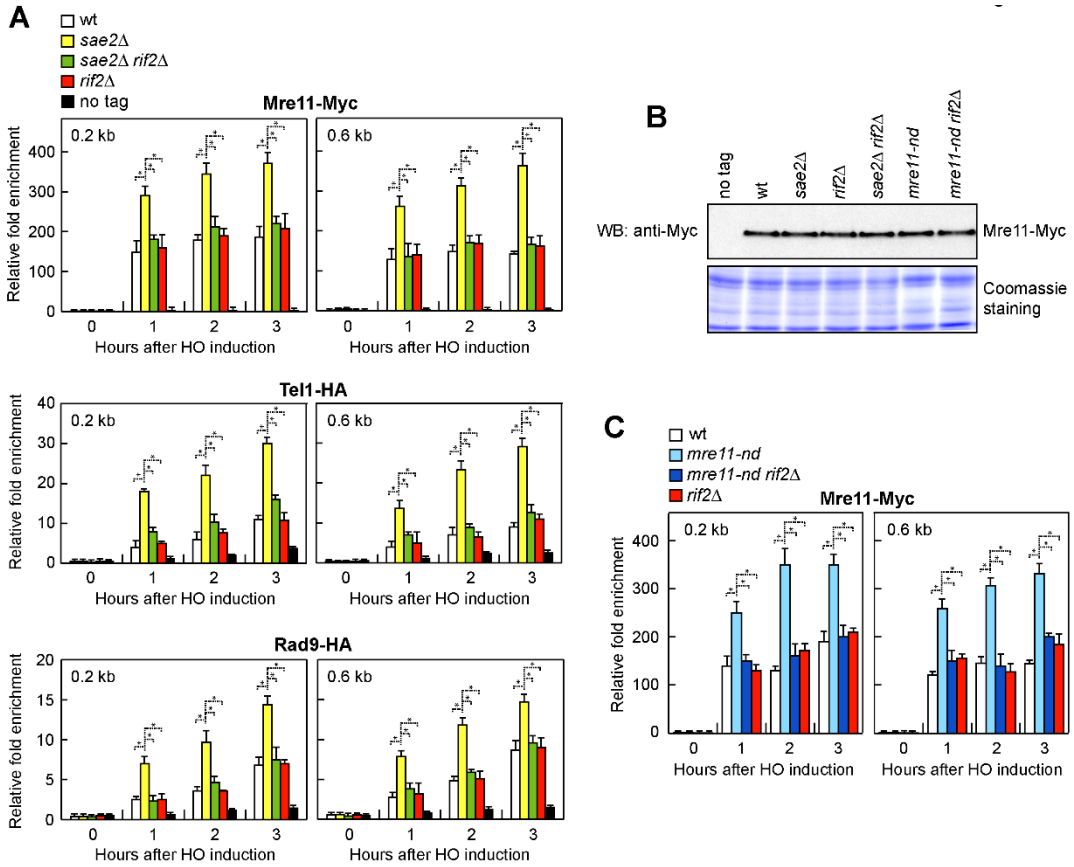

Figure 32 ***The lack of Rif2 decreases MRX abundance at DSBs in both sae2Δ and mre11-nd cells.***
*(A) ChIP and qPCR. Exponentially growing YEPR cell cultures were transferred to YEPRG to induce HO expression, followed by ChIP analysis of the recruitment of the indicated proteins at the indicated distance from the HO-cut site. In all diagrams, ChIP signals were normalized for each time point to the corresponding input signal. The mean values of three independent experiments are represented with error bars denoting s.d. *p<0.005 (Student's t-test).*
(B) Western blot with anti-Myc antibodies of extracts used for the ChIP analysis shown in (A). The same amount of protein extracts was separated on a SDS-PAGE and stained with Coomassie Blue as loading control.
*(C) ChIP and qPCR. Exponentially growing YEPR cell cultures were transferred to YEPRG to induce HO expression, followed by ChIP analysis of the recruitment of Mre11-Myc as described in panel (A). The mean values of three independent experiments are represented with error bars denoting s.d. *p<0.005 (Student's t-test).*

Rad50-N18S mimics *RIF2* deletion with respect to *sae2Δ* suppression and checkpoint inhibition

The MR complex was shown to efficiently bind dsDNA in presence of ATP-bound Rad50, which generates a groove that can host dsDNA [176], [175], [222], [138]. The finding that Rif2 increases the ATPase activity by Rad50 suggests that Rif2 can regulate MRX persistence at DSBs by acting on Rad50. Thus, to better understand the interplay between Rif2 and Rad50, we searched for *rad50* mutants that are insensitive to Rif2 inhibition. As *RIF2* deletion suppresses the DNA damage sensitivity of *sae2Δ* cells, we screened for *rad50* alleles that were capable to restore DNA damage resistance of *sae2Δ* cells. *RAD50* gene was amplified by low-fidelity PCR, followed by transformation with the linear *RAD50* PCR products into *sae2Δ* cells in order to replace the corresponding *RAD50* wild type sequence with the mutagenized DNA fragments. Transformants were then screened for high viability in the presence of CPT compared to *sae2Δ* cells. This analysis allowed us to identify the *rad50-N18S* mutation, causing the replacement of the Rad50 Arg18 residue with Ser. As shown in Figure 33A, *rad50-N18S* partially suppressed the sensitivity of *sae2Δ* cells not only to CPT, but also to MMS.

The *rad50-N18S* and *rif2Δ* alleles suppressed the DNA damage sensitivity of *sae2Δ* cells by altering the same pathway. In support, *sae2Δ rif2Δ rad50-N18S* triple mutant cells were resistant to DNA damaging agents as *sae2Δ rif2Δ* double mutant cells (Figure 33A). The pathway affected by *rif2Δ* and *rad50-N18S* alleles is different from that altered by the Ku complex, whose removal has been shown to suppress the CPT sensitivity of *sae2*Δ cells by increasing Exo1-mediated resection [47], [85], [86]. In fact, *sae2Δ ku70Δ rad50-N18S* triple mutant cells were considerably more resistant to DNA damaging agents than both *sae2Δ ku70Δ* and *sae2Δ rad50-N18S* double mutant cells (Figure 33B).

As the lack of Rif2 decreases the hyperactivation of the checkpoint in *sae2Δ* cells, we investigated the effect of *rad50-N18S* on Rad53 phosphorylation and MRX association at DSBs. Similar to *RIF2* deletion, expression of the *rad50-N18S* allele in *sae2Δ* cells decreased both HO-induced Rad53 phosphorylation (Figure 32C)

and Mre11 persistence at the HO-induced DSB to almost wild type levels (Figure 33C). The decreased Mre11 association at DSBs in *rad50-N18S sae2Δ* cells is not due to a reduced DNA binding activity of $MR^{N18S}X$, as the amount of Mre11 bound at DSBs in *rad50-N18S* cells was similar to that of wild type cells (Figure 33C). The finding that the lack of *RIF2* did not decrease further the amount of Mre11 bound at DSBs in *rad50-N18S sae2Δ* cells (Figure 33C) indicates again that the lack of Rif2 and the presence of Rad50-N18S destabilize Mre11 association to DSBs in *sae2Δ* cells by altering the same pathway.

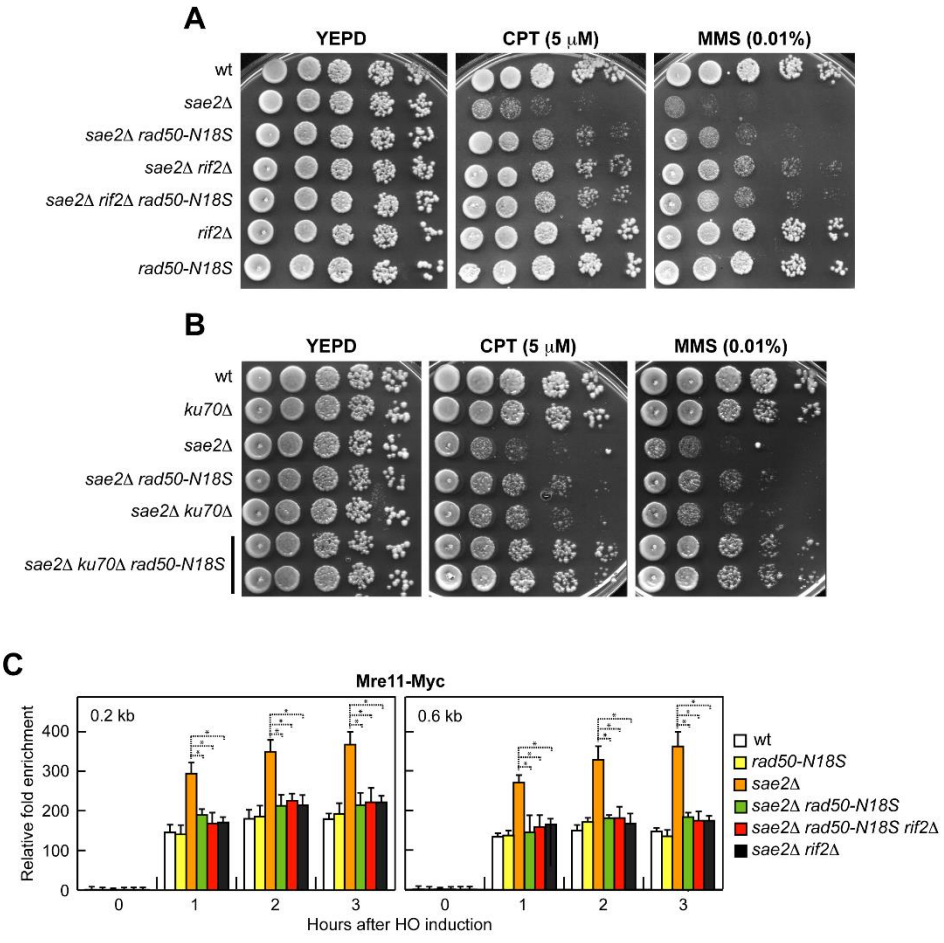

Figure 33 ***The rad50-N18S mutation suppresses the DNA damage sensitivity of sae2△ cells by decreasing MRX abundance at DSBs****.*
(A,B) Exponentially growing cultures were serially diluted (1:10) and each dilution was spotted out onto YEPD plates with or without CPT or MMS.
*(C) ChIP and qPCR. Exponentially growing YEPR cell cultures were transferred to YEPRG to induce HO expression, followed by ChIP analysis of the recruitment of Mre11-Myc at the indicated distance from the HO-cut. In all diagrams, ChIP signals were normalized for each time point to the corresponding input signal. The mean values of three independent experiments are represented with error bars denoting s.d. *p<0.005 (Student's t-test).*

Rif2 inhibits Mre11-Rad50 endonuclease activity and Mre11-Rad50^{N18S} is refractory to Rif2-mediated inhibition

To gain insights into the function of Rif2 in downregulating MRX association at DSBs in *sae2Δ* cells, we expressed and purified recombinant full-length Rif2 and tested its effect on Mre11-Rad50 (MR) ATPase (Figure 34A) and nuclease activities (Figure 34B). Xrs2 is largely dispensable for the endonuclease activities of the MRX complex [182]. As previously observed [114], [227], Rif2 stimulated the ATPase activity of MR (Figure 34A). Interestingly, Rif2 strongly inhibited the endonuclease activity of MR in conjunction with phosphorylated Sae2 (pSae2) (Figure 34C and D), whereas it had no effect on its exonuclease activity (Figure 34C and E). As the ATPase hydrolysis by Rad50 is required for Sae2 to stimulate Mre11 endonuclease activity [28], [230], this finding suggests that Rif2 stimulates the ATP hydrolysis by Rad50 in a nonproductive manner, leading to the discharge of the ATP-bound state into a post-hydrolysis MR conformation that is not competent for DNA cleavage.

As *rad50-N18S* mimics *RIF2* deletion with respect to *sae2Δ* checkpoint inhibition and MRX destabilization at DSBs, we purified Mre11-Rad50^{N18S} (Figure 34F) and tested whether the ATPase and nuclease activities of MR^{N18S} are still sensitive to inhibition by Rif2. We observed two main differences compared to wild type MR. First, Sae2 was capable to stimulate the endonuclease activity of MR^{N18S}, although less efficiently than wild type MR (Figure 34D and G). Second, Rif2 was less efficient in inhibiting the MR^{N18S} endonuclease activity compared to that of wild type MR (Figure 34D and G), while it stimulated the ATPase activity of both MR and MR^{N18S}

with similar efficiency (Figure 34A). This finding suggests that Rad50-N18S partially escapes the inhibitory function exerted by Rif2 on Mre11 endonuclease activity.

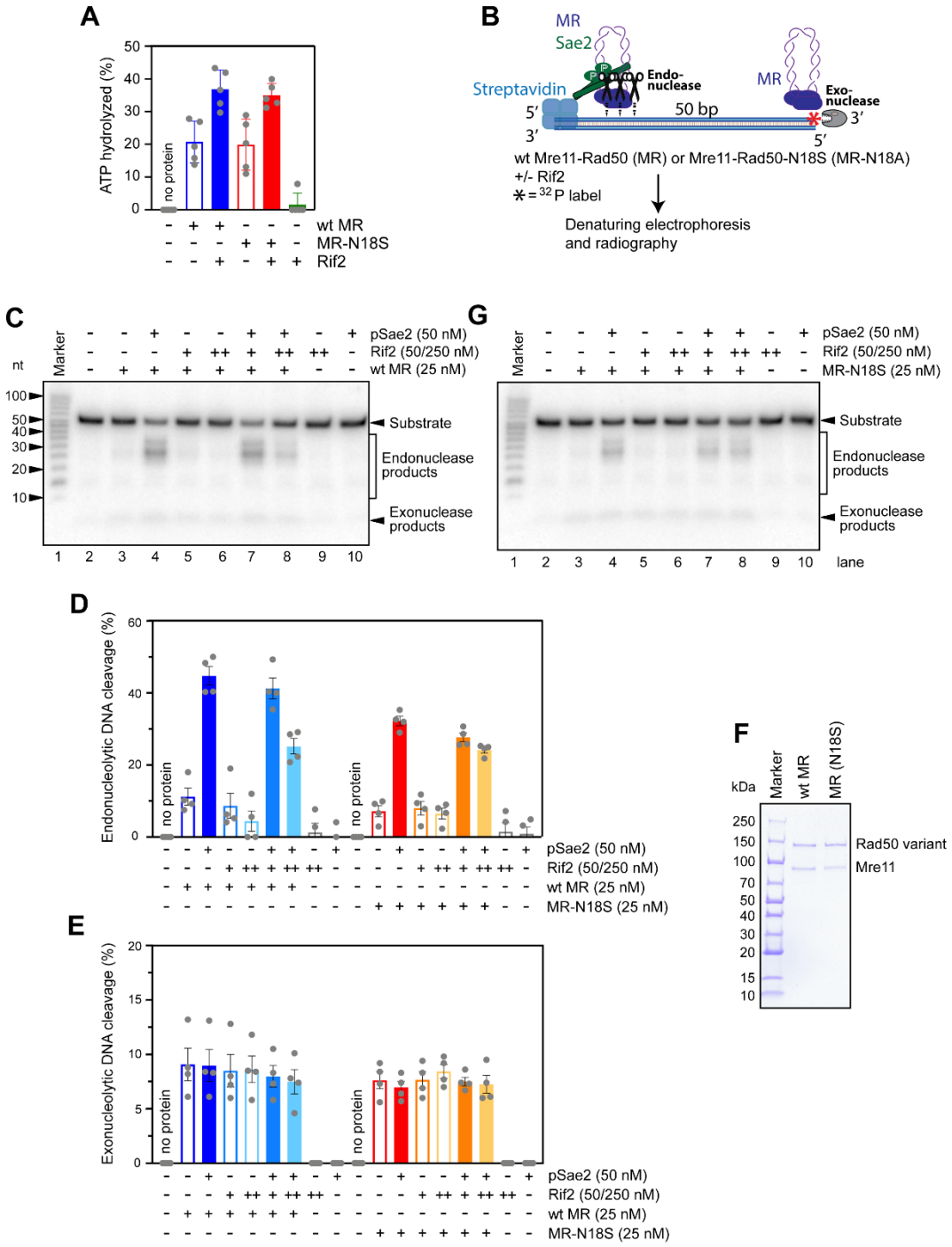

Figure 34 ***Rif2 inhibits the endonuclease activity of Mre11-Rad50 and Mre11-Rad50^{N18S} escapes this inhibition.***
(A) Quantitation of ATPase assays carried out with wild type MR or MR-N18S (both 100 nM) and Rif2 (500 nM), as indicated. Averages shown from 5 independent experiments; error bars, SEM.
(B) A scheme of the assay used to analyze the effect of Rif2 on the endonuclease activity of MR (which requires phosphorylated Sae2, pSae2), and the exonuclease activity of MR. 50 bp-long dsDNA, blocked with streptavidin on one end, was used a substrate.
(C) Representative nuclease assays with Mre11-Rad50 (MR), phosphorylated Sae2 (pSae2) and Rif2, as indicated.
(D) Quantitation of endonuclease activity from experiments such as shown in panels C and G. Averages shown from 4 independent experiments; error bars, SEM.
(E) Quantitation of exonuclease activity from experiments such as shown in panels C and G. Averages shown from 4 independent experiments; error bars, SEM.
(G) Representative assays as in (C), but with MR-N18S.
(F) MR and MR^{N18S} used in this study.

Rif2 binds a Rad50 surface that is essential for Sae2 to stimulate Mre11 nuclease activity

As Rif2 is known to interact with Rad50 [227], we tested whether the *rad50-N18S* mutation impairs Rad50-Rif2 interaction. In pull-down assays, Rif2 was able to interact with Mre11-Rad50 and the N18S mutation reduced this interaction (Figure 35A), thus explaining the partial escaping of Rif2-mediated inhibition of Mre11-Rad50^{N18S} endonuclease activity. Rif2 association to DSBs has been reported to be partially dependent on MRX [114]. Consistent with an impaired Rad50^{N18S}-Rif2 interaction, the amount of Rif2 bound at the HO-induced DSBs was reduced in *rad50-N18S* cells compared to wild type cells (Figure 35B).

In the ATP-bound state (resting state), Mre11 binding to dsDNA is blocked by Rad50 [138], [174], [176], [178], [179], [196], [222]. A recent cryo-electron microscopy of the *E. coli* Mre11-Rad50 homolog SbcCD has revealed that, upon DNA binding and ATP hydrolysis, the two Rad50 coiled coil domains zip up and, together with the Rad50 NBDs, form a clamp around dsDNA [231]. This structural change allows Mre11 dimer to move to the side of Rad50, where it binds a DNA end and assembles a DNA cutting channel for nucleolytic reactions (cutting state). Importantly, formation of the cutting state has been shown to require that the phosphodiesterase domain of *E. coli* Mre11 is locked onto Rad50 NBD by a “fastener” loop in Mre11, which binds the outer β sheet of Rad50 [231]. This interface is important for the nuclease

activity of the complex, as mutants losing the binding between Mre11 fastener and Rad50 NBD show reduced Mre11 nuclease activity [231]. Although the fastener loop is not conserved in eukaryotes, comparison of the cutting state structures of *E. coli* sbcCD with that of *S. cerevisiae* MR generated by homology modeling [212] reveals that the fastener loop of *E. coli* sbcC (Mre11 ortholog) binds to the surface of sbcD (Rad50 ortholog) in the same region where a cluster of Rad50 residues (K6, R20 and K81), corresponding to the *S. cerevisiae rad50-s* mutations, is located [232] (Figure 35C). Furthermore, the T188 residue affected by the *mre11-s* mutation in budding yeast [233] is localized in the Mre11 α helix facing the same region of the fastener loop (Figure 35C). The *rad50-K81I* mutation, representative of *rad50-s* mutations, is known to impair Mre11 endonuclease activity by disrupting the physical interaction of Sae2 with Rad50 [28], [230]. This finding suggests that, instead of the fastener loop, formation of a ternary complex with phosphorylated Sae2 can stabilize Mre11-Rad50 NBD interface and therefore the transition to the cutting state.

The N18 residue, which is important for Rad50 to interact with Rif2, is located nearby the Rad50 K6, R20 and K81 residues altered by the *rad50-s* mutations (Figure 5C), suggesting that Rif2 can also bind to this site. To test this hypothesis, we analyzed whether the Rad50 K81I mutation affects the interaction with Rif2 by coimmunoprecipitation. Since Rif2 binds also Xrs2 and the Rad50-Rif2 interaction occurs independently of Xrs2 [191], [227], we performed the experiment in *xrs2Δ* cells. When Rif2-Myc was immunoprecipitated with anti-Myc antibodies, a reduced amount of $Rad50^{K81I}$-HA could be detected in Myc-tagged Rif2 immunoprecipitates compared to wild type Rad50-HA (Figure 35D). The finding that the K81I mutation weakens the interaction of Rad50 not only with Sae2 but also with Rif2 suggests that Rif2 can inhibit Mre11 endonuclease by binding to this site and interfering with the adoption of a cutting state.

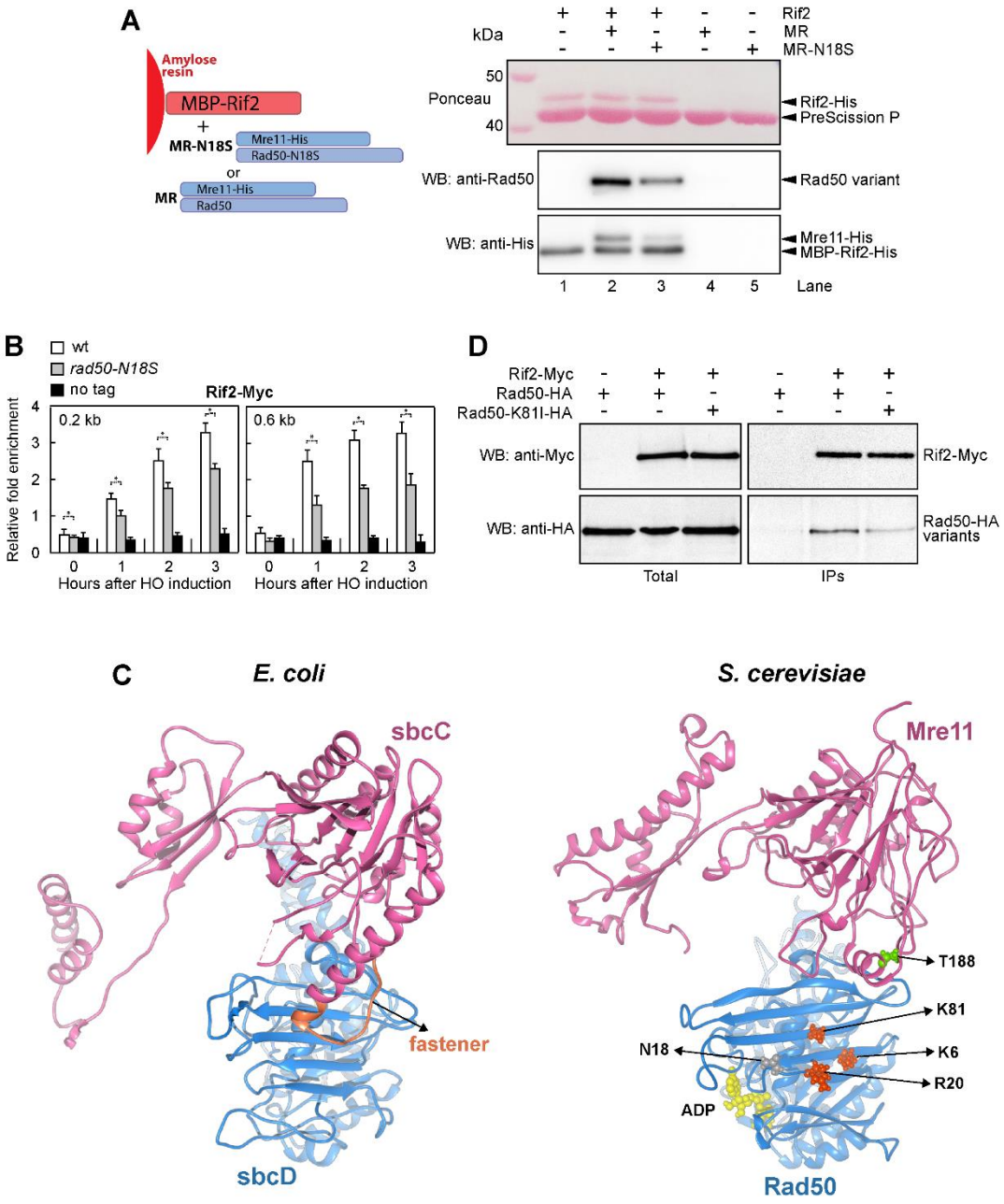
A
Amylose resin
MBP-Rif2
+
MR-N18S
Mre11-His
Rad50-N18S
or
MR
Mre11-His
Rad50
kDa
Rif2
MR
MR-N18S
50
Ponceau
40
Rif2-His
PreScission P
WB: anti-Rad50
Rad50 variant
WB: anti-His
Mre11-His
MBP-Rif2-His
1 2 3 4 5 Lane
B
wt
rad50-N18S
no tag
Rif2-Myc
Relative fold enrichment
0.2 kb
0.6 kb
Hours after HO induction
Hours after HO induction
D
Rif2-Myc
Rad50-HA
Rad50-K81I-HA
WB: anti-Myc
Rif2-Myc
WB: anti-HA
Rad50-HA variants
Total
IPs
C
E. coli
sbcC
fastener
sbcD
S. cerevisiae
Mre11
T188
K81
N18
K6
R20
ADP
Rad50

Figure 35 ***The N18S mutation weakens Rad50-Rif2 interaction and is located close to the rad50-s mutations****.*
(A) Recombinant MBP-Rif2 was immobilized on amylose resin (lanes 1 and 2). Subsequently, MR or MR-N18S were added, as indicated. The resin with bound proteins was washed, eluted with maltose, and the MBP tag on Rif2 was cleaved with PreScission protease. The protein in the eluate were analyzed by Ponceau (Rif2) and Western blotting (anti-Rad50 and anti-His to detect Mre11-His).
*(B) ChIP and qPCR. Exponentially growing YEPR cell cultures were transferred to YEPRG to induce HO expression, followed by ChIP analysis of the recruitment of Rif2-Myc at the indicated distance from the HO-cut. In all diagrams, ChIP signals were normalized for each time point to the corresponding input signal. The mean values of three independent experiments are represented with error bars denoting s.d. *p<0.005 (Student's t-test).*
(C) Comparison of E. coli sbcC (Mre11 ortholog, pink) and sbcD (Rad50 ortholog, blue) in the cutting state (PDB ID: 6S85) and S. cerevisiae Mre11 and Rad50 models, obtained by homology modeling, positioned by structural alignment to mimic the same cutting state conformation. The Rad50 residues (K6, R20 and K81) involved in Sae2 interaction and affected by the rad50-s mutations are shown as orange spheres. The Mre11 residue affected by mre11-s mutation (T188) is shown as green spheres. The Rad50 residue N18 is drawn in gray spheres, while the ADP nucleotide is in yellow.
(D) Protein extracts from exponentially growing cells were analyzed by western blotting with anti-HA and anti-Myc antibodies either directly (Total) or after immunoprecipitation (IPs) with anti-Myc antibody.

Discussion

In the first part of my thesis, I contributed to understanding how these diverse Sae2-MRX functions contribute to DNA damage resistance by searching and characterizing *S. cerevisiae mre11* mutants that suppress the ***sae2Δ*** hypersensitivity to phleomycin, which generates chemically complex DNA termini, and/or to camptothecin (CPT), which extends the half-life of topoisomerase 1 (Top1)-DNA cleavable complexes (Top1ccs) [212]. We identified and characterized several *mre11* mutants that restored the DNA damage resistance of ***sae2Δ*** cells. Among them, the *mre11-H98Y*, *mre11-K292E* and *mre11- R389C* mutations, which restore resistance to both CPT and phleomycin, also increase the resection efficiency of ***sae2Δ*** cells. By contrast, the *mre11-R522H* and *mre11-N631Y* mutations, which restore resistance only to phleomycin, bypass Sae2 function in end-tethering but not in end-resection. These findings indicate that an end-tethering defect by itself is not sufficient to account for the CPT hypersensitivity of ***sae2Δ*** cells, whereas Sae2 function in end-resection can be dispensable to repair phleomycin-induced DNA lesions. CPT cytotoxicity is due to the reversibly trapping of Top1 on nicked DNA intermediates[212]. The endonucleolytic activity of MRX has been implicated in the nucleolytic removal of Top1-DNA adducts [236]–[239]. Our findings that Mre11-H98Y, Mre11-K292E and Mre11-R389C do not bypass the requirement for Sae2 in either Spo11 removal or activation of Mre11 endonuclease strongly suggest that the suppression of ***sae2Δ*** CPT sensitivity is not due to a more efficient endonucleolytic removal of Top1ccs. Rather, Mre11-H98Y, Mre11-K292E and Mre11- R389C were found to increase the resection efficiency of ***sae2Δ*** cells by potentiating the Sgs1-Dna2 resection machinery. Since DNA replication and/or transcription can convert the Top1ccs that are reversibly trapped by CPT into DSBs and/or unusual replication intermediates [240], [241], both of which require homologous recombination to be repaired/resolved, a more efficient DNA-end resection by the above mutant variants could restore CPT resistance in ***sae2Δ*** cells by facilitating the repair of these secondary DNA lesions.

By contrast, Sae2-MRX function in end-tethering appears to be more important to repair phleomycin-induced rather than CPT-induced DNA lesions. As phleomycin leads directly to DNA cleavage and DSB repair by HR has been shown to require

limited amount of ssDNA at DSB ends (69,70), the amount of ssDNA generated in *sae2Δ* cells may be sufficient to repair by HR phleomycin-induced DSBs, whose DNA ends are readily accessible to the resection machinery. By contrast, a more efficient and faster resection could be required to repair by HR CPT-induced lesions, which are accessible to the resection nucleases only once DNA replication and/or transcription have processed the Top1-DNA cleavage complexes.

The primary cause of the resection defect of *sae2Δ* cells is a reduction of the Sgs1-Dna2 activity that is due to enhanced Rad9 binding to DSBs. Mre11-H98Y, Mre11-K292E and Mre11-R389C were found to restore DNA damage resistance and resection in *sae2Δ* cells by relieving Rad9-mediated inhibition of the Sgs1-Dna2 resection machinery. In fact, these mutant variants poorly bind to DNA ends and this defect causes decreased Tel1 association to DSBs. Consequently, diminished Tel1 binding leads to a decreased amount of Rad9 bound at DSBs and therefore to the relief of Sgs1-Dna2 inhibition. Structural studies on Mre11–Rad50 complex from archaea and bacteria have shown that Mre11 has an extended structure that can be divided into two functional domains connected by a poorly structured linker (C-linker): a nuclease module at the N-terminus, which comprises the phosphodiesterase and the capping domains, and a Rad50-binding domain at the C-terminus that binds the Rad50 coiled-coils [174], [176], [196]. Notably, the *mre11* mutations restoring both CPT resistance and efficient DSB resection in *sae2Δ* cells are all located upstream of the C-linker domain. This observation is further strengthened by two other works that identified changes in amino acids (H37, Q70, T74, L77, L89, E101, P110) all located in Mre11 N-terminus as suppressors of the CPT sensitivity of *sae2Δ* cells [42], [197]. The common feature of all these *mre11* mutations is a reduction of Mre11 association to DSBs [42], [197]. Structural studies by homology modeling and molecular dynamics of ScMre11–Rad50 indicate that the H98Y and R389C amino acid substitutions reduce Mre11 association to DSBs by different means. In particular, the H98Y substitution alters the formation of hydrogen bonds in the Mre11 dimer interface and reduces in vivo Mre11 dimer formation, which is known to facilitate MRX- DNA association [203]. Interestingly, our inter-chain hydrogen bond analysis of the ScMre11 dimer interface indicates that other

residues play similar roles, such as Q70 and E101, whose substitutions have been shown to bypass Sae2 function in CPT resistance possibly by lowering MRX association to DSBs [42], [197]. By contrast, the R389 residue is involved in mediating the interactions of the ScMre11 capping domain with both Rad50 and branched DNA. Substitution of R389 with C could alter the Mre11 DNA-binding interface by losing the attractive force between the arginine and the phosphate group of DNA. In addition, it could overcome the need of a salt bridge rupture during the ATP-driven rotation of the Rad50 subunits, thus facilitating the conformational transition of Mre11 and Rad50 to an open configuration that possesses a lower DNA binding affinity [179]. Consistent with this hypothesis, substitution of residues mediating the interaction between the Mre11 capping domain and Rad50 have been shown to facilitate the disengagement of Mre11 capping domain and disclosure of the Mre11 endonucleolytic site [196]. By contrast, the *mre11-R522H* and *mre11-N631Y* mutations, which are located at the C-terminus, restore resistance only to phleomycin and bypass Sae2 function in end-tethering but not in end-resection, suggesting that an end-tethering defect by itself is sufficient to account for the hypersensitivity of ***sae2Δ*** cells to phleomycin. Despite causing reduced end-tethering, the lack of Sae2 leads to in- creased NHEJ frequency [242] that can be explained by the reduced 5' resection, as the extent of nucleolytic degradation can be an impediment for NHEJ. Therefore, it is unlikely that the increased end-tethering activity conferred by the *mre11-R522H* and *mre11-N631Y* mutations might suppress the phleomycin sensitivity of ***sae2Δ*** cells by increasing the NHEJ efficiency. Rather, we found that ***sae2Δ*** cells are specifically defective in DSB repair by SDSA and that the *mre11-R522H* mutation suppresses this defect. Given that the end-tethering function of MRX is particularly important for DSB repair by SDSA, possibly because it facilitates the annealing of the displaced strand to the other DSB end [114], the increased phleomycin resistance conferred by the *mre11-R522H* and *mre11-N631Y* mutations is likely due to a more efficient DSB repair by SDSA.

The Mre11-R522 residue is located in the RBD domain that, together with the capping domain, mediates the interaction between Mre11 and ATP-bound Rad50 [196]. The conformational change induced by ATP hydrolysis leads to dissociation

of the Mre11 capping domain from Rad50, which remains associated to Mre11 mainly through the RBD [196]. We found that the R522H substitution affects neither MRX complex formation nor Rad50 ATPase activity, while our structural analysis reveals that it might confer more mobility to the whole RBD. Based on this finding and on the observation that Mre11-R522H possesses an increased tethering activity by itself, we speculate that the substitution of R522 with H might lead to a slight destabilization of the Mre11–Rad50 interaction that could be unmasked only after ATP hydrolysis, when the RBD becomes essential to maintain Mre11 fastened to Rad50 in the ADP-bound state. Consequently, a defect in accommodating the ATP-hydrolysis-dependent conformational transitions of the complex could lead to increased association at DSBs of MRX in its ATP-bound conformation and therefore to a more efficient end-tethering. In summary, we provide evidence that two structurally distinct N-terminal and C-terminal domains of Mre11 have different roles in supporting the functions of the MRX complex in DNA damage resistance.

In the second part of my thesis, I contributed to elucidate the mechanism of Tel1/ATM activation by MRX/MRN by characterizing the separation-of-function *mre11-S499P* and *rad50-A78T* mutations that specifically impair activation of Tel1/ATM but no other MRX functions. In fact, both *mre11-S499P* and *rad50-A78T* cells phenocopy *tel1Δ* cells with respect to DNA damage resistance, telomere metabolism, DSB resection and checkpoint signaling. We found that the defective Tel1 activation by both Mre11-S499P and Rad50-A78T is due to a poor Tel1 association to DSBs that is caused by reduced MRX–Tel1 interaction. This decreased MRX–Tel1 association does not depend on impaired Xrs2-MR interaction, as Xrs2 interacts equally well with wild type MR, $M^{S499P}R$ andMR^{A78T} subcomplexes. Interestingly, the *mre11-S499P* mutation is localized at the Mre11–Rad50 interface and reduces Mre11–Rad50 association, suggesting that Rad50 plays an important function in Tel1/ATM activation that is specifically impaired by the *rad50-A78T* mutation. *In vitro* activation of human ATM by MRN was shown to require ATP binding but not ATP hydrolysis [221], raising the possibility that MRX/MRN activates Tel1/ATM when it is present in the ATP-bound state. By molecular dynamics, we showed that, in the presence of ATP, wild type MR lingers

in a tightly closed conformation, with the two ATP molecules deeply buried at the interface between the Rad50 subunits. In the presence of ADP, the Rad50 homodimer loosens up due to the conformational change occurring in Rad50 when bound to ADP compared to ATP. ADP-bound Rad50 exposes the nucleotide binding sites, and its association with Mre11 is also destabilized. These events are the earlier stages of the large-scale conformational changes occurring upon ATP hydrolysis and required for MRX engagement in resection [174], [176], [196], [222]. The *rad50-A78T* mutation induces conformational rearrangements in MR^{A78T} bound to ATP similar to those observed when wild type MR is bound to ADP, thus impinging on the ability of MR^{A78T}-ATP complex to maintain the closed conformation. In particular, substitution of A78 with T already induces a higher mobility of the $\alpha 1$-$\beta 4$ loop in the ATP-bound state, triggering a series of motions that lead to the C-terminal lobe rotation and interfering with the dimer interface affinity. Interestingly, similar motions have been revealed by NMR also in the *P. furiosus* Rad50-R805E mutant [225], suggesting that the inability of this mutant to elicit Tel1 activation is caused by a spontaneous conformational change that occurs independently of ATP hydrolysis (which is actually impaired in this mutant) [179]. In any case, these changes in the stability of the ATP-bound MR^{A78T} conformational state greatly reduce Tel1 activation, but do not impair the ability of the mutant complex to support both DNA damage resistance and ligation of broken DNA ends, suggesting different requirements for the ATP-bound conformational state in promoting either Tel1 activation or efficient DSB repair. In summary, we provide evidence that the ATP-bound Mre11–Rad50 conformation is important to sustain Tel1/ATM binding and activation. The finding that the *in vitro* binding of Xrs2/NBS1 with Mre11–Rad50 is increased in the presence of ATP [243] supports the view that these Mre11 and Rad50 structural features reflect an important function of MRX in Tel1/ATM activation.

In the last part of my thesis, I studied the regulation of Mre11 endonucleolytic cleavage. Indeed, phosphorylated Sae2 interacts with Rad50 and stimulates the Mre11 endonucleolytic activity through an unknown mechanism [28]Although Sae2 does not affect the overall ATP hydrolysis rate by Rad50, Sae2-mediated stimulation

of MRX endonuclease requires ATP hydrolysis by Rad50, suggesting that Sae2 acts on Rad50 to stimulate Mre11 nuclease activity [226]. Interestingly, the nuclease activity of *E. coli* Mre11 requires the fastener loop, which stabilizes the Mre11-Rad50 DNA cutting configuration by locking the phosphodiesterase domain of Mre11 onto Rad50 NBD [231]. The fastener loop of *E. coli* Mre11 binds to the Rad50 cluster of residues corresponding to the *rad50-s* mutations in yeast Rad50. As the *rad50-s* mutations abrogate the physical interaction of Rad50 with Sae2 [230], [232], we propose that, instead of the fastener loop, Sae2 binding to Rad50-Mre11 interface is necessary to stabilize a post-hydrolysis MRX conformation (cutting state) that is competent to cleave DNA (Figure 36), thus explaining the requirement of Sae2 to stimulate Mre11 endonuclease activity.

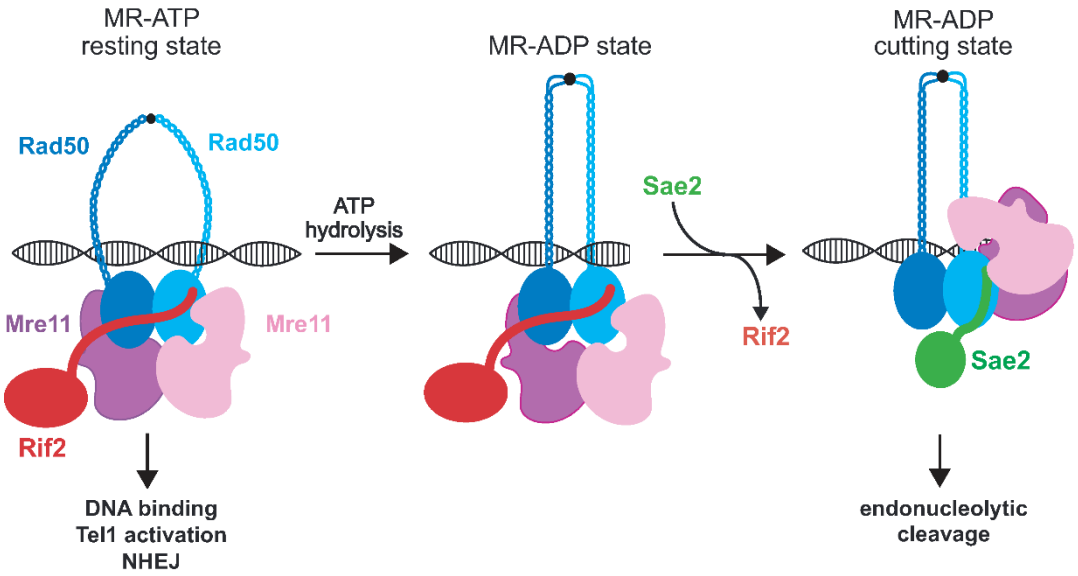

Figure 36 ***Model for Sae2 and Rif2 regulation of MRX activity at DNA ends****.*
In the ATP-bound state (resting state), Mre11 embraces Rad50-ATP dimer, resulting in Mre11 being completely inaccessible to dsDNA. After ATP hydrolysis, Rad50 adopts a conformation that induces a rotation of the coiled-coils arms, which clamp upon DNA binding. Mre11 dimer is able to move from the Rad50 dimer and reaches the DNA end. The resulting conformation (cutting state) is stabilized by the presence of Sae2 on the Rad50-Mre11 interface. Rif2 binding near the Sae2-interacting site on Rad50 interferes with the adoption of the cutting state and stabilizes the complex in a conformation that is not competent for DNA cleavage.

We show that this Sae2-mediated stimulation of Mre11 endonuclease activity is inhibited by Rif2. MRX endonuclease requires ATP hydrolysis by Rad50 [226]. Paradoxically, Rif2 has been shown to stimulate ATP hydrolysis by Rad50 [114], [227], raising the possibility that this stimulation leads to a MR ADP-bound

conformation that is not productive for nuclease activity. The Rad50 N18S mutation escapes the Rif2-mediated negative regulation of Mre11 nuclease by weakening Rad50-Rif2 interaction. Interestingly, this mutation, which also renders Mre11-Rad50 less sensitive to Sae2 stimulation, is located nearby the Rad50 residues altered by the *rad50-s* mutations [230], [232], suggesting that the Rif2 and Sae2 binding sites on Rad50 can overlap. In accord with this hypothesis, the *rad50-K81I* mutation, phenocopying the *rad50-s* mutations, impairs not only Sae2-Rad50 interaction but also Rad50-Rif2 interaction, indicating that Rif2 inhibits MR nuclease by competing with Sae2 for Rad50 binding. This Rif2 function in antagonizing Sae2 binding can lead to a destabilization of the MR cutting state and can explain why the stimulation of Rad50 ATPase activity by Rif2 results into a post-hydrolysis MR conformation that is non-productive for nuclease activity. Although Mre11-Rad50-N18S partially escapes the Rif2-mediated inhibition of Mre11 endonuclease activity, Rad50-N18S ATPase activity is still sensitive to Rif2 stimulation. This finding suggests that the residual interaction between Rif2 and Rad50-N18S is sufficient for Rif2 to stimulate ATP hydrolysis by Rad50, but not for competing with Sae2 for Rad50 binding and therefore for destabilizing a post-hydrolysis MR cutting state.

The lack of either Sae2 or Mre11 nuclease activity increases MRX and Tel1 retention at DSBs, which leads to a persistent Rad53 activation that decreases DNA damage resistance at least in *sae2Δ* cells [114], [194], [195]. We found that Rif2 is responsible for the increased MRX association at DSBs and that the *rad50-N18S* mutation escapes the Rif2-mediated increase of MRX retention at DSBs in both *sae2Δ* and *mre11-nd* cells. Thus, we propose that failure to stabilize the MRX cutting state by Sae2 favors the return to a post-hydrolysis MR conformation that is bound by Rif2 at the Mre11-Rad50 interface. Rif2 binding stabilizes this MR conformation that, due to the lack of Sae2 or the presence of a catalytically inactive Mre11, is not proficient for cleavage but is still capable to bind DSB ends (Figure 35). Since MRX was shown to undergo stepwise incision of dsDNA and therefore to move on dsDNA during cleavage reactions [226], the inability of this clamp state to cleave DNA can favor interactions among MR complexes brought near each other by DNA binding

to generate higher order oligomeric assemblies that lead to a Rif2-dependent increase of MRX association at DSBs.

Which are the biological consequences of Rif2-mediated MRX regulation when Sae2 is present? Indeed, DSBs are more avidly bound by Sae2 than by Rif2, whereas the opposite occurs at telomeres that are more avidly bound by Rif2 than by Sae2 [184], [191], [244], [245]. The lack of Rif2 was shown to increase NHEJ at both DSBs and telomeres [114] [246], whereas it increases MRX-mediated resection only at telomeres and not at DSBs [191], [245], [247]–[249]. NHEJ has been shown to rely on the ATP-bound state of Rad50 (Deshpande et al., 2014; Cassani et al., 2018), which generates a groove that can host dsDNA [138], [176], [222], [250]. Thus, Rif2 binding at both DSBs and telomeres inhibits NHEJ by discharging the MRX ATP-bound state though stimulation of Rad50 hydrolysis. By contrast, as MRX function in resection strictly depends on Sae2, the high amount of Rif2 at telomeres antagonizes Sae2 binding to Rad50, thus destabilizing the MRX cutting state and inhibiting resection, whereas its amount is not enough to destabilize the MRX cutting state at DSBs. Likewise, the lack of Rif2 decreases MRX and Tel1 association at DSBs only when Sae2 is absent or Mre11 is nucleolytically inactive. Rather, *rif2Δ* cells show an increase of MRX and Tel1 persistence at both DSBs and telomeres [114], [191]. This inhibition of MRX and Tel1 association at both DSBs and telomeres can be due to the ability of Rif2 to discharge the MRX ATP-bound state.

In summary, we propose that Sae2 and Rif2 regulate the MRX endonuclease activity in opposite manners. While Sae2 stimulates Mre11 nuclease activity by stabilizing a post-hydrolysis MR conformation that is competent for DNA cleavage, Rif2 inhibits it by antagonizing this Sae2 function.

In conclusion, in this thesis, we demonstrated that the multiple roles of the MRX complex are modulated by the complex ability to transduce its conformational change between Rad50 and Mre11 subunit, but they are also finely regulated by the interaction with other proteins. Since this complex is highly conserved in humans, this more in-depth understanding of its roles and regulation might apply to human

cells to improve our knowledge of the consequences of MRX dysfunctions in human diseases and cancer.

Material and methods

Yeast strains and growth conditions

Strain genotypes are listed in **Table *2***. Strain JKM139, used to detect DSB resection, was kindly provided by J. Haber (Brandeis University, Waltham, USA). Strain tGI354, used to detect ectopic recombination, was kindly provided by G. Liberi (CNR, Pavia, Italy). Strain JYK40.6, used to detect end-tethering, was kindly provided by D.P. Toczyski (University of California, San Francisco, USA). Cells were grown in YEP medium (1% yeast extract, 2% bactopeptone) supplemented with 2% glucose (YEPD), 2% raffinose (YEPR) or 2% raffinose and 3% galactose (YEPRG). Gene disruptions were generated by one-step PCR disruption method. All the experiments have been performed at 27°C.

Search for *mre11* mutants

Genomic DNA from a strain carrying the *HPHMX* gene located 250 bp downstream of the *MRE11* stop codon was used as template to amplify by low-fidelity PCR a *MRE11* region spanning from position –460 bp to +500 bp from the *MRE11* coding region. Thirty independent PCR reaction mixtures were prepared, each containing 5U EuroTaq DNA polymerase (Euroclone), 10 ng genomic DNA, 500 ng each primer, 0.5 mM each dNTP (dATP, dTTP, dCTP), 0.1 mM dGTP, 0.5 mM $MnCl_2$, 10 mM ßmercaptoethanol, 10 mM Tris–HCl (pH 9), 50 mM KCl and 1.5 mM $MgCl_2$. The resulting PCR amplification products contained the *MRE11* coding sequence and the *HPHMX* resistance gene were used to transform a *sae2*Δ mutant strain (YLL 1070.1). 3000 transformants were selected on YEPD medium added with Hygromycin B (0.3 mg/ml) and then assayed by drop tests for the ability to grow on YEPD plates containing phleomycin or camptothecin.

Search for *mre11* and *rad50* mutants

The screen for *mre11* and *rad50* mutations has been carried out as previously described [212]. Briefly, genomic DNA from strains carrying either the *HPHMX* gene located 250 bp downstream of the *MRE11* stop codon or the *KANMX* gene located

570 bp upstream of the *RAD50* ORF was used as template to amplify by low-fidelity PCR the *MRE11* and the *RAD50* coding region, respectively. Thirty independent PCR reaction mixtures were prepared, each containing 5U EuroTaq DNA polymerase (Euroclone), 10 ng genomic DNA, 500 ng each primer, 0.5 mM each dNTP (dATP, dTTP, dCTP), 0.1 mM dGTP, 0.5 mM $MnCl_2$, 10 mM ß-mercaptoethanol, 10 mM Tris–HCl (pH9), 50 mM KCl and 1.5 mM $MgCl_2$. The resulting PCR amplification products, containing the *MRE11* or *RAD50* coding sequence and the *HPHMX* or *KANMX* resistance gene, respectively, were used to transform a wild type strain. Three thousand transformants were selected and then assayed by drop tests for hypersensitivity to high doses of camptothecin but not to phleomycin or methyl methansulfonate (MMS). The selected clones were then analyzed by Southern blot for telomere shortening similar to *tel1*Δ cells.

Table 2 – *Saccharomyces cerevisiae* strains used in this study.

Strain	Relevant genotype	Source
W303	*MATa/α ade2-1 can1-100 his3-11,15 leu2-3,112 trp1-1 ura3-1 rad5-535*	
YLL3658.3	W303 *MATa MRE11::HPHMX*	This study
YLL1070.1	W303 *MATa sae2Δ::HIS*	This study
YLL1069.3	W303 *MATa sae2Δ::KANMX*	[201]
YLL3743.8	W303 *MATa mre11-H98Y::HPHMX sae2Δ::HIS3*	This study
YLL3760.1	W303 *MATa mre11-K292E::HPHMX sae2Δ::KANMX*	This study
YLL3735.4	W303 *MATa mre11-R389C::HPHMX sae2Δ::KANMX*	This study
YLL3766.1	W303 *MATa mre11-T426I- HPHMX sae2Δ::KANMX*	This study
YLL3736.2	W303 *MATa mre11-R522H::HPHMX sae2Δ::KANMX*	This study
YLL3737.1	W303 *MATa mre11-N631Y::HPHMX sae2Δ::KANMX*	This study
YLL3738.1	W303 *MATa mre11-R651X::HPHMX sae2Δ::KANMX*	This study
DMP6605/3C	W303 *MATa mre11-H98Y::HPHMX*	This study
DMP6413/3D	W303 *MATa mre11-K292E::HPHMX*	This study
DMP6562/2A	W303 *MATa mre11-R389C::HPHMX*	This study
DMP6700/1A	W303 *MATa mre11-T426I::HPHMX*	This study
DMP6441/1D	W303 *MATa mre11-R522H::HPHMX*	This study
DMP6399/9C	W303 *MATa mre11-N631Y::HPHMX*	This study

DMP6400/4C	W303 *MATa mre11-R651X::HPHMX*	This study
DMP6041/6B	W303 *MATa mre11-H125N::URA3 sae2Δ::KANMX*	This study
YLL4019.1	W303 *MATa mre11- H98Y, H125N::URA3 sae2Δ::KANMX*	This study
YLL4020.2	W303 *MATa mre11-H125N, K292E::URA3 sae2Δ::KANMX*	This study
YLL4021.1	W303 MATa mre11-H125N, R389C::URA3 sae2Δ::KANMX	This study
DMP6082/6D	W303 *MATα sae2Δ::KANMX exo1Δ::LEU2*	This study
DMP6659/6C	W303 *MATa mre11-H98Y::HPHMX sae2Δ::KANMX exo1Δ::LEU2*	This study
DMP6660/8A	W303 *MATa mre11-K292E::HPHMX sae2Δ::KANMX exo1Δ::LEU2*	This study
DMP6661/6A	W303 *MATa mre11-R389C::HPHMX sae2Δ::KANMX exo1Δ::LEU2*	This study
DMP6110/10A	W303 *MATa sae2Δ::KANMX dna2 -1*	This study
DMP6605/1C	W303 *MATa sae2Δ::KANMX mre11-H98Y::HPHMX dna2-1*	This study
DMP6658/10D	W303 *MATα sae2Δ::KANMX mre11-K292E::HPHMX dna2-1*	This study
DMP6606/8A	W303 *MATα sae2Δ::KANMX mre11-R389C::HPHMX dna2-1*	This study
DMP5066/2A	W303 *MATα sgs1Δ::TRP1*	This study
JKM139	*MATa hml Δ::ADE1, hmrΔ ::ADE1, ade1-100, lys5, leu2-3,112, trp1::hisG ura3-52, ho, ade3::GAL-HO site*	[218]
YLL3188.3	JKM139 *MATa MRE11-3HA::URA3*	This study
YLL3879.2	JKM139 *MATa mre11-H98Y-3HA::URA3*	This study
YLL3868.1	JKM139 *MATa mre11-K292E-3HA::URA3*	This study
YLL3880.6	JKM139 *MATa mre11-R389C-3HA::URA3*	This study
YLL4022.1	JKM139 *MATa mre11-T426I-3HA::URA3*	This study
YLL3841.2	JKM139 *MATa mre11-R522H-3HA::URA3*	This study
YLL3070.1	JKM139 *MATa mre11-N631Y-3HA::URA3*	This study
DMP6488/10B	JKM139 *MATa mre11-R651X-3HA::URA3*	This study
YLL1523.3	JKM139 *MATa sae2Δ::KANMX*	[201]
DMP6574/9C	JKM139 *MATa mre11-H98Y::HPHMX*	This study
YLL3869.1	JKM139 *MATa mre11-H98Y::HPHMX sae2Δ::KANMX*	This study
DMP6414/1C	JKM139 *MATa mre11-K292E::HPHMX*	This study
YLL3768.11	JKM139 *MATa mre11-K292E::HPHMX sae2Δ::KANMX*	This study
DMP6556/1A	JKM139 *MATa mre11-R389C::HPHMX*	This study
YLL3739.1	JKM139 *MATa mre11-R389C::HPHMX sae2Δ::KANMX*	This study

DMP6401/9B	JKM139 *MATa mre11-R522H::HPHMX*	This study
YLL3740.4	JKM139 *MATa mre11-R522H::HPHMX sae2Δ::KANMX*	This study
DMP6415/9D	JKM139 *MATa mre11-N631Y::HPHMX*	This study
DMP6515/8C	JKM139 *MATa mre11-N631Y::HPHMX sae2Δ::KANMX*	This study
DMP6023/5A	JKM139 *MATa SGS1-3HA::URA3*	[201]
DMP6239/8C	JKM139 *MATa SGS1-3HA::URA3 sae2Δ::KANMX*	This study
DMP6688/2C	JKM139 *MATa SGS1-3HA::URA3 mre11-H98Y-HPHMX*	This study
DMP6647/2D	JKM139 *MATa SGS1-3HA::URA3 mre11-K292E::HPHMX*	This study
DMP6689/4C	JKM139 *MATa SGS1-3HA::URA3 mre11-R389C::HPHMX*	This study
DMP6688/4A	JKM139 *MATa SGS1-3HA::URA3 mre11-H98Y::HPHMX sae2Δ::KANMX*	This study
DMP6647/7C	JKM139 *MATa SGS1-3HA::URA3 mre11-K292E::HPHMX sae2Δ::KANMX*	This study
DMP6648/5D	JKM139 *MATa SGS1-3HA::URA3 mre11-R389C::HPHMX sae2Δ::KANMX*	This study
YLL3421.2	JKM139 *MATa RAD9-3HA::TRP1*	This study
DMP6574/8A	JKM139 *MATa RAD9-3HA::TRP1 mre11-H98Y::HPHMX*	This study
DMP6555/6B	JKM139 *MATa RAD9-3HA::TRP1 mre11-K292E::HPHMX*	This study
DMP6557/6C	JKM139 *MATa RAD9-3HA::TRP1 mre11-R389C::HPHMX*	This study
DMP6766/1A	JKM139 *MATa RAD9-3HA::TRP1 MRE11-H98Y::HPHMX sae2Δ::KANMX*	This study
DMP6767/2A	JKM139 *MATa RAD9-3HA::TRP1 MRE11-K292E::HPHMX sae2Δ::KANMX*	This study
DMP6768/3A	JKM139 *MATa RAD9-3HA::TRP1 MRE11-R389C::HPHMX sae2Δ::KANMX*	This study
DMP5816/1A	JKM139 *MATa RAD9-3HA::TRP1 sae2Δ::KANMX*	[201]
YLL3222.6	JKM139 *MATa TEL1-3HA::NATMX*	[201]
DMP6435/1A	JKM139 *MATa TEL1-3HA::NATMX sae2Δ::KANMX*	This study
DMP6628/11C	JKM139 *MATa TEL1-3HA::NATMX mre11-H98Y::HPHMX*	This study
DMP6627/2D	JKM139 *MATa TEL1-3HA::NATMX mre11-K292E::HPHMX*	This study
DMP6626/1C	JKM139 *MATa TEL1-3HA::NATMX mre11-R389C::HPHMX*	This study
DMP6628/1B	JKM139 *MATa TEL1-3HA::NATMX mre11-H98Y::HPHMX sae2Δ::KANMX*	This study
DMP6627/10D	JKM139 *MATa TEL1-3HA::NATMX mre11-K292E::HPHMX sae2Δ::KANMX*	This study

DMP6628/3B	JKM139 *MATa TEL1-3HA::NATMX mre11-R389C::HPHMX sae2Δ::KANMX*	This study
YLL3572.11	JKM139 *MATa XRS2-18MYC::TRP1*	This study
DMP6649/1C	JKM139 *MATa XRS2-18MYC::TRP1 MRE11-3HA::URA3*	This study
DMP6669/1B	JKM139 *MATa XRS2-18MYC::TRP1 mre11-H98Y-3HA::URA3*	This study
DMP6680/5A	JKM139 *MATa XRS2-18MYC::TRP1 mre11-K292E-3HA::URA3*	This study
DMP6681/8C	JKM139 *MATa XRS2-18MYC::TRP1 mre11-R389C-3HA::URA3*	This study
DMP6769/5A	JKM139 *MATa RAD9-3HA::TRP1 mre11-R522H-HPHMX*	This study
DMP6559/1C	JKM139 *MATa RAD9-3HA::TRP1 mre11-N631Y-HPHMX*	This study
DMP6463/3D	JKM139 *MATa TEL1-3HA::NATMX mre11-R522H-HPHMX*	This study
DMP6645/5D	JKM139 *MATa TEL1-3HA::NATMX mre11-N631Y-HPHMX*	This study
YJK40.6	*MATΔ hmlΔ hmrΔ can1 lys5 ade2 leu2 trp1 ura3 his3 ade3::GAL-HO VII::TRP1-HO LacI-GFP::URA3 LacO::LYS5 LacO::KanR*	[206]
YLL4008.1	YJK40.6 *mre11-H98Y::HPHMX*	This study
YLL4001.1	YJK40.6 *mre11-K292E::HPHMX*	This study
YLL4002.4	YJK40.6 *mre11-R389C::HPHMX*	This study
YLL3811.1	YJK40.6 *mre11-R522H::HPHMX*	This study
YLL3812.2	YJK40.6 *mre11-N631Y::HPHMX*	This study
YLL1709.11	YJK40.6 *sae2Δ::NATMX*	[41]
YLL4023.1	YJK40.6 *mre11-H98Y::HPHMX sae2Δ::NATMX*	This study
YLL4014.3	YJK40.6 *mre11-K292E::HPHMX sae2Δ::NATMX*	This study
YLL4022.4	YJK40.6 *mre11-R389C::HPHMX sae2Δ::NATMX*	This study
YLL3820.2	YJK40.6 *mre11-R522H::HPHMX sae2Δ::NATMX*	This study
YLL3821.4	YJK40.6 *mre11-N631Y::HPHMX sae2Δ::NATMX*	This study
DMP6733	JKM139 *MATa/α MRE11-18MYC::TRP1/MRE11-18MYC::TRP1*	This study
DMP6803	JKM139 *MATa/α MRE11-3HA::URA3/MRE11-3HA::URA3*	This study
DMP6734	JKM139 *MATa/α MRE11-18MYC::TRP1/MRE11-3HA::URA3*	This study
DMP6735	JKM139 *MATa/α MRE11-H98Y-18MYC::TRP1 /MRE11-H98Y-3HA::URA3*	This study

tGI354	*ho hmlΔ::ADE1 MATa inc hmrΔ::ADE1 ade1 leu2-3;112 lys5 trp1::hisG ura3-52 ade3::GAL::HO arg5,6::MATa::HPHMX*	[210]
YLL3996.1	tGI354 *mre11-R522H::KANMX*	This study
YLL3964.4	tGI354 *mre11-R522H::KANMX sae2Δ::NATMX*	This study
YLL3914.2	tGI354 *sae2Δ::NATMX*	This study
YLL3657.1	W303 MATa *KANMX::RAD50*	This study
YLL490.4	W303 MATa *mec1Δ::HIS3 sml1Δ::KANMX*	[244]
DMP6983/4B	W303 MATa *mec1Δ::HIS3 sml1Δ::KANMX mre11-S499P-HPHMX*	This study
DMP6984/9D	W303 MATa *mec1Δ::HIS3 sml1Δ::KANMX KANMX-rad50-A78T*	This study
DMP4243/4C	W303 MATa *mec1Δ::HIS3 sml1Δ::KANMX sae2Δ::KANM*	This study
DMP6983/2D	W303 MATa *mec1Δ::HIS3 sml1Δ::KANMX sae2Δ::KANM mre11-S499P-HPHMX*	This study
DMP6984/10B	W303 MATa *mec1Δ::HIS3 sml1Δ::KANMX sae2Δ::KANM KANMX-rad50-A78T*	This study
YLL1794.3	JKM139 MATa *tel1Δ::NATMX*	[214]
YLL3748.1	JKM139 MATa *mre11-S499P::HPHMX*	This study
YLL3751.2	JKM139 MATa *KANMX::rad50-A78T*	This study
YLL1769.1	JKM139 MATa *mre11Δ::NATMX*	[251]
YLL2119.2	JKM139 MATa *mre11Δ::NAT::mre11-H125N::URA3*	This study
DMP6664/11D	JKM139 MATa *mre11-S499P-HPHMX tel1Δ::NATMX*	This study
DMP6908/10B	JKM139 MATa *KANMX-rad50-A78T tel1Δ::NATMX*	This study
184-10A	JKM139 MATa *mec1Δ::HIS3 sml1Δ::KANMX*	[214]
YLL1523.3	JKM139 MATa *sae2Δ::KANMX*	[201]
YLL2766.7	JKM139 MATa *sae2Δ::KANMX tel1Δ::NATMX*	[201]
DMP6799/1B	JKM139 MATa *sae2Δ::KANMX mre11-S499P-HPHMX*	This study
DMP6907/12D	JKM139 MATa *sae2Δ::KANMX KANMX::rad50-A78T*	This study
YLL3222.6	JKM139 MATa *TEL1-3HA::NATMX*	[201]
DMP6459/4B	JKM139 MATa *TEL1-3HA::NATMX mre11-S499P::HPHMX*	This study
DMP6489/3A	JKM139 MATa *TEL1-3HA::NATMX KANMX::rad50-A78T*	This study
YLL1854.2	JKM139 MATa *MRE11-18MYC::TRP1*	
DMP6535/3A	JKM139 MATa *MRE11-18MYC::TRP1 TEL1-3HA::NATMX*	This study
DMP6540/1B	JKM139 MATa *mre11-S499P-18MYC::URA3 TEL1-3HA::NATMX*	This study
YLL3786.1	JKM139 MATa *RAD50-18MYC::URA3*	This study

DMP6905/1C	JKM139 MATa *RAD50-18MYC::URA3 TEL1-3HA::NATMX*	This study
DMP6904/24	JKM139 MATa *rad50-A78T-18MYC::URA3 TEL1-3HA::NATMX*	This study
YLL3572.11	JKM139 MATa *XRS2-18MYC::TRP1*	This study
DMP6649/1C	JKM139 MATa *MRE11-3HA::URA3 XRS2-MYC::TRP1*	This study
DMP6773/7B	JKM139 *MATa mre11-S499P-3HA::URA3 XRS2-18MYC::TRP1*	This study
YLL3786.1	JKM139 *MATa RAD50-18MYC::URA3*	This study
DMP6932/4B	JKM139 *MATa XRS2-3HA::URA3 RAD50-18MYC::URA3*	This study
DMP6933/9D	JKM139 *MATa XRS2-3HA::URA3 rad50-A78T-18MYC::URA3*	This study
DMP6787	JKM139 *MATa/α mre11-S499P-18MYC::URA3/ mre11-S499P-3HA::URA3*	This study
YLL3188.3	JKM139 *MATa MRE11-3HA::URA3*	This study
DMP6940/1D	JKM139 *MATa RAD50-18MYC::URA3 MRE11-3HA::URA3*	This study
DMP6952/4B	JKM139 *MATa rad50-A78T-18MYC::URA3 MRE11-3HA::URA3*	This study
DMP6771/3D	JKM139 *MATa MRE11-18MYC::TRP1 RAD50-3HA::URA3*	This study
DMP6772/2B	JKM139 *MATa mre11-S499P-18MYC::URA3 RAD50-3HA::URA3*	This study
YLL3782.1	JKM139 *MATa mre11-S499P-18MYC::URA3*	This study
DMP6458/2A	JKM139 *MATa KANMX::rad50-A78T MRE11-18MYC::URA3*	This study
DMP6214/1D	JKM139 *MATa tel1Δ::NATMX MRE11-18MYC::URA3*	This study
DMP6539/2C	JKM139 *MATa tel1Δ::NATMX mre11-S499P-18MYC::URA3*	This study
DMP6540/1C	JKM139 MATa *tel1Δ::NATMX KANMX-rad50-A78T MRE11-18MYC::URA3*	This study
YLL 1134.2	W303 *rif2Δ::KANMX*	[114]
DMP 6166/2D	W303 *MATα rif2Δ::HIS3 sae2Δ::KANMX*	This study
HS21	*MATα ade5-1 his7-2 ura3Δ trp1-289 leu2-3,112::p305L3 LEU2 lys2::AluIR*	[252]
YLL 4197.1	HS21 *rif2Δ::TRP1*	This study
YLL 3773.3	HS21 *sae2Δ::KANMX*	This study
YLL 4348.1	HS21 *mre11-H15N::LEU2*	This study
DMP 7294/6A	HS21 *rif2Δ::TRP1 sae2Δ::KANMX*	This study
YLL 4349.2	HS21 *mre11_H15N::LEU2 rif2Δ::TRP1*	This study
YLL 1712.6	JKM139 *rif2Δ::HPHMX*	This study
DMP 5113/5A	JKM139 *KANMX::rad50-N18S*	This study

YLL 3627.3	JKM139 *sae2Δ::HPHMX*	This study
DMP 7144/8C	JKM139 *rif2Δ::KANMX sae2Δ::HPHMX*	This study
YLL 3757.1	JKM139 *KANMX::rad50-N18S sae2Δ::HPHMX*	This study
DMP 6149/2D	JKM139 *sae2Δ::KANMX MRE11-18MYC::TRP1*	This study
DMP 7248/3A	JKM139 *rif2Δ::KANMX sae2Δ::HPHMX MRE11-18MYC::TRP1*	This study
DMP 6211/5B	JKM139 *rif2Δ::HPHMX MRE11-18MYC::TRP1*	This study
DMP 6435/1A	JKM139 *sae2Δ::KANMX TEL1-3HA::NATMX*	This study
DMP 7250/8D	JKM139 *sae2Δ::HPHMX rif2Δ::KANMX TEL1-3HA::NATMX*	This study
DMP 7250/8A	JKM139 *rif2Δ::KANMX TEL1-3HA::NATMX*	This study
YLL 3421.2	JKM139 *RAD9-3HA::TRP1*	This study
DMP 7192/6B	JKM139 *sae2Δ::HPHMX RAD9-3HA::TRP1*	This study
DMP 7192/8C	JKM139 *sae2Δ::HPHMX rif2Δ::KANMX RAD9-3HA::TRP1*	This study
DMP 7192/3A	JKM139 *rif2Δ::KANMX RAD9-3HA::TRP1*	This study
YLL 4104.2	JKM139 *MRE11-H125N-18MYC::TRP1*	[15]
DMP 7283/3D	JKM139 *rif2Δ::KANMX MRE11-H125N-18MYC::TRP1*	This study
YLL 3754.1	W303 *KANMX::rad50-N18S sae2Δ::HIS3*	This study
DMP 7007/8B	W303 *KANMX::rad50-N18S sae2Δ::HIS3 rif2Δ::HIS3*	This study
DMP 6449/1C	W303 *KANMX::rad50-N18S*	This study
YLL 941.1	W303 *yku70Δ::HIS3*	This study
DMP 4374/6B	W303 *sae2Δ::KANMX yku70Δ::HIS3*	This study
DMP 6903/18D	W303 *KANMX::rad50-N18S ykuΔ::HIS3*	This study
DMP 6903/7D	W303 *KANMX::rad50-N18S sae2Δ::KANMX yku70Δ::HIS3*	This study
DMP 6903/9A	W303 *KANMX::rad50-N18S sae2Δ::KANMX yku70Δ::HIS3*	This study
DMP 7238/2A	JKM139 *KANMX::rad50-N18S MRE11-18MYC::TRP1*	This study
DMP 7238/7A	JKM139 *KANMX::rad50-N18S sae2Δ::HPHMX MRE11-18MYC::TRP1*	This study
DMP 7238/7A	JKM139 *KANMX::rad50-N18S sae2Δ::HPHMX rif2Δ::KANMX MRE11-18MYC::TRP1*	This study
YLL 3612.2	JKM139 *RIF2-18MYC::URA3*	This study
DMP 7059/2A	JKM139 *RIF2-18MYC::URA3 KANMX::rad50-N18S*	This study

Spot assays

Cells grown overnight were diluted to $1x10^7$ cells/ml. 10-fold serial dilutions were spotted on YEPD with or without indicated DNA damaging drugs. Plates were incubated for 3 days at 28°C.

DSB resection and ectopic recombination

DSB end resection at the *MAT* locus in JKM139 derivative strains was analyzed on alkaline agarose gels, by using a single-stranded probe complementary to the unresected DSB strand, as previously described [114]. Quantitative analysis of DSB resection was performed by calculating the ratio of band intensities for ssDNA and total amount of DSB products. DSB repair by ectopic recombination was detected by using the tGI354 strain as previously described [114]. To determine the repair efficiency, the intensity of the uncut band at 2 h after HO induction (maximum efficiency of DSB formation), normalized with respect to a loading control, was subtracted to the normalized values of NCO and CO bands at the subsequent time points after galactose addition. The obtained values were divided by the normalized intensity of the uncut *MAT*a band at time zero before HO induction (100%).

Plasmid religation assay

The centromeric plasmid pRS316 was digested with the BamH1 restriction enzyme before being transformed into the cells. Parallel transformation with undigested pRS316 DNA was used to determine the transformation efficiency. Efficiency of re-ligation was calculated by determining the number of colonies able to grow on medium selective for the plasmid marker and was normalized to the transformation efficiency for each sample. The re-ligation efficiency in mutant cells was compared to that of wild type cells that was set up to 100%.

Western blotting and immunoprecipitation

Trichloroacetic acid protein extracts were separated on 10% polyacrylamide gels and Rad53 detection was carried out by using anti-Rad53 polyclonal antibodies (ab104232) from Abcam. Immunoprecipitations were performed as previously described [253], with the following modifications: protein extracts were prepared in a lysis buffer containing 50 mM HEPES (pH 7.5), 140 mM NaCl, 1 mM EDTA (pH 7.5), 10% glycerol, 0.5% NP40, 1 mM phenylmethylsulfonyl fluoride, 60 mM β-glycerophosphate, 1 mM sodium orthovanadate and a protease inhibitor cocktail (Roche Diagnostics).

ChIP and qPCR

ChIP analysis was performed as previously described [114]. Quantification of immunoprecipitated DNA was achieved by quantitative real-time PCR (qPCR) on a Bio-Rad MiniOpticon apparatus. Triplicate samples in 20 µl reaction mixture containing 10 ng of template DNA, 300 nM for each primer, 2× SsoFast™ EvaGreen® supermix (Bio-Rad #1725201) (2× reaction buffer with dNTPs, Sso7d-fusion polymerase, $MgCl_2$, EvaGreen dye, and stabilizers) were run in white 48-well PCR plates Multiplate™ (Bio-Rad #MLL4851). The qPCR program was as follows: step 1, 98°C for 2 min; step 2, 98°C for 5 s; step 3, 60°C for 10 s; step 4, return to step 2 and repeat 30 times. At the end of the cycling program, a melting program (from 65°C to 95°C with a 0.5°C increment every 5 s) was run to test the specificity of each qPCR. Data are expressed as fold enrichment at the HO-induced DSB over that at the non-cleaved *ARO1* locus, after normalization of each ChIP signals to the corresponding input for each time point. Fold enrichment was then normalized to the efficiency of DSB induction.

Preparation of recombinant proteins

The Mre11-Rad50 complex was expressed in *Spodoptera frugiperda 9* (*Sf9*) cells using constructs coding for His-tagged Mre11 and untagged Rad50 and purified by

NiNTA (Qiagen) affinity chromatography followed by ion-exchange chromatography with HiTrap SP HP (Cytiva) and HiTrap Q HP (Cytiva) columns (Oh et al., 2016). For the preparation of the Mre11-Rad50-N18S mutant complex, the construct for the expression of untagged Rad50 was mutagenized by site-specific mutagenesis with 5'-CCG CAG CTT CGA TAG CAG CGA TCG CGA GAC CAT CG-3' and 5'-CGA TGG TCT CGC GAT CGC TGC TAT CGA AGC TGC GG-3'oligonucleotides. The mutant complex was purified using the same procedure as for the wild type MR. Phosphorylated Sae2 was prepared in *Sf*9 cells as previously described (Cannavo et al., 2018). Recombinant Rif2 was prepared as a fusion with N-terminal MBP tag and a C-terminal 10xHis-tag in *Sf*9 cells. The construct was a kind gift from A. Bianchi (University of Sussex) and the preparation procedure for Rif2 will be described elsewhere.

ATPase assays

The ATPase assays were carried out in 10 μl reactions in 25 mM Tris-acetate pH 7.5, 1 mM dithiothreitol, 5 mM magnesium acetate, 20 mM NaCl, 0.25 mg/ml bovine serum albumin (NEB), 150 μM unlabeled ATP, 4 nM γ-^{32}P-ATP (Perkin Elmer) and 200 ng of dsDNA. The reaction buffer was assembled on ice, the recombinant proteins were added, as indicated, and the reactions were incubated at 30°C for 4 h. The ATP hydrolysis was analyzed by thin layer chromatography using a standard procedure, the plates were exposed to storage phosphor screens and processed by a Typhoon Imager (GE Healthcare/Cytiva). The data were quantitated using Image J and plotted with Prism software.

Nuclease assays

Nuclease assays were carried out as previously described [28], [230] in 15 μl reactions in 25 mM Tris-acetate pH 7.5, 1 mM dithiothreitol, 5 mM magnesium acetate, 1 mM manganese acetate, 0.25 mg/ml bovine serum albumin (NEB), 1 mM phosphoenolpyruvate, 80 U/ml pyruvate kinase (Sigma), 1 mM ATP and 1 nM (in molecules) 3'-labeled dsDNA substrate (oligonucleotides PC1253C and PC1253B).

Streptavidin (15 nM final, Sigma) was added to block one of the DNA ends, and the reactions were pre-incubated for 5 min at room temperature. Subsequently, where applicable, Rif2 was added and the reactions were incubated for 5 min at room temperature. The additional recombinant proteins (MR variants, phosphorylated Sae2, pSae2) were then added as indicated, and the reactions were incubated for 30 min at 30°C. The reaction products were analyzed by denaturing electrophoresis, the gels were dried and exposed to storage phosphor screens and processed by a Typhoon Imager (GE Healthcare/Cytiva). The data were quantitated using Image J and plotted with Prism software.

Protein interaction assays

*Sf*9 cell lysate expressing MBP-Rif2-his was bound to amylose resin (NEB) and washed with wash buffer 1 M (50 mM Tris-HCl pH 7.5, 1 M NaCl, 0.2 % [v/v] NP40, 2 mM EDTA, 1:1000 protease inhibitory cocktail (Sigma P8340) and then with wash buffer 0.1 M (same as wash buffer 1 M, but only 0.1 M NaCl). The recombinant MR variants (1 μg) were then added, incubated for 1 h at 4°C and the resin was then washed with wash buffer 0.1 M. As a negative control, the MR proteins were added to the amylose resin without MBP-Rif2-his to test for non-specific binding. The proteins were eluted with 0.1 M wash buffer supplemented with 20 mM maltose, and cleaved with PreScission protease. The eluates were analyzed by Ponceau staining or by Western blotting with anti-His (MBL, D291-3, 1:5,000) or anti-Rad50 antibodies (Thermo Scientific, PA5-32176, 1:1,000).

Expression and purification of Mre11, Mre11-R522H, Rad50 and Xrs2

The pFB-Mre11–6xHis plasmid for Mre11 expression in insect cells was obtained from P. Cejka (University of Zurich, Switzerland). Bacmid and P3 baculovirus were prepared in *Escherichia coli* DH10Bac and *Spodoptera frugiperda* Sf9 cells, respectively, according to the manufacturer's protocols (Invitrogen). To express Mre11, 800 ml *Trichoplusia ni* High Five cells were grown to a density of 1×10^6

cells/ml and infected with 24 ml high-titer P3 baculovirus. After 44 h infection, cells were harvested, washed with PBS, snap frozen in liquid nitrogen, and stored at –80°C. All the subsequent purification steps were carried out at 4°C. The cell pellet (~7 g from 800 ml of culture) was thawed and resuspended in 65 ml T buffer (25 mM Tris–HCl, pH 7.5, 10% glycerol, 0.5 mM EDTA) supplemented with fresh DTT (1 mM), Igepal (0.01%), KCl (300 mM) and protease inhibitors (5 μg/ml each of aprotinin, chymostatin, leupeptin and pepstatin A; 1 mM phenylmethylsulfonyl fluoride). After sonication for 1 min, the cell lysate was clarified by ultracentrifugation at 100 000×g for 45 min and mixed with 4 ml Ni-NTA agarose (Qiagen) together with 20 mM imidazole for 1 h. The resin was washed with 250 ml of T buffer containing 1 M KCl and 20 mM imidazole and bound proteins were eluted with 15 ml of 200 mM imidazole in T buffer containing 300 mM KCl. The eluate was diluted with an equal volume of T buffer and then applied onto a 4-ml Q Sepharose Fast Flow column (GE healthcare). The column was washed with 24 ml T buffer containing 150 mM KCl before being developed with an 80 ml gradient of KCl (150–500 mM) in T buffer. The fractions containing Mre11 were pooled, concentrated to 0.5 ml using an Amicon Ultra 30K filter (Millipore), and further fractionated in a 24-ml Superose 6 column (GE healthcare) in T buffer containing 300 mM KCl. The peak fractions were pooled, concentrated to ~4 μg/μl and stored in small aliquots at -80°C. The typical yield of Mre11 was ~2.5 mg from 800 ml of cell culture. The Mre11-R522H expression vector was constructed by site-directed mutagenesis of the pFB-Mre11–6xHis plasmid. The Mre11-R522H protein was purified using the procedure described above. Rad50 was overexpressed in yeast and purified as described previously [114]. The pFB-Xrs2-Flag plasmid for Xrs2 expression in insect cells was obtained from P. Cejka, and the cell extract was prepared as described above for Mre11 purification. The clarified lysate was mixed with 6 ml anti-Flag affinity resin (Sigma) for 2 h incubation. After washing the resin with 250 ml of T buffer containing 500 mM KCl, bound proteins were eluted with 6 ml of T buffer containing 300 mM KCl and 250 ng/μl Flag peptide. The protein pool was diluted with 6 ml of T buffer and further fractionated in a 1-ml Mono S column (GE healthcare) with a 40 ml gradient of 100–400 mM KCl in T buffer. The Xrs2 peak

fractions were pooled, concentrated to 0.5 ml using an Amicon Ultra 30K filter (Millipore), and further fractionated in a 24-ml Superose 6 column as described above for Mre11. The Xrs2 peak fractions were pooled, concentrated to ~5 μg/μl and stored in small aliquots at −80°C. The typical yield of Xrs2 was ~2.7 mg from 1 L of cell culture.

Affinity pull-down assay

To evaluate the assembly of the MRX complex, 0.9 μg His-tagged Mre11 or Mre11-R522H was mixed with Rad50 (1.5 μg) and Xrs2 (1 μg) in 30 μl T buffer containing 200 mM KCl, incubated on ice for 1 h, and imidazole was added to 20 mM. The reaction mixtures were incubated with Ni-NTA agarose for 1 h on ice with frequent tapping. The supernatant was removed, and the affinity resin was washed three times with 50 μl of the same buffer. Then, bound proteins were eluted with 40 μl 2% SDS. The supernatant, wash, and eluate fractions were resolved by SDS-PAGE and proteins were revealed using the Oriole fluorescent gel stain (BioRad).

ATPase and nuclease assays

The ATPase assay was performed as described previously [114] with slight modifications. Briefly, Mre11 or Mre11-R522H, 100 nM each, was incubated with an equimolar concentration of Rad50 and Xrs2 in 12 μl of reaction buffer (25 mM Tris–HCl, pH 7.5, 5 mM $MgCl_2$, 1 mM DTT, 100 μg/ml BSA) that also contained 75 mM KCl (final concentration), 100 bp dsDNA (200 nM), 300 μM of ATP, and 1.7 nM of [γ-^{32}P]ATP at 30°C. At the indicated times, 2 μl of the reaction mixture was mixed with an equal volume of EDTA (0.5 M, pH 8.0) and placed on ice. Reaction samples were resolved by thin layer chromatography followed by phosphorimaging analysis as previously described [166]. The nuclease activity of Mre11 or Mre11-R522H was tested on a DNA substrate with 5-nt 3′ overhangs and a nick in 12 μl reaction buffer (25 mM Tris–HCl, pH 7.5, 1 mM $MnCl_2$, 1 mM DTT, 100 μg/ml BSA) containing 100 mM KCl (final concentration). After a 30 min incubation at 30°C, reaction mixtures

were resolved in a denaturing polyacrylamide gel, followed by gel drying and phosphorimaging analysis.

Structural models

A starting structural model of Mre11–Rad50 (ATP-bound) complex was built by homology modelling (HM) technique, as previously described [212]. Briefly, Mre11 and Rad50 subunits were built using as templates the homologs of *S. pombe* (PDB ID: 4FCX) and *Chaetomium thermophilum* (PDB ID: 5DA9), respectively. Then, the Mre11–Rad50 complex was assembled using the tetrameric structure of the complex of *Methanocaldococcus jannaschii* (PDB ID: 5F3W). Maestro Mutagenesis Wizard (https://www.schrodinger.com/maestro) was used to mutate alanine 78 to threonine and to change ATP into ADP to obtain ATP-bound Mre11–Rad50 (MR-ATP), ADP-bound Mre11–Rad50 (MR-ADP), ATP-bound Mre11–Rad50^{A78T} (MR^{A78T}-ATP) and ADP-bound Mre11–Rad50^{A78T} (MR^{A78T}-ADP) systems. Proper protonation states of amino acids were assigned using Maestro Protein Preparation Wizard at pH 7.0 [254]. All models were refined through Molecular Dynamics (MD) simulations. MD simulations were performed using Gromacs 5.1.2 (https://www.gromacs.org) and CHARMM36 force field [255]. All bonds involving hydrogen were constrained by linear constrained solver algorithm [256]. Non-bonded interaction pair list was calculated with Verlet algoritm [257] every 20 fs using a cutoff of 1.2 nm. Long range electrostatic interactions were treated using PME method [258] setting a cut-off of 1.2 nm. Each complex was solvated in a dodecahedral box with TIP3P water model [259] at a minimum distance of 1.2 nm from solute to box edges. K^+ ions were added as counter ions to obtain electroneutral models.

Refinement of Homology Modelling (HM) structures

Structures obtained by HM were subsequently optimized by steepest descent energy minimization with a limit of 50000 steps and a convergence criterion on the maximum force (<10 kJ mol^{-1} nm^{-1}). Temperature and pressure were equilibrated

at 300 K with NVT simulation of 4 ns and 1 atm with NPT simulation of 400 ps, respectively. MD simulations were carried out for 500 ns in NPT ensemble at 300 K and 1 atm with a time step of 2 fs. All trajectories of MR-ATP, MR-ADP, MR^{A78T}-ATP, MR^{A78T}-ADP systems were analysed using Gromos algorithm [260] for cluster analysis with a cutoff of 0.30, 0.35, 0.35 and 0.32 respectively. Centroids of the first five clusters of each model were used as starting points for further simulations.

MD production

Productive MD simulations were performed within an NPT thermodynamic ensemble at 300 K and 1 atm. More in detail, five simulations (200 ns) were carried out using centroid structures of the first five clusters obtained from previous simulations, as starting points of each system. To improve conformational sampling, two independent replicas were carried out using different initial atomic velocities for each structure for a total of ten simulations on each system. As a result, 2000 ns of simulation time have been collected for each model.

Post-production trajectory analysis

Analysis tools of GROMACS package were used to perform the analyses on the concatenated trajectories. Backbone root-mean-square deviation (RMSD) was used to evaluate trajectory stability of each replica, computed using the initial structure of each replica as reference. Principal Component Analysis (PCA) was performed on ATP/ADP and backbone atoms in order to identify globally correlated motions from MD trajectories. This method is based on dimensionality reduction of trajectory through the construction and diagonalization of the covariance matrix [261]. Free Energy Landscapes (FELs) were constructed using the probability distribution along two reaction coordinates (the first two eigenvectors, PC1 and PC2) in order to identify the dominant conformations with lower energy for each system. The joint-probability distribution is estimated by $\Delta G(X) = -k_B T \ln P(X)$, where k_B is the Boltzmann constant, T is the absolute temperature and $P(X)$ is the probability distribution along reaction coordinates X.

Homology modeling

A BLASTX search of the Protein Data Bank (PDB) using *Saccharomyces cerevisiae* Mre11 (ScMre11) protein sequence as a query showed high sequence identity (52%) with *Schizosaccharomyces pombe* Mre11 (SpMre11) (PDB ID: 4FCX) [164]and also (50%) with *Chaetomium thermophilum* Mre11 (CtMre11) (PDB ID: 4YKE) [262]. A homology-based model of ScMre11 protein spanning endonuclease and capping domains (1–416 aa) was constructed based on the crystal structure coordinates of 4FCX. The pairwise alignment was performed using the homology module of Prime through the Maestro interface (Schrodinger, LLC, and New York, USA) (https://www.schrodinger.com/citations#Maestro). The pairwise alignment was improved manually by minor editing based on the secondary structure predictions as well, and the energy-driven modeling option was used in order to allow energy minimization using the force-field OPLS-2005. The initial structure for Rad50 binding domain (RBD) of ScMre11, spanning residues 443–526, was obtained by homology modeling based on the crystal coordinates of the RBD of CtMre11 in complex with Rad50 (PDB ID: 5DA9) [138]. Since the sequence identity between the two proteins is limited in this domain, the pairwise alignment obtained using the Prime homology module was improved manually by minor editing based on the secondary structure predictions and imposing conservation of the relevant Rad50 interacting surface residues. The disordered connecting regions between the first model and the RBD model were designed ex novo by the energy-driven Prime homology module and then refined by Prime loops refinement module. The whole model of ScMre11, spanning residues 1–542, was then processed for molecular dynamics as a heterodimer with Rad50. A model for ScRad50 globular domain and initial coiled-coil regions, bound to ATP, was obtained by homology modeling as described above based on the crystal coordinates of CtRad50 (PDB ID: 5DA9), sharing 58% identity with ScRad50. An initial model of the tetrameric structure of ScMre11–Rad50 complex was obtained by superposition of Mre11 and Rad50 (ATP-bound) on the tetrameric complex structure from *M. jannaschii* (PDB ID:

5F3W) [222]. This structure was then refined by molecular dynamics. A multiple alignment based on AL2CO structural conservation [263]) of ScMre11 with Mre11 orthologs from *Homo sapiens* (PDB ID:3T1I), *Schizosaccharomyces pombe* (PDB ID:4FCX), *Chaetomium thermophilum* (PDB ID:4KYE and 5DA9 for RBD region), *Methanococcus jannaschii* (PDB ID:3AV0) and *Pyrococcus furiosus* (PDB ID:1II7) was built by UCSF Chimera software (http://www.cgl.ucsf.edu/chimera/).

Molecular dynamics

MD simulations were performed using gromacs 5.0.4 software package (www.gromacs.org) and the AMBER99 force field [264]. During the simulations, the interactions between magnesium ions (Mg^{2+}) and their coordinating residues were treated using non-bonded model with van der Waals and electrostatic terms present in the AMBER99 force field. Protein structures were soaked in a cubic box of SPC/E (Extended Single Point Charge) [85]water molecules and simulated using periodic boundary conditions. All protein atoms were at the distance of 1 nm from the box edges. The ionization state of residues was set to be consistent with physiological pH (7.0 pH ± 0.2). Na^+ ions were added to all molecular systems as counterions to obtain electroneutral models. All systems were relaxed through a steepest descent minimization with a limit of 50,000 cycles. Temperature and pressure were equilibrated at 300 K and 1 atm with a NVT (isothermal-isochoric) simulation of 2 ns and a NPT (isothermal-isobaric) simulation of 100 ps, respectively. Productive MD simulations were carried out in the NPT ensemble at 300 K with a time step of 2 fs. Quality assessment of the MD simulations was performed by backbone root-mean-square deviation (RMSD) analysis (Supplementary Figure S1). Hydrogen bonds are computed and analyzed using the g_hbond tool of GROMACS. Hydrogen bonds are determined based on cutoffs for the angle Hydrogen-Donor-Acceptor (30°) and the distance donor-acceptor (3.5 Å). OH and NH groups are regarded as donors, O and N are acceptors. Salt bridges were analysed monitoring the distance between any of the oxygen atoms of acidic residues and the nitrogen atoms of basic residues along all the simulation. A salt bridge was considered formed if the distance between oxygen and nitrogen is within 4 Å.

Quantification And Statistical Analysis

Data are expressed as mean values ± standard deviation. Quantification and statistical analysis were done using PRISM (GraphPad). *p* values for the ChIP-qPCR and recombination experiments were calculated by two-tailed Student's *t* test. No statistical methods or criteria were used to estimate sample size or to include or exclude samples.

References

[1] G. Giglia-Mari, A. Zotter, and W. Vermeulen, “DNA Damage Response,” *Cold Spring Harb. Perspect. Biol.*, vol. 3, no. 1, pp. a000745–a000745, Jan. 2011, doi: 10.1101/cshperspect.a000745.

[2] N. Chatterjee and G. C. Walker, “Mechanisms of DNA damage, repair, and mutagenesis,” *Environ. Mol. Mutagen.*, vol. 58, no. 5, pp. 235–263, 2017, doi: 10.1002/em.22087.

[3] D. Nakada, K. Matsumoto, and K. Sugimoto, “ATM-related Tel1 associates with double-strand breaks through an Xrs2-dependent mechanism,” *Genes Dev.*, vol. 17, no. 16, pp. 1957–1962, 2003, doi: 10.1101/gad.1099003.

[4] C. J. Lord and A. Ashworth, “The DNA damage response and cancer therapy,” *Nature*, vol. 481, no. 7381, pp. 287–294, 2012, doi: 10.1038/nature10760.

[5] D. Hanahan and R. A. Weinberg, “Hallmarks of cancer: The next generation,” *Cell*, vol. 144, no. 5. pp. 646–674, 2011, doi: 10.1016/j.cell.2011.02.013.

[6] M. P. Longhese, D. Bonetti, I. Guerini, N. Manfrini, and M. Clerici, “DNA double-strand breaks in meiosis: Checking their formation, processing and repair,” *DNA Repair (Amst).*, vol. 8, no. 9, pp. 1127–1138, Sep. 2009, doi: 10.1016/j.dnarep.2009.04.005.

[7] A. Mehta and J. E. J. E. Haber, “Sources of DNA double-strand breaks and models of recombinational DNA repair,” *Cold Spring Harb. Perspect. Biol.*, vol. 6, no. 9, p. a016428, Aug. 2014, doi: 10.1101/cshperspect.a016428.

[8] A. Aguilera and B. Gómez-González, “Genome instability: A mechanistic view of its causes and consequences,” *Nature Reviews Genetics*. 2008, doi: 10.1038/nrg2268.

[9] H. Ulukan and P. W. Swaan, “Camptothecins: a review of their chemotherapeutic potential.,” *Drugs*, vol. 62, no. 14, pp. 2039–2057, 2002, doi: 621404 [pii].

[10] V. Pagès and R. P. P. Fuchs, “How DNA lesions are turned into mutations within cells?,” *Oncogene*, vol. 21, pp. 8957–8966, 2002, doi: 10.1038/sj.onc.1206006.

[11] M. R. Lieber, “The Mechanism of Double-Strand DNA Break Repair by the

Nonhomologous DNA End Joining Pathway THE BIOLOGICAL CONTEXT OF NHEJ," *Annu Rev Biochem*, vol. 79, pp. 181–211, 2010, doi: 10.1146/annurev.biochem.052308.093131.

[12] H. H. Y. Y. Chang, N. R. Pannunzio, N. Adachi, and M. R. Lieber, "Non-homologous DNA end joining and alternative pathways to double-strand break repair," *Nat. Rev. Mol. Cell Biol.*, vol. 18, no. 8, pp. 495–506, 2017, doi: 10.1038/nrm.2017.48.

[13] E. Casari *et al.*, "Processing of DNA double-strand breaks by the MRX complex in a chromatin context," *Frontiers in Molecular Biosciences*, vol. 6, no. JUN. Frontiers Media S.A., 2019, doi: 10.3389/fmolb.2019.00043.

[14] E. Gobbini, C. Cassani, M. Villa, D. Bonetti, and M. P. M. Longhese, "Functions and regulation of the MRX complex at DNA double-strand breaks," *Microb. Cell*, vol. 3, no. 8, pp. 329–337, 2016, doi: 10.15698/mic2016.08.517.

[15] C. V. Colombo, L. Menin, R. Ranieri, D. Bonetti, M. Clerici, and M. P. Longhese, "Uncoupling SAE2 functions in downregulation of tel1 and RAD53 signaling activities," *Genetics*, vol. 211, no. 2, pp. 515–530, Feb. 2019, doi: 10.1534/genetics.118.301830.

[16] T. E. Wilson, U. Grawunder, and M. R. Lieber, "Yeast DNA ligase IV mediates non-homologous DNA end joining," *Nature*, 1997, doi: 10.1038/41365.

[17] M. L. Hefferin and A. E. Tomkinson, "Mechanism of DNA double-strand break repair by non-homologous end joining," *DNA Repair (Amst).*, vol. 4, no. 6, pp. 639–648, 2005, doi: 10.1016/j.dnarep.2004.12.005.

[18] Z. Dudášová, A. Dudáš, and M. Chovanec, "Non-homologous end-joining factors of Saccharomyces cerevisiae," *FEMS Microbiology Reviews*, vol. 28, no. 5. No longer published by Elsevier, pp. 581–601, Nov. 01, 2004, doi: 10.1016/j.femsre.2004.06.001.

[19] A. J. Davis and D. J. Chen, "DNA double strand break repair via non-homologous end-joining.," *Transl. Cancer Res.*, vol. 2, no. 3, pp. 130–143, Jun. 2013, doi: 10.3978/j.issn.2218-676X.2013.04.02.

[20] D. P. Mathiasen and M. Lisby, "Cell cycle regulation of homologous recombination in *Saccharomyces cerevisiae*," *FEMS Microbiol. Rev.*, vol. 38,

no. 2, pp. 172–184, Mar. 2014, doi: 10.1111/1574-6976.12066.

[21] X. Zhao *et al.*, “Cell cycle-dependent control of homologous recombination,” *Acta Biochimica et Biophysica Sinica*. 2017, doi: 10.1093/abbs/gmx055.

[22] L. P. Ferretti, L. Lafranchi, and A. A. Sartori, “Controlling DNA-end resection: A new task for CDKs,” *Front. Genet.*, vol. 4, no. JUN, pp. 1–7, 2013, doi: 10.3389/fgene.2013.00099.

[23] H. Van Attikum and S. M. Gasser, “ATP-dependent chromatin remodeling and DNA double-strand break repair,” *Cell Cycle*, vol. 4, no. 8. Taylor and Francis Inc., pp. 1011–1014, 2005, doi: 10.4161/cc.4.8.1887.

[24] J. Bartek and J. Lukas, “DNA damage checkpoints: from initiation to recovery or adaptation,” *Current Opinion in Cell Biology*. 2007, doi: 10.1016/j.ceb.2007.02.009.

[25] J. M. Daley, H. Niu, A. S. Miller, and P. Sung, “Biochemical mechanism of DSB end resection and its regulation,” *DNA Repair (Amst).*, 2015, doi: 10.1016/j.dnarep.2015.04.015.

[26] E. P. Mimitou and L. S. Symington, “DNA end resection: Many nucleases make light work,” *DNA Repair (Amst).*, vol. 8, no. 9, pp. 983–995, 2009, doi: 10.1016/j.dnarep.2009.04.017.

[27] D. Bonetti, C. V. Colombo, M. Clerici, and M. P. Longhese, “Processing of DNA ends in the maintenance of genome stability,” *Front. Genet.*, vol. 9, no. SEP, pp. 1–11, 2018, doi: 10.3389/fgene.2018.00390.

[28] E. Cannavo and P. Cejka, “Sae2 promotes dsDNA endonuclease activity within Mre11-Rad50-Xrs2 to resect DNA breaks,” *Nature*, vol. 514, no. 7520, pp. 122–125, 2014, doi: 10.1038/nature13771.

[29] G. Reginato, E. Cannavo, and P. Cejka, “Physiological protein blocks direct the Mre11-Rad50-Xrs2 and Sae2 nuclease complex to initiate DNA end resection,” *Genes Dev.*, vol. 31, no. 23–24, pp. 2325–2330, 2017, doi: 10.1101/gad.308254.117.

[30] W. Wang, J. M. Daley, Y. Kwon, D. S. D. S. Krasner, and P. Sung, “Plasticity of the Mre11-Rad50-Xrs2-Sae2 nuclease ensemble in the processing of DNA-bound obstacles,” *Genes Dev.*, vol. 31, no. 23–24, pp. 2331–2336,

2017, doi: 10.1101/gad.307900.117.

[31] Z. Zhu, W.-H. W.-H. H. Chung, E. Y. E. Y. Shim, S. E. S. E. Lee, and G. Ira, “Sgs1 Helicase and Two Nucleases Dna2 and Exo1 Resect DNA Double-Strand Break Ends,” *Cell*, vol. 134, no. 6, pp. 981–994, Sep. 2008, doi: 10.1016/j.cell.2008.08.037.

[32] P. Cejka *et al.*, “DNA end resection by Dna2-Sgs1-RPA and its stimulation by Top3-Rmi1 and Mre11-Rad50-Xrs2,” *Nature*, vol. 467, no. 7311, Sep. 2010, doi: 10.1038/nature09355.

[33] M. L. Nicolette *et al.*, “Mre11-Rad50-Xrs2 and Sae2 promote 5’ strand resection of DNA double-strand breaks.,” *Nat. Struct. Mol. Biol.*, 2010, doi: 10.1038/nsmb.1957.

[34] H. Niu *et al.*, “Mechanism of the ATP-dependent DNA endresection machinery from Saccharomyces cerevisiae,” *Nature*, vol. 467, no. 7311, pp. 108–111, 2010, doi: 10.1038/nature09318.

[35] E. Cannavo, P. Cejka, and S. C. Kowalczykowski, “Relationship of DNA degradation by Saccharomyces cerevisiae Exonuclease 1 and its stimulation by RPA and Mre11-Rad50-Xrs2 to DNA end resection,” *Proc. Natl. Acad. Sci. U. S. A.*, vol. 110, no. 18, pp. E1661-8, Apr. 2013, doi: 10.1073/pnas.1305166110.

[36] L. S. Symington, “End resection at double-strand breaks: Mechanism and regulation,” *Cold Spring Harb. Perspect. Biol.*, vol. 6, no. 8, Aug. 2014, doi: 10.1101/cshperspect.a016436.

[37] A. A. Sartori *et al.*, “Human CtIP promotes DNA end resection,” *Nature*, 2007, doi: 10.1038/nature06337.

[38] P. Cejka, “DNA end resection: Nucleases team up with the right partners to initiate homologous recombination,” *J. Biol. Chem.*, vol. 290, no. 38, pp. 22931–22938, Sep. 2015, doi: 10.1074/jbc.R115.675942.

[39] I. Ceppi *et al.*, “CtIP promotes the motor activity of DNA2 to accelerate long-range DNA end resection,” *Proc. Natl. Acad. Sci. U. S. A.*, vol. 117, no. 16, pp. 8859–8869, Apr. 2020, doi: 10.1073/pnas.2001165117.

[40] N. N. Hoa *et al.*, “Erratum: Mre11 Is Essential for the Removal of Lethal

Topoisomerase 2 Covalent Cleavage Complexes (Molecular Cell (2016) 64(3) (580–592) (S1097276516306347) (10.1016/j.molcel.2016.10.011)),” *Molecular Cell*, vol. 64, no. 5. 2016, doi: 10.1016/j.molcel.2016.11.028.

[41] M. Clerici, D. Mantiero, G. Lucchini, and M. P. M. P. Longhese, “The Saccharomyces cerevisiae Sae2 protein promotes resection and bridging of double strand break ends,” *J. Biol. Chem.*, vol. 280, no. 46, pp. 38631–38638, 2005, doi: 10.1074/jbc.M508339200.

[42] H. Chen *et al.*, “Sae2 promotes DNA damage resistance by removing the Mre11-Rad50-Xrs2 complex from DNA and attenuating Rad53 signaling,” *Proc. Natl. Acad. Sci. U. S. A.*, vol. 112, no. 15, Apr. 2015, doi: 10.1073/pnas.1503331112.

[43] N. Tomimatsu *et al.*, “Exo1 plays a major role in DNA end resection in humans and influences double-strand break repair and damage signaling decisions,” *DNA Repair (Amst).*, 2012, doi: 10.1016/j.dnarep.2012.01.006.

[44] E. P. E. P. Mimitou and L. S. L. S. Symington, “Sae2, Exo1 and Sgs1 collaborate in DNA double-strand break processing,” *Nature*, vol. 455, no. 7214, pp. 770–774, 2008, doi: 10.1038/nature07312.

[45] A. V. A. V. Nimonkar *et al.*, “BLM-DNA2-RPA-MRN and EXO1-BLM-RPA-MRN constitute two DNA end resection machineries for human DNA break repair,” *Genes Dev.*, vol. 25, no. 4, pp. 350–362, 2011, doi: 10.1101/gad.2003811.

[46] F. Marini, C. C. Rawal, G. Liberi, and A. Pellicioli, “Regulation of DNA Double Strand Breaks Processing: Focus on Barriers,” *Frontiers in Molecular Biosciences*. 2019, doi: 10.3389/fmolb.2019.00055.

[47] E. Y. E. Y. Shim *et al.*, “Saccharomyces cerevisiae Mre11/Rad50/Xrs2 and Ku proteins regulate association of Exo1 and Dna2 with DNA breaks,” *EMBO J.*, vol. 29, no. 19, pp. 3370–3380, 2010, doi: 10.1038/emboj.2010.219.

[48] W. Eid *et al.*, “DNA end resection by CtIP and exonuclease 1 prevents genomic instability,” *EMBO Rep.*, 2010, doi: 10.1038/embor.2010.157.

[49] E. Gobbini *et al.*, “ The MRX complex regulates Exo1 resection activity by altering DNA end structure ,” *EMBO J.*, 2018, doi:

10.15252/embj.201798588.

[50] N. Tomimatsu *et al.*, “Phosphorylation of EXO1 by CDKs 1 and 2 regulates DNA end resection and repair pathway choice,” *Nat. Commun.*, vol. 5, p. 3561, 2014, doi: 10.1038/ncomms4561.

[51] N. Tomimatsu *et al.*, “DNA-damage-induced degradation of EXO1 exonuclease limits DNA end resection to ensure accurate DNA repair,” *J. Biol. Chem.*, vol. 292, no. 26, pp. 10779–10790, Jun. 2017, doi: 10.1074/jbc.M116.772475.

[52] S. H. Bae and Y. S. Seo, “Characterization of the enzymatic properties of the yeast Dna2 helicase/endonuclease suggests a new model for Okazaki fragment processing,” *J. Biol. Chem.*, vol. 275, no. 48, pp. 38022–38031, Dec. 2000, doi: 10.1074/jbc.M006513200.

[53] Y. H. Kang, C. H. Lee, and Y. S. Seo, “Dna2 on the road to Okazaki fragment processing and genome stability in eukaryotes,” *Critical Reviews in Biochemistry and Molecular Biology*, vol. 45, no. 2. pp. 71–96, Apr. 2010, doi: 10.3109/10409230903578593.

[54] J. A. Stewart, J. L. Campbell, and R. A. Bambara, “Flap endonuclease disengages Dna2 helicase/nuclease from Okazaki fragment flaps,” *J. Biol. Chem.*, vol. 281, no. 50, pp. 38565–38572, Dec. 2006, doi: 10.1074/jbc.M606884200.

[55] S. H. Bae *et al.*, “Coupling of DNA helicase and endonuclease activities of yeast Dna2 facilitates Okazaki fragment processing,” *J. Biol. Chem.*, vol. 277, no. 29, pp. 26632–26641, Jul. 2002, doi: 10.1074/jbc.M111026200.

[56] T. Masuda-Sasa, P. Polaczek, and J. L. Campbell, “Single strand annealing and ATP-independent strand exchange activities of yeast and human DNA2: Possible role in okazaki fragment maturation,” *J. Biol. Chem.*, vol. 281, no. 50, pp. 38555–38564, Dec. 2006, doi: 10.1074/jbc.M604925200.

[57] L. Zheng, Y. Meng, J. L. Campbell, and B. Shen, “Multiple roles of DNA2 nuclease/helicase in DNA metabolism, genome stability and human diseases,” *Nucleic Acids Research*, vol. 48, no. 1. Oxford University Press, pp. 16–35, Jan. 10, 2020, doi: 10.1093/nar/gkz1101.

[58] H. I. Kao, J. Veeraraghavan, P. Polaczek, J. L. Campbell, and R. A. Bambara, “On the Roles of Saccharomyces cerevisiae Dna2p and Flap Endonuclease 1 in Okazaki Fragment Processing,” *J. Biol. Chem.*, vol. 279, no. 15, pp. 15014–15024, Apr. 2004, doi: 10.1074/jbc.M313216200.

[59] Y. Liu, H. I. Kao, and R. A. Bambara, “Flap Endonuclease 1: A central component of DNA metabolism,” *Annual Review of Biochemistry*, vol. 73. pp. 589–615, 2004, doi: 10.1146/annurev.biochem.73.012803.092453.

[60] H. I. H.-I. Kao, J. L. J. L. Campbell, and R. A. R. A. Bambara, “Dna2p helicase/nuclease is a tracking protein, like FEN1, for flap cleavage during okazaki fragment maturation,” *J. Biol. Chem.*, vol. 279, no. 49, pp. 50840–50849, Dec. 2004, doi: 10.1074/jbc.M409231200.

[61] L. Mariotti *et al.*, “The iron–sulphur cluster in human DNA2 is required for all biochemical activities of DNA2,” *Commun. Biol.*, vol. 3, no. 1, Dec. 2020, doi: 10.1038/s42003-020-1048-4.

[62] K. Kasaciunaite, F. Fettes, M. Levikova, P. Daldrop, P. Cejka, and R. Seidel, “Competing interactions modulate the activity of Sgs1 during DNA end resection,” *bioRxiv*. 2019, doi: 10.1101/515791.

[63] E. P. Mimitou and L. S. Symington, “DNA end resection-Unraveling the tail,” *DNA Repair (Amst).*, 2011, doi: 10.1016/j.dnarep.2010.12.004.

[64] R. Sharma, S. Lewis, and M. W. Wlodarski, “DNA Repair Syndromes and Cancer: Insights Into Genetics and Phenotype Patterns,” *Front. Pediatr.*, vol. 8, Oct. 2020, doi: 10.3389/fped.2020.570084.

[65] J. A. Newman and O. Gileadi, “RecQ helicases in DNA repair and cancer targets,” *Essays in Biochemistry*, vol. 64, no. 5. Portland Press Ltd, Oct. 01, 2020, doi: 10.1042/EBC20200012.

[66] A. Sturzenegger *et al.*, “DNA2 cooperates with the WRN and BLM RecQ helicases to mediate long-range DNA end resection in human cells,” *J. Biol. Chem.*, vol. 289, no. 39, pp. 27314–27326, Sep. 2014, doi: 10.1074/jbc.M114.578823.

[67] A. S. Miller *et al.*, “A novel role of the Dna2 translocase function in DNA break resection,” *Genes Dev.*, vol. 31, no. 5, pp. 503–510, Mar. 2017, doi:

10.1101/gad.295659.116.

[68] M. Levikova, C. Pinto, and P. Cejka, “The motor activity of dna2 functions as an ssdna translocase to promote dna end resection,” *Genes Dev.*, vol. 31, no. 5, pp. 493–502, Mar. 2017, doi: 10.1101/gad.295196.116.

[69] D. K. Singh, B. Ahn, and V. A. Bohr, “Roles of RECQ helicases in recombination based DNA repair, genomic stability and aging,” *Biogerontology*, vol. 10, no. 3. pp. 235–252, 2009, doi: 10.1007/s10522-008-9205-z.

[70] D. L. Croteau, V. Popuri, P. L. Opresko, and V. A. Bohr, “Human RecQ helicases in DNA repair, recombination, and replication,” *Annual Review of Biochemistry*, vol. 83. Annual Reviews Inc., pp. 519–552, 2014, doi: 10.1146/annurev-biochem-060713-035428.

[71] S. Rezazadeh, “RecQ helicases; at the crossroad of genome replication, repair, and recombination,” *Molecular Biology Reports*, vol. 39, no. 4. Mol Biol Rep, pp. 4527–4543, Apr. 2012, doi: 10.1007/s11033-011-1243-y.

[72] V. A. Bohr, “Rising from the RecQ-age: the role of human RecQ helicases in genome maintenance,” *Trends in Biochemical Sciences*, vol. 33, no. 12. pp. 609–620, Dec. 2008, doi: 10.1016/j.tibs.2008.09.003.

[73] J. M. Daley *et al.*, “Enhancement of BLM-DNA2-Mediated Long-Range DNA End Resection by CtIP,” *Cell Rep.*, 2017, doi: 10.1016/j.celrep.2017.09.048.

[74] C. Soustelle, M. Vedel, R. Kolodner, and A. Nicolas, “Replication protein A is required for meiotic recombination in Saccharomyces cerevisiae,” *Genetics*, vol. 161, no. 2, pp. 535–547, 2002, Accessed: Aug. 19, 2017. [Online]. Available: http://www.genetics.org/content/161/2/535.long.

[75] C. F. Cheok, C. Z. Bachrati, K. L. Chan, C. Ralf, L. Wu, and I. D. Hickson, “Roles of the Bloom’s syndrome helicase in the maintenance of genome stability,” in *Biochemical Society Transactions*, Dec. 2005, vol. 33, no. 6, pp. 1456–1459, doi: 10.1042/BST20051456.

[76] J. M. Daley, T. Chiba, X. Xue, H. Niu, and P. Sung, “Multifaceted role of the Topo IIIα-RMI1-RMI2 complex and DNA2 in the BLM-dependent pathway of DNA break end resection,” *Nucleic Acids Res.*, vol. 42, no. 17, pp. 11083–

11091, Jun. 2014, doi: 10.1093/nar/gku803.

[77] L. S. Symington and J. Gautier, “Double-strand break end resection and repair pathway choice,” *Annu. Rev. Genet.*, 2011, doi: 10.1146/annurev-genet-110410-132435.

[78] Z. You and J. M. Bailis, “DNA damage and decisions: CtIP coordinates DNA repair and cell cycle checkpoints,” *Trends in Cell Biology*. 2010, doi: 10.1016/j.tcb.2010.04.002.

[79] P. Zegerman, “Evolutionary conservation of the CDK targets in eukaryotic DNA replication initiation,” *Chromosoma*, vol. 124, no. 3. Springer Science and Business Media Deutschland GmbH, pp. 309–321, Sep. 26, 2015, doi: 10.1007/s00412-014-0500-y.

[80] C. V. Colombo, M. Gnugnoli, E. Gobbini, and M. P. Longhese, “How do cells sense DNA lesions?,” *Biochem. Soc. Trans.*, vol. 48, no. 2, pp. 677–691, 2020, doi: 10.1042/BST20191118.

[81] N. Manfrini, I. Guerini, A. Citterio, G. Lucchini, and M. P. Longhese, “Processing of meiotic DNA double strand breaks requires cyclin-dependent kinase and multiple nucleases,” *J. Biol. Chem.*, 2010, doi: 10.1074/jbc.M110.104083.

[82] P. Huertas, F. Cortés-Ledesma, A. A. Sartori, A. Aguilera, and S. P. Jackson, “CDK targets Sae2 to control DNA-end resection and homologous recombination.,” *Nature*, vol. 455, no. 7213, pp. 689–92, Oct. 2008, doi: 10.1038/nature07215.

[83] M. Clerici, D. Mantiero, I. Guerini, G. Lucchini, and M. P. Longhese, “The Yku70-Yku80 complex contributes to regulate double-strand break processing and checkpoint activation during the cell cycle.,” *EMBO Rep.*, vol. 9, no. 8, pp. 810–818, 2008, doi: 10.1038/embor.2008.121.

[84] E. Gobbini, D. Cesena, A. Galbiati, A. Lockhart, and M. P. M. P. Longhese, “Interplays between ATM/Tel1 and ATR/Mec1 in sensing and signaling DNA double-strand breaks,” *DNA Repair (Amst).*, vol. 12, no. 10, pp. 791–799, Oct. 2013, doi: 10.1016/j.dnarep.2013.07.009.

[85] E. P. E. P. Mimitou and L. S. L. S. Symington, “Ku prevents Exo1 and Sgs1-

dependent resection of DNA ends in the absence of a functional MRX complex or Sae2," *EMBO J.*, vol. 29, no. 19, pp. 3358–3369, Oct. 2010, doi: 10.1038/emboj.2010.193.

[86] P. Langerak, E. Mejia-Ramirez, O. Limbo, and P. Russell, "Release of Ku and MRN from DNA ends by Mre11 nuclease activity and Ctp1 is required for homologous recombination repair of double-strand breaks," *PLoS Genet.*, 2011, doi: 10.1371/journal.pgen.1002271.

[87] J. Sun, K. J. Lee, A. J. Davis, and D. J. Chen, "Human Ku70/80 protein blocks exonuclease 1-mediated DNA resection in the presence of human Mre11 or Mre11/Rad50 protein complex," *J. Biol. Chem.*, 2012, doi: 10.1074/jbc.M111.306167.

[88] M. Ferrari *et al.*, "Functional Interplay between the 53BP1-Ortholog Rad9 and the Mre11 Complex Regulates Resection, End-Tethering and Repair of a Double-Strand Break," *PLoS Genet.*, vol. 11, no. 1, 2015, doi: 10.1371/journal.pgen.1004928.

[89] D. Bonetti *et al.*, "Escape of Sgs1 from Rad9 inhibition reduces the requirement for Sae2 and functional MRX in DNA end resection.," *EMBO Rep.*, vol. 16, no. 3, pp. 351–361, 2015, doi: 10.15252/embr.201439764.

[90] F. Lazzaro *et al.*, "Histone methyltransferase Dot1 and Rad9 inhibit single-stranded DNA accumulation at DSBs and uncapped telomeres," *EMBO J.*, vol. 2781, pp. 1502–1512, 2008, doi: 10.1038/emboj.2008.81.

[91] G. T. & M. P. L. Diego Bonetti, Matteo Villa, Elisa Gobbini, Corinne Cassani, "Escape of Sgs1 from Rad9 inhibition reduces the requirement for Sae2 and functional MRX in DNA end resection.," *EMBO Rep.*, 2015, doi: 10.15252/embr.201439764.

[92] C. Escribano-Díaz *et al.*, "A Cell Cycle-Dependent Regulatory Circuit Composed of 53BP1-RIF1 and BRCA1-CtIP Controls DNA Repair Pathway Choice," *Mol. Cell*, 2013, doi: 10.1016/j.molcel.2013.01.001.

[93] M. Di Virgilio *et al.*, "Rif1 prevents resection of DNA breaks and promotes immunoglobulin class switching," *Science (80-.).*, 2013, doi: 10.1126/science.1230624.

[94] M. Zimmermann, F. Lottersberger, S. B. Buonomo, A. Sfeir, and T. De Lange, “53BP1 regulates DSB repair using Rif1 to control 5′ end resection,” *Science (80-.).*, 2013, doi: 10.1126/science.1231573.

[95] M. Grenon *et al.*, “Docking onto chromatin via the Saccharomyces cerevisiae Rad9 Tudor domain,” *Yeast*, 2007, doi: 10.1002/yea.1441.

[96] R. Wysocki, A. Javaheri, S. Allard, F. Sha, J. Côté, and S. J. Kron, “Role of Dot1-Dependent Histone H3 Methylation in G1 and S Phase DNA Damage Checkpoint Functions of Rad9,” *Mol. Cell. Biol.*, 2005, doi: 10.1128/mcb.25.19.8430-8443.2005.

[97] C. C. Nnakwe, M. Altaf, J. Côté, and S. J. Kron, “Dissection of Rad9 BRCT domain function in the mitotic checkpoint response to telomere uncapping,” *DNA Repair (Amst).*, 2009, doi: 10.1016/j.dnarep.2009.09.010.

[98] M. Giannattasio, F. Lazzaro, P. Plevani, and M. Muzi-Falconi, “The DNA damage checkpoint response requires histone H2B ubiquitination by Rad6-Bre1 and H3 methylation by Dot1,” *J. Biol. Chem.*, 2005, doi: 10.1074/jbc.M414453200.

[99] A. Hammet, C. Magill, J. Heierhorst, and S. P. Jackson, “Rad9 BRCT domain interaction with phosphorylated H2AX regulates the G1 checkpoint in budding yeast,” *EMBO Rep.*, 2007, doi: 10.1038/sj.embor.7401036.

[100] R. Shroff *et al.*, “Distribution and dynamics of chromatin modification induced by a defined DNA double-strand break,” *Curr. Biol.*, 2004, doi: 10.1016/j.cub.2004.09.047.

[101] G. W. L. Toh *et al.*, “Histone H2A phosphorylation and H3 methylation are required for a novel Rad9 DSB repair function following checkpoint activation,” *DNA Repair (Amst).*, 2006, doi: 10.1016/j.dnarep.2006.03.005.

[102] J. A. Downs, N. F. Lowndes, and S. P. Jackson, “A role for Saccharomyces cerevisiae histone H2A in DNA repair,” *Nature*, 2000, doi: 10.1038/35050000.

[103] A. Javaheri, R. Wysocki, O. Jobin-Robitaille, M. Altaf, J. Côté, and S. J. Kron, “Yeast G1 DNA damage checkpoint regulation by H2A phosphorylation is independent of chromatin remodeling,” *Proc. Natl. Acad. Sci. U. S. A.*, 2006, doi: 10.1073/pnas.0511192103.

[104] M. Granata *et al.*, “To trim or not to trim Progression and control of DSB end resection,” *Cell Cycle*, vol. 12, no. 12, pp. 1848–1860, 2013, doi: 10.4161/cc.25042.

[105] M. Granata *et al.*, “Dynamics of RAD9 chromatin binding and checkpoint function are mediated by its dimerization and are cell cycle-regulated by CDK1 activity,” *PLoS Genet.*, 2010, doi: 10.1371/journal.pgen.1001047.

[106] B. Pfander and J. F. X. Diffley, “Dpb11 coordinates Mec1 kinase activation with cell cycle-regulated Rad9 recruitment,” *EMBO J.*, 2011, doi: 10.1038/emboj.2011.345.

[107] X. Chen *et al.*, “The Fun30 nucleosome remodeller promotes resection of DNA double-strand break ends,” *Nature*, 2012, doi: 10.1038/nature11355.

[108] T. Costelloe *et al.*, “The yeast Fun30 and human SMARCAD1 chromatin remodellers promote DNA end resection,” *Nature*, 2012, doi: 10.1038/nature11353.

[109] V. V. Eapen, N. Sugawara, M. Tsabar, W.-H. Wu, and J. E. Haber, “The Saccharomyces cerevisiae Chromatin Remodeler Fun30 Regulates DNA End Resection and Checkpoint Deactivation,” *Mol. Cell. Biol.*, 2012, doi: 10.1128/mcb.00566-12.

[110] S. C. S. Bantele, P. Ferreira, D. Gritenaite, D. Boos, and B. Pfander, “Targeting of the Fun30 nucleosome remodeller by the Dpb11 scaffold facilitates cell cycle-regulated DNA end resection,” *Elife*, 2017, doi: 10.7554/eLife.21687.

[111] X. Bi, Q. Yu, J. Siler, C. Li, and A. Khan, “Functions of Fun30 chromatin remodeler in regulating cellular resistance to genotoxic stress,” *PLoS One*, 2015, doi: 10.1371/journal.pone.0121341.

[112] D. Dibitetto *et al.*, “Slx4 and Rtt107 control checkpoint signalling and DNA resection at double-strand breaks,” *Nucleic Acids Res.*, 2015, doi: 10.1093/nar/gkv1080.

[113] P. Y. Ohouo, F. M. Bastos De Oliveira, Y. Liu, C. J. Ma, and M. B. Smolka, “DNA-repair scaffolds dampen checkpoint signalling by counteracting the adaptor Rad9,” *Nature*, 2013, doi: 10.1038/nature11658.

[114] C. Cassani *et al.*, “Tel1 and Rif2 Regulate MRX Functions in End-Tethering and Repair of DNA Double-Strand Breaks,” *PLOS Biol.*, vol. 14, no. 2, p. e1002387, Feb. 2016, doi: 10.1371/journal.pbio.1002387.

[115] I. Morin, H. P. Ngo, A. Greenall, M. K. Zubko, N. Morrice, and D. Lydall, “Checkpoint-dependent phosphorylation of Exo1 modulates the DNA damage response,” *EMBO J.*, 2008, doi: 10.1038/emboj.2008.171.

[116] X. Jia, T. Weinert, and D. Lydall, “Mec1 and Rad53 Inhibit Formation of Single-Stranded DNA at Telomeres of Saccharomyces cerevisiae cdc13-1 Mutants,” *Genetics*, 2004, doi: 10.1534/genetics.166.2.753.

[117] M. Clerici, C. Trovesi, A. Galbiati, G. Lucchini, and M. P. M. P. Longhese, “Mec1/ATR regulates the generation of single-stranded DNA that attenuates Tel1/ATM signaling at DNA ends,” *EMBO J.*, vol. 33, no. 3, pp. 198–216, Feb. 2014, doi: 10.1002/embj.201386041.

[118] E. Gobbini, M. Villa, M. Gnugnoli, L. Menin, M. Clerici, and M. P. Longhese, “Sae2 Function at DNA Double-Strand Breaks Is Bypassed by Dampening Tel1 or Rad53 Activity,” *PLoS Genet.*, vol. 11, no. 11, 2015, doi: 10.1371/journal.pgen.1005685.

[119] H. Cartagena-Lirola, I. Guerini, V. Viscardi, G. Lucchini, and M. P. Longhese, “Budding yeast Sae2 is an in vivo target of the Mec1 and Tel1 checkpoint kinases during meiosis,” *Cell Cycle*, 2006, doi: 10.4161/cc.5.14.2916.

[120] Y. Liu *et al.*, “TOPBP1Dpb11 plays a conserved role in homologous recombination DNA repair through the coordinated recruitment of 53BP1Rad9,” *J. Cell Biol.*, 2017, doi: 10.1083/jcb.201607031.

[121] L. S. Symington, “Mechanism and regulation of DNA end resection in eukaryotes,” *Critical Reviews in Biochemistry and Molecular Biology*. 2016, doi: 10.3109/10409238.2016.1172552.

[122] G. H. P. Ngo, L. Balakrishnan, M. Dubarry, J. L. Campbell, and D. Lydall, “The 9-1-1 checkpoint clamp stimulates DNA resection by Dna2-Sgs1 and Exo1,” *Nucleic Acids Res.*, 2014, doi: 10.1093/nar/gku746.

[123] L. Krejci, V. Altmannova, M. Spirek, and X. Zhao, “Homologous recombination and its regulation,” *Nucleic Acids Res.*, vol. 40, no. 13, pp.

5795–5818, Jul. 2012, doi: 10.1093/nar/gks270.

[124] J. San Filippo, P. Sung, and H. Klein, “Mechanism of eukaryotic homologous recombination.,” *Annu. Rev. Biochem.*, vol. 77, no. 1, pp. 229–257, Jun. 2008, doi: 10.1146/annurev.biochem.77.061306.125255.

[125] W. K. Holloman, “Unraveling the mechanism of BRCA2 in homologous recombination,” *Nature Structural and Molecular Biology*. 2011, doi: 10.1038/nsmb.2096.

[126] P. Sung, L. Krejci, S. Van Komen, and M. G. Sehorn, *Rad51 Recombinase and Recombination Mediators*, vol. 278, no. 44. American Society for Biochemistry and Molecular Biology, 2003, pp. 42729–32.

[127] G. N. Krishnaprasad, M. T. Anand, G. Lin, M. M. Tekkedil, L. M. Steinmetz, and K. T. Nishant, “Variation in crossover frequencies perturb crossover assurance without affecting meiotic chromosome segregation in Saccharomyces cerevisiae,” *Genetics*, vol. 199, no. 2, pp. 399–412, Feb. 2014, doi: 10.1534/genetics.114.172320.

[128] S. C. Y. Ip, U. Rass, M. G. Blanco, H. R. Flynn, J. M. Skehel, and S. C. West, “Identification of Holliday junction resolvases from humans and yeast.,” *Nature*, 2008, doi: 10.1038/nature07470.

[129] A. Ciccia and S. J. Elledge, *The DNA Damage Response: Making It Safe to Play with Knives*, vol. 40, no. 2. 2010, pp. 179–204.

[130] S. Sarbajna and S. C. West, “Holliday junction processing enzymes as guardians of genome stability,” *Trends in Biochemical Sciences*. 2014, doi: 10.1016/j.tibs.2014.07.003.

[131] A. H. Bizard and I. D. Hickson, “The dissolution of double Holliday junctions,” *Cold Spring Harb. Perspect. Biol.*, 2014, doi: 10.1101/cshperspect.a016477.

[132] J. M. Chen, D. N. Cooper, N. Chuzhanova, C. Férec, and G. P. Patrinos, “Gene conversion: Mechanisms, evolution and human disease,” *Nature Reviews Genetics*. 2007, doi: 10.1038/nrg2193.

[133] M. E. Moynahan and M. Jasin, “Mitotic homologous recombination maintains genomic stability and suppresses tumorigenesis,” *Nat. Rev. Mol. Cell Biol.*, vol. 11, no. 3, pp. 196–207, 2010, doi: 10.1038/nrm2851.

[134] D. Branzei and M. Foiani, “Template Switching: From Replication Fork Repair to Genome Rearrangements,” *Cell*. 2007, doi: 10.1016/j.cell.2007.12.007.

[135] J. C. Harrison and J. E. Haber, *Surviving the breakup: The DNA damage checkpoint*, vol. 40, no. 1. 2006, pp. 209–235.

[136] R. Bosotti, A. Isacchi, and E. L. L. Sonnhammer, “FAT: A novel domain in PIK-related kinases,” *Trends Biochem. Sci.*, 2000, doi: 10.1016/S0968-0004(00)01563-2.

[137] E. Gino, D. Domenico, E. Romano, P. Del Porto, and F. Ascenzioni, “Multifunctional Role of ATM/Tel1 Kinase in Genome Stability: From the DNA Damage Response to Telomere Maintenance,” 2014, doi: 10.1155/2014/787404.

[138] F. U. Seifert, K. Lammens, G. Stoehr, B. Kessler, and K.-P. Hopfner, “Structural mechanism of ATP-dependent DNA binding and DNA end bridging by eukaryotic Rad50,” *EMBO J.*, vol. 35, no. 7, pp. 759–772, 2016, doi: 10.15252/embj.201592934.

[139] H. Lempiäinen and T. D. Halazonetis, “Emerging common themes in regulation of PIKKs and PI3Ks,” *EMBO Journal*. 2009, doi: 10.1038/emboj.2009.281.

[140] J. Smith, L. Mun Tho, N. Xu, and D. A. Gillespie, “The ATM-Chk2 and ATR-Chk1 pathways in DNA damage signaling and cancer,” in *Advances in Cancer Research*, 2010.

[141] Z. You, C. Chahwan, J. Bailis, T. Hunter, and P. Russell, “ATM activation and its recruitment to damaged DNA require binding to the C terminus of Nbs1.,” *Mol. Cell. Biol.*, vol. 25, no. 13, pp. 5363–5379, 2005, doi: 10.1128/MCB.25.13.5363-5379.2005.

[142] T. T. Paull, “Mechanisms of ATM activation,” *Annual Review of Biochemistry*. 2015, doi: 10.1146/annurev-biochem-060614-034335.

[143] A. Guleria and S. Chandna, “ATM kinase: Much more than a DNA damage responsive protein,” *DNA Repair*. 2016, doi: 10.1016/j.dnarep.2015.12.009.

[144] A. Dupré, L. Boyer-Chatenet, and J. Gautier, “Two-step activation of ATM by DNA and the Mre11-Rad50-Nbs1 complex,” *Nat. Struct. Mol. Biol.*, 2006, doi:

10.1038/nsmb1090.

[145] K. Fukunaga, Y. Kwon, P. Sung, and K. Sugimoto, “Activation of Protein Kinase Tel1 through Recognition of Protein-Bound DNA Ends,” *Mol. Cell. Biol.*, 2011, doi: 10.1128/mcb.05157-11.

[146] L. Zou *et al.*, “Sensing DNA damage through ATRIP recognition of RPA-ssDNA complexes,” *Science (80-.).*, vol. 300, no. 5625, Jun. 2003, doi: 10.1126/science.1083430.

[147] V. Paciotti, M. Clerici, G. Lucchini, and M. P. Longhese, “The checkpoint protein Ddc2, functionally related to S. pombe Rad26, interacts with Mec1 and is regulated by Mec1-dependent phosphorylation in budding yeast,” *Genes Dev.*, 2000, doi: 10.1101/gad.14.16.2046.

[148] D. Cortez, S. Guntuku, J. Qin, and S. J. Elledge, “ATR and ATRIP: Partners in checkpoint signaling,” *Science (80-.).*, 2001, doi: 10.1126/science.1065521.

[149] H. L. Ball, M. R. Ehrhardt, D. A. Mordes, G. G. Glick, W. J. Chazin, and D. Cortez, “Function of a Conserved Checkpoint Recruitment Domain in ATRIP Proteins,” *Mol. Cell. Biol.*, 2007, doi: 10.1128/mcb.02238-06.

[150] C. A. MacDougall, T. S. Byun, C. Van, M. C. Yee, and K. A. Cimprich, “The structural determinants of checkpoint activation,” *Genes Dev.*, 2007, doi: 10.1101/gad.1522607.

[151] V. M. Navadgi-Patil and P. M. Burgers, “A tale of two tails: Activation of DNA damage checkpoint kinase Mec1/ATR by the 9-1-1 clamp and by Dpb11/TopBP1,” *DNA Repair (Amst).*, vol. 8, no. 9, pp. 996–1003, Sep. 2009, doi: 10.1016/j.dnarep.2009.03.011.

[152] K. Finn, N. F. Lowndes, and M. Grenon, “Eukaryotic DNA damage checkpoint activation in response to double-strand breaks,” *Cell. Mol. Life Sci.*, vol. 69, no. 9, pp. 1447–1473, May 2012, doi: 10.1007/s00018-011-0875-3.

[153] A. M. Duursma, R. Driscoll, J. E. Elias, and K. A. Cimprich, “A Role for the MRN Complex in ATR Activation via TOPBP1 Recruitment,” *Mol. Cell*, 2013, doi: 10.1016/j.molcel.2013.03.006.

[154] D. A. Mordes, E. A. Nam, and D. Cortez, “Dpb11 activates the Mec1-Ddc2

complex," *Proc. Natl. Acad. Sci. U. S. A.*, vol. 105, no. 48, pp. 18730–18734, Dec. 2008, doi: 10.1073/pnas.0806621105.

[155] F. Puddu *et al.*, "Phosphorylation of the Budding Yeast 9-1-1 Complex Is Required for Dpb11 Function in the Full Activation of the UV-Induced DNA Damage Checkpoint," *Mol. Cell. Biol.*, vol. 28, no. 15, pp. 4782–4793, Aug. 2008, doi: 10.1128/mcb.00330-08.

[156] B. Shiotani and L. Zou, "Single-Stranded DNA Orchestrates an ATM-to-ATR Switch at DNA Breaks," *Mol. Cell*, 2009, doi: 10.1016/j.molcel.2009.01.024.

[157] A. Pellicioli and M. Foiani, "Signal transduction: How Rad53 kinase is activated," *Current Biology*. 2005, doi: 10.1016/j.cub.2005.08.057.

[158] J. Bartek, J. Falck, and J. Lukas, "Milestones chk2 kinase: a busy messenger," *Nat Rev Mol Cell Biol*, 2001.

[159] F. D. Sweeney, F. Yang, A. Chi, J. Shabanowitz, D. F. Hunt, and D. Durocher, "Saccharomyces cerevisiae Rad9 acts as a Mec1 adaptor to allow Rad53 activation," *Curr. Biol.*, vol. 15, no. 15, pp. 1364–1375, Aug. 2005, doi: 10.1016/j.cub.2005.06.063.

[160] C. S. Gilbert, C. M. Green, and N. F. Lowndes, "Budding yeast Rad9 is an ATP-dependent Rad53 activating machine," *Mol. Cell*, vol. 8, no. 1, pp. 129–136, Jul. 2001, doi: 10.1016/S1097-2765(01)00267-2.

[161] L. Zannini, D. Delia, and G. Buscemi, "CHK2 kinase in the DNA damage response and beyond," *J. Mol. Cell Biol.*, 2014, doi: 10.1093/jmcb/mju045.

[162] M. Patil, N. Pabla, and Z. Dong, "Checkpoint kinase 1 in DNA damage response and cell cycle regulation," *Cellular and Molecular Life Sciences*. 2013, doi: 10.1007/s00018-013-1307-3.

[163] Y. Zhang and T. Hunter, "Roles of Chk1 in cell biology and cancer therapy," *International Journal of Cancer*. 2014, doi: 10.1002/ijc.28226.

[164] C. B. Schiller *et al.*, "Structural biology of the Mre11:Nbs1 complex structure yields insights into ataxia–telangiectasia–like disease mutations and DNA damage signaling," *Nat. Struct. Mol. Biol.*, vol. 19, no. 7, pp. 693–700, 2012, doi: 10.1038/nbt.3121.ChIP-nexus.

[165] M. T. Mcpherson, A. S. Holub, A. Y. Husbands, and R. C. Petreaca, "NBS1 /

NBN) Break Sensor in Cancer Cells," pp. 1–20, 2020.

[166] K. M. K. M. Trujillo, S.-S. F. S. S. F. Yuan, E. Y.-H. P. E. Y. H. P. Lee, and P. Sung, "Nuclease activities in a complex of human recombination and DNA repair factors Rad50, Mre11, and p95," *J. Biol. Chem.*, vol. 273, no. 34, pp. 21447–21450, Aug. 1998, doi: 10.1074/jbc.273.34.21447.

[167] T. T. T. Paull and M. Gellert, "The 3′ to 5′ Exonuclease Activity of Mre11 Facilitates Repair of DNA Double-Strand Breaks," *Mol. Cell*, vol. 1, no. 7, pp. 969–979, 1998, doi: 10.1016/S1097-2765(00)80097-0.

[168] S. Moreau, J. R. J. R. Ferguson, and L. S. L. S. Symington, "The Nuclease Activity of Mre11 Is Required for Meiosis but Not for Mating Type Switching, End Joining, or Telomere Maintenance," *Mol. Cell. Biol.*, vol. 19, no. 1, pp. 556–566, 1999, doi: 10.1128/MCB.19.1.556.

[169] B. J. Lamarche, N. I. Orazio, and M. D. Weitzman, *The MRN complex in double-strand break repair and telomere maintenance*, vol. 584, no. 17. NIH Public Access, 2010, pp. 3682–95.

[170] J. Oh and L. S. Symington, "Role of the Mre11 Complex in Preserving Genome Integrity," *Genes (Basel).*, vol. 9, no. 12, p. 589, Nov. 2018, doi: 10.3390/genes9120589.

[171] A. Rupnik, N. F. Lowndes, and M. Grenon, "MRN and the race to the break," *Chromosoma*. 2010, doi: 10.1007/s00412-009-0242-4.

[172] T. H. Stracker and J. H. J. Petrini, "The MRE11 complex: Starting from the ends," *Nature Reviews Molecular Cell Biology*. 2011, doi: 10.1038/nrm3047.

[173] K.-P. K. P. Hopfner *et al.*, "Structural biology of Rad50 ATPase: ATP-driven conformational control in DNA double-strand break repair and the ABC-ATPase superfamily," *Cell*, vol. 101, no. 7, pp. 789–800, 2000, doi: 10.1016/S0092-8674(00)80890-9.

[174] G. J. G. J. Williams *et al.*, "ABC ATPase signature helices in Rad50 link nucleotide state to Mre11 interface for DNA repair," *Nat. Struct. Mol. Biol.*, vol. 18, no. 4, pp. 423–431, 2011, doi: 10.1038/nsmb.2038.

[175] A. Rojowska, K. Lammens, F. U. Seifert, C. Direnberger, H. Feldmann, and K. Hopfner, " Structure of the Rad50 DNA double-strand break repair protein

in complex with DNA ," *EMBO J.*, 2014, doi: 10.15252/embj.201488889.

[176] K. Lammens *et al.*, "The Mre11:Rad50 structure shows an ATP-dependent molecular clamp in DNA double-strand break repair," *Cell*, vol. 145, no. 1, pp. 54–66, 2011, doi: 10.1016/j.cell.2011.02.038.

[177] T. T. Paull and R. A. Deshpande, "The Mre11/Rad50/Nbs1 complex: Recent insights into catalytic activities and ATP-driven conformational changes," *Experimental Cell Research*. 2014, doi: 10.1016/j.yexcr.2014.07.007.

[178] C. Möckel, K. Lammens, A. Schele, and K.-P. Hopfner, "ATP driven structural changes of the bacterial Mre11:Rad50 catalytic head complex," *Nucleic Acids Res.*, vol. 40, no. 2, pp. 914–927, 2012, doi: 10.1093/nar/gkr749.

[179] R. A. R. A. Deshpande *et al.*, "ATP-driven Rad50 conformations regulate DNA tethering, end resection, and ATM checkpoint signaling," *EMBO J.*, vol. 33, no. 5, pp. 482–500, 2014, doi: 10.1002/embj.201386100.

[180] J. C. Connelly, E. S. De Leau, and D. R. F. Leach, "Nucleolytic processing of a protein-bound DNA end by the E. coli SbcCD (MR) complex," *DNA Repair (Amst).*, vol. 2, no. 7, pp. 795–807, Jul. 2003, doi: 10.1016/S1568-7864(03)00063-6.

[181] J. Oh, S. J. Lee, R. Rothstein, and L. S. Symington, "Xrs2 and Tel1 Independently Contribute to MR-Mediated DNA Tethering and Replisome Stability," *Cell Rep.*, vol. 25, no. 7, pp. 1681-1692.e4, 2018, doi: 10.1016/j.celrep.2018.10.030.

[182] J. Oh, A. Al-Zain, E. Cannavo, P. Cejka, and L. S. Symington, "Xrs2 Dependent and Independent Functions of the Mre11-Rad50 Complex," *Mol. Cell*, vol. 64, no. 2, pp. 405–415, Oct. 2016, doi: 10.1016/j.molcel.2016.09.011.

[183] J. Liang, R. T. Suhandynata, and H. Zhou, "Phosphorylation of Sae2 mediates Forkhead-associated (FHA) domain-specific interaction and regulates its DNA repair function," *J. Biol. Chem.*, vol. 290, no. 17, pp. 10751–10763, 2015, doi: 10.1074/jbc.M114.625293.

[184] H. Wang *et al.*, "The Interaction of CtIP and Nbs1 Connects CDK and ATM to Regulate HR-Mediated Double-Strand Break Repair," *PLoS Genet.*, 2013,

doi: 10.1371/journal.pgen.1003277.

[185] E. Becker, V. Meyer, H. Madaoui, and R. Guerois, “Detection of a tandem BRCT in Nbs1 and Xrs2 with functional implications in the DNA damage response,” *Bioinformatics*, 2006, doi: 10.1093/bioinformatics/btl075.

[186] S. N. Andres and R. S. Williams, “CtIP/Ctp1/Sae2, molecular form fit for function,” *DNA Repair*. 2017, doi: 10.1016/j.dnarep.2017.06.013.

[187] L. S. Symington, R. Rothstein, and M. Lisby, “Mechanisms and regulation of mitotic recombination in saccharomyces cerevisiae,” *Genetics*, vol. 198, no. 3, 2014, doi: 10.1534/genetics.114.166140.

[188] J. E. Haber, “The Many Interfaces of Mre11 Minireview,” *Cell*, 1998.

[189] K. M. Trujillo and P. Sung, “DNA Structure-specific Nuclease Activities in the Saccharomyces cerevisiae Rad50-Mre11 Complex,” *J. Biol. Chem.*, vol. 276, no. 38, pp. 35458–35464, 2001, doi: 10.1074/jbc.M105482200.

[190] T. J. Herdendorf and S. W. Nelson, “Functional evaluation of bacteriophage T4 Rad50 signature motif residues,” *Biochemistry*, 2011, doi: 10.1021/bi200184w.

[191] Y. Hirano, K. Fukunaga, and K. Sugimoto, “Rif1 and Rif2 Inhibit Localization of Tel1 to DNA Ends,” *Mol. Cell*, 2009, doi: 10.1016/j.molcel.2008.12.027.

[192] M. Clerici, D. Mantiero, G. Lucchini, M. P. M. P. Longhese, and M. P. M. P. Longhese, “The Saccharomyces cerevisiae Sae2 protein negatively regulates DNA damage checkpoint signalling,” *EMBO Rep.*, vol. 7, no. 2, pp. 212–218, Feb. 2006, doi: 10.1038/sj.embor.7400593.

[193] M. Lisby, J. H. Barlow, R. C. Burgess, and R. Rothstein, “Choreography of the DNA damage response: Spatiotemporal relationships among checkpoint and repair proteins,” *Cell*, 2004, doi: 10.1016/j.cell.2004.08.015.

[194] T. Usui, H. Ogawa, and J. H. . J. H. J. Petrini, “A DNA damage response pathway controlled by Tel1 and the Mre11 complex,” *Mol. Cell*, vol. 7, no. 6, pp. 1255–1266, 2001, doi: 10.1016/S1097-2765(01)00270-2.

[195] T. Y. Yu, M. T. Kimble, and L. S. Symington, “Sae2 antagonizes Rad9 accumulation at DNA double-strand breaks to attenuate checkpoint signaling and facilitate end resection,” *Proc. Natl. Acad. Sci. U. S. A.*, 2018, doi:

10.1073/pnas.1816539115.

[196] H. S. H. S. Lim, J. S. J. S. Kim, Y. B. Y. B. Park, G. H. G. H. Gwon, and Y. Cho, “Crystal structure of the Mre11-Rad50-ATP??S complex: Understanding the interplay between Mre11 and Rad50,” *Genes Dev.*, vol. 25, no. 10, May 2011, doi: 10.1101/gad.2037811.

[197] F. Puddu *et al.*, “Synthetic viability genomic screening defines Sae2 function in DNA repair,” *EMBO J.*, vol. 34, no. 11, pp. 1509–1522, 2015, doi: 10.15252/embj.201590973.

[198] T. Usui, T. Ohta, H. Oshiumi, J.-I. Tomizawa, H. Ogawa, and T. Ogawa, “Complex formation and functional versatility of Mre11 of budding yeast in recombination.,” *Cell*, vol. 95, no. 5, pp. 705–716, 1998, doi: 10.1016/S0092-8674(00)81640-2.

[199] V. Garcia, S. E. L. Phelps, S. Gray, and M. J. Neale, “Bidirectional resection of DNA double-strand breaks by Mre11 and Exo1 Valerie,” vol. 479, no. 7372, pp. 241–244, 2012, doi: 10.1038/nature10515.Bidirectional.

[200] S. Keeney and N. Kleckner, “Covalent protein-DNA complexes at the 5’ strand termini of meiosis-specific double-strand breaks in yeast.,” *Proc. Natl. Acad. Sci. U. S. A.*, vol. 92, no. 24, pp. 11274–11278, Nov. 1995, doi: 10.1073/pnas.92.24.11274.

[201] E. Gobbini, M. Villa, M. Gnugnoli, L. Menin, M. Clerici, and M. P. M. P. Longhese, “Sae2 Function at DNA Double-Strand Breaks Is Bypassed by Dampening Tel1 or Rad53 Activity,” *PLoS Genet.*, vol. 11, no. 11, pp. 1–24, 2015, doi: 10.1371/journal.pgen.1005685.

[202] J. Falck, J. Coates, and S. P. S. P. Jackson, “Conserved modes of recruitment of ATM, ATR and DNA-PKcs to sites of DNA damage,” *Nature*, vol. 434, no. 7033, pp. 605–611, 2005, doi: 10.1038/nature03442.

[203] R. S. S. Williams *et al.*, “Mre11 Dimers Coordinate DNA End Bridging and Nuclease Processing in Double-Strand-Break Repair,” *Cell*, vol. 135, no. 1, pp. 97–109, Oct. 2008, doi: 10.1016/j.cell.2008.08.017.

[204] S. Sung *et al.*, “DNA end recognition by the Mre11 nuclease dimer: Insights into resection and repair of damaged DNA,” *EMBO J.*, vol. 33, no. 20, pp.

2422–2435, 2014, doi: 10.15252/embj.201488299.

[205] K. Lee, Y. Y. Zhang, and S. E. S. E. Lee, “Saccharomyces cerevisiae ATM orthologue suppresses break-induced chromosome translocations,” *Nature*, vol. 454, no. 7203, pp. 543–546, 2008, doi: 10.1038/nature07054.

[206] J. A. J. A. J. A. Kaye, J. A. J. A. J. A. Melo, S. K. S. K. Cheung, M. B. M. B. Vaze, J. E. J. E. Haber, and D. P. D. P. Toczyski, “DNA breaks promote genomic instability by impeding proper chromosome segregation,” *Curr. Biol.*, vol. 14, no. 23, pp. 2096–2106, 2004, doi: 10.1016/j.cub.2004.10.051.

[207] W. Nakai, J. Westmoreland, E. Yeh, K. Bloom, and M. A. M. A. Resnick, “Chromosome integrity at a double-strand break requires exonuclease 1 and MRX,” *DNA Repair (Amst).*, vol. 10, no. 1, pp. 102–110, 2011, doi: 10.1016/j.dnarep.2010.10.004.

[208] J. M. Daley, W. A. W. A. Gaines, Y. H. Kwon, and P. Sung, *Regulation of DNA pairing in homologous recombination*, vol. 6, no. 11. 2014, p. a017954.

[209] A. Mehta and J. E. Haber, “Sources of DNA double-strand breaks and models of recombinational DNA repair,” *Cold Spring Harb. Perspect. Biol.*, vol. 6, no. 9, 2014, doi: 10.1101/cshperspect.a016428.

[210] M. Saponaro *et al.*, “Cdk1 targets Srs2 to complete synthesis-dependent strand annealing and to promote recombinational repair,” *PLoS Genet.*, vol. 6, no. 2, 2010, doi: 10.1371/journal.pgen.1000858.

[211] L. Menin *et al.*, “Tel1/ATM prevents degradation of replication forks that reverse after topoisomerase poisoning,” *EMBO Rep.*, vol. 19, no. 7, 2018, doi: 10.15252/embr.201745535.

[212] C. Cassani *et al.*, “Structurally distinct Mre11 domains mediate MRX functions in resection, end-tethering and DNA damage resistance,” *Nucleic Acids Res.*, vol. 46, no. 6, pp. 2990–3008, Apr. 2018, doi: 10.1093/nar/gky086.

[213] K. B. Ritchie and T. D. Petes, “The Mre11p/Rad50p/Xrs2p complex and the Tellp function in a single pathway for telomere maintenance in yeast,” *Genetics*, vol. 155, no. 1, pp. 475–479, 2000.

[214] D. Mantiero, M. Clerici, G. Lucchini, and M. P. M. P. Longhese, “Dual role for

Saccharomyces cerevisiae Tel1 in the checkpoint response to double-strand breaks," *EMBO Rep.*, vol. 8, no. 4, pp. 380–387, Apr. 2007, doi: 10.1038/sj.embor.7400911.

[215] S. Keeney, C. N. Giroux, and N. Kleckner, "Meiosis-specific DNA double-strand breaks are catalyzed by Spo11, a member of a widely conserved protein family," *Cell*, vol. 88, no. 3, pp. 375–384, 1997, doi: 10.1016/S0092-8674(00)81876-0.

[216] A. Pellicioli, S. E. Lee, C. Lucca, M. Foiani, and J. E. Haber, "Regulation of Saccharomyces Rad53 checkpoint kinase during adaptation from DNA damage-induced G2/M arrest," *Mol. Cell*, vol. 7, no. 2, pp. 293–300, 2001, doi: 10.1016/S1097-2765(01)00177-0.

[217] E. L. Ivanov, N. Sugawara, C. I. White, F. Fabre, and J. E. Haber, "Mutations in XRS2 and RAD50 delay but do not prevent mating-type switching in Saccharomyces cerevisiae," *Mol. Cell. Biol.*, vol. 14, no. 5, pp. 3414–3425, 1994, doi: 10.1128/MCB.14.5.3414.

[218] S. E. S. E. Lee, J. K. K. Moore, A. Holmes, K. Umezu, R. D. R. D. Kolodner, and J. E. J. E. Haber, "Saccharomyces Ku70, Mre11/Rad50, and RPA proteins regulate adaptation to G2/M arrest after DNA damage," *Cell*, vol. 94, no. 3, pp. 399–409, 1998, doi: 10.1016/S0092-8674(00)81482-8.

[219] D. P. Toczyski, D. J. Galgoczy, and L. H. Hartwell, "CDC5 and CKII control adaptation to the yeast DNA damage checkpoint," *Cell*, vol. 90, no. 6, pp. 1097–1106, 1997, doi: 10.1016/S0092-8674(00)80375-X.

[220] M. Villa, C. Cassani, E. Gobbini, D. Bonetti, and M. P. M. P. Longhese, "Coupling end resection with the checkpoint response at DNA double-strand breaks," *Cell. Mol. Life Sci.*, vol. 73, no. 19, pp. 3655–3663, 2016, doi: 10.1007/s00018-016-2262-6.

[221] J.-H. Lee *et al.*, "Ataxia Telangiectasia-Mutated (ATM) kinase activity is regulated by ATP-driven conformational changes in the Mre11/Rad50/Nbs1 (MRN) complex," *J. Biol. Chem.*, vol. 288, no. 18, pp. 12840–12851, 2013, doi: 10.1074/jbc.M113.460378.

[222] Y. Liu *et al.*, "ATP-dependent DNA binding, unwinding, and resection by the

Mre11/Rad50 complex," *EMBO J.*, vol. 35, no. 7, pp. 743–758, 2016, doi: 10.15252/embj.201592462.

[223] M. C. Zwier and L. T. Chong, "Reaching biological timescales with all-atom molecular dynamics simulations," *Curr. Opin. Pharmacol.*, vol. 10, no. 6, pp. 745–752, 2010, doi: 10.1016/j.coph.2010.09.008.

[224] G. Bhabha, J. T. Biel, and J. S. Fraser, "Keep on moving: Discovering and perturbing the conformational dynamics of enzymes," *Acc. Chem. Res.*, vol. 48, no. 2, pp. 423–430, 2015, doi: 10.1021/ar5003158.

[225] Z. K. Boswell, S. Rahman, M. D. Canny, and M. P. Latham, "A dynamic allosteric pathway underlies Rad50 ABC ATPase function in DNA repair," *Sci. Rep.*, vol. 8, no. 1, 2018, doi: 10.1038/s41598-018-19908-8.

[226] E. Cannavo, G. Reginato, and P. Cejka, "Stepwise 5′ DNA end-specific resection of DNA breaks by the Mre11-Rad50-Xrs2 and Sae2 nuclease ensemble," *Proc. Natl. Acad. Sci. U. S. A.*, vol. 116, no. 12, pp. 5505–5513, Mar. 2019, doi: 10.1073/pnas.1820157116.

[227] S. Hailemariam, P. De Bona, R. Galletto, M. Hohl, J. H. Petrini, and P. M. Burgers, "The telomere-binding protein Rif2 and ATP-bound Rad50 have opposing roles in the activation of yeast Tel1ATM kinase.," *J. Biol. Chem.*, no. 8, 2019, doi: 10.1074/jbc.RA119.011077.

[228] K. S. Lobachev, D. A. Gordenin, and M. A. Resnick, "The Mre11 complex is required for repair of hairpin-capped double-strand breaks and prevention of chromosome rearrangements," *Cell*, 2002, doi: 10.1016/S0092-8674(02)00614-1.

[229] M. F. Schwartz, J. K. Duong, Z. Sun, J. S. Morrow, D. Pradhan, and D. F. Stern, "Rad9 phosphorylation sites couple Rad53 to the Saccharomyces cerevisiae DNA damage checkpoint," *Mol. Cell*, 2002, doi: 10.1016/S1097-2765(02)00532-4.

[230] E. Cannavo *et al.*, "Regulatory control of DNA end resection by Sae2 phosphorylation," *Nat. Commun.*, vol. 9, no. 1, pp. 1–14, 2018, doi: 10.1038/s41467-018-06417-5.

[231] L. Käshammer *et al.*, "Mechanism of DNA End Sensing and Processing by

the Mre11-Rad50 Complex," *Mol. Cell*, vol. 76, no. 3, pp. 382-394.e6, Nov. 2019, doi: 10.1016/j.molcel.2019.07.035.

[232] E. Alani, R. Padmore, and N. Kleckner, "Analysis of wild-type and rad50 mutants of yeast suggests an intimate relationship between meiotic chromosome synapsis and recombination," *Cell*, vol. 61, no. 3, pp. 419–436, May 1990, doi: 10.1016/0092-8674(90)90524-I.

[233] K. Nairz and F. Klein, "mre11S - A yeast mutation that blocks double-strand-break processing and permits nonhomologous synapsis in meiosis," *Genes Dev.*, vol. 11, no. 17, pp. 2272–2290, 1997, doi: 10.1101/gad.11.17.2272.

[234] B. B. Zhou and S. J. Elledge, "The DNA damage response: putting checkpoints in perspective.," *Nature*, vol. 408, no. 6811, pp. 433–9, 2000, doi: 10.1038/35044005.

[235] T. Helleday *et al.*, "Mechanisms underlying mutational signatures in human cancers," *Nat. Rev. Genet.*, vol. 15, no. 9, pp. 585–598, May 2014, doi: 10.1038/nrg3729.

[236] C. Liu, J. J. Pouliot, and H. A. Nash, "Repair of topoisomerase I covalent complexes in the absence of the tyrosyl-DNA phosphodiesterase Tdp1," *Proc. Natl. Acad. Sci. U. S. A.*, vol. 99, no. 23, pp. 14970–14975, 2002, doi: 10.1073/pnas.182557199.

[237] E. Hartsuiker, M. J. Neale, and A. M. Carr, "Distinct Requirements for the $Rad32^{Mre11}$ Nuclease and $Ctp1^{CtIP}$ in the Removal of Covalently Bound Topoisomerase I and II from DNA," *Mol. Cell*, vol. 33, no. 1, pp. 117–123, 2009, doi: 10.1016/j.molcel.2008.11.021.

[238] E. J. Sacho and N. Maizels, "DNA repair factor MRE11/RAD50 cleaves 3′-phosphotyrosyl bonds and resects DNA to repair damage caused by topoisomerase 1 poisons," *J. Biol. Chem.*, vol. 286, no. 52, pp. 44945–44951, 2011, doi: 10.1074/jbc.M111.299347.

[239] K. C. Lee *et al.*, "MRE11 facilitates the removal of human topoisomerase II complexes from genomic DNA," *Biol. Open*, vol. 1, no. 9, pp. 863–873, 2012, doi: 10.1242/bio.20121834.

[240] Y. Pommier, Y. Sun, S.-Y. N. Huang, and J. L. Nitiss, "Roles of eukaryotic

topoisomerases in transcription, replication and genomic stability," *Nat. Rev. Mol. Cell Biol.*, vol. 17, no. 11, pp. 703–721, 2016, doi: 10.1038/nrm.2016.111.

[241] A. Ray Chaudhuri *et al.*, "Topoisomerase i poisoning results in PARP-mediated replication fork reversal," *Nat. Struct. Mol. Biol.*, vol. 19, no. 4, pp. 417–423, 2012, doi: 10.1038/nsmb.2258.

[242] K. Lee and E. L. Sang, "Saccharomyces cerevisiae Sae2- and Tel1-dependent single-strand DNA formation at DNA break promotes microhomology-mediated end joining," *Genetics*, vol. 176, no. 4, pp. 2003–2014, 2007, doi: 10.1534/genetics.107.076539.

[243] T. Uziel, Y. Lerenthal, L. Moyal, Y. Andegeko, L. Mittelman, and Y. Shiloh, "Requirement of the MRN complex for ATM activation by DNA damage," *EMBO J.*, vol. 22, no. 20, pp. 5612–5621, 2003, doi: 10.1093/emboj/cdg541.

[244] M. Martina, M. Clerici, V. Baldo, D. Bonetti, G. Lucchini, and M. P. Longhese, "A Balance between Tel1 and Rif2 Activities Regulates Nucleolytic Processing and Elongation at Telomeres," *Mol. Cell. Biol.*, 2012, doi: 10.1128/mcb.06547-11.

[245] C. Ribeyre and D. Shore, "Anticheckpoint pathways at telomeres in yeast," *Nat. Struct. Mol. Biol.*, 2012, doi: 10.1038/nsmb.2225.

[246] S. Marcand, B. Pardo, A. Gratias, S. Cahun, and I. Callebaut, "Multiple pathways inhibit NHEJ at telomeres," *Genes Dev.*, 2008, doi: 10.1101/gad.455108.

[247] J. S. McGee, J. A. Phillips, A. Chan, M. Sabourin, K. Paeschke, and V. A. Zakian, "Reduced Rif2 and lack of Mec1 target short telomeres for elongation rather than double-strand break repair," *Nat. Struct. Mol. Biol.*, vol. 17, no. 12, pp. 1438–1445, Dec. 2010, doi: 10.1038/nsmb.1947.

[248] S. C. Teng, J. Chang, B. McCowan, and V. A. Zakian, "Telomerase-independent lengthening of yeast telomeres occurs by an abrupt Rad50p-dependent, Rif-inhibited recombinational process," *Mol. Cell*, vol. 6, no. 4, pp. 947–952, 2000, doi: 10.1016/S1097-2765(05)00094-8.

[249] D. Bonetti, M. Clerici, N. Manfrini, G. Lucchini, and M. P. Longhese, "The

MRX complex plays multiple functions in resection of Yku- and Rif2-protected DNA ends," *PLoS One*, vol. 5, no. 11, 2010, doi: 10.1371/journal.pone.0014142.

[250] A. Rojowska, K. Lammens, F. U. Seifert, C. Direnberger, H. Feldmann, and K. Hopfner, "Structure of the Rad50 <scp>DNA</scp> double-strand break repair protein in complex with <scp>DNA</scp>," *EMBO J.*, vol. 33, no. 23, pp. 2847–2859, Dec. 2014, doi: 10.15252/embj.201488889.

[251] N. Manfrini *et al.*, " RNA -processing proteins regulate Mec1/ ATR activation by promoting generation of RPA -coated ss DNA ," *EMBO Rep.*, 2015, doi: 10.15252/embr.201439458.

[252] E. Baroni, V. Viscardi, H. Cartagena-Lirola, G. Lucchini, and M. P. Longhese, "The Functions of Budding Yeast Sae2 in the DNA Damage Response Require Mec1- and Tel1-Dependent Phosphorylation," *Mol. Cell. Biol.*, vol. 24, no. 10, pp. 4151–4165, May 2004, doi: 10.1128/mcb.24.10.4151-4165.2004.

[253] V. Baldo, V. Testoni, G. Lucchini, and M. P. Longhese, "Dominant TEL1-hy mutations compensate for Mec1 lack of functions in the DNA damage response," *Mol. Cell. Biol.*, vol. 28, no. 1, pp. 358–375, 2008, doi: 10.1128/MCB.01214-07.

[254] G. Madhavi Sastry, M. Adzhigirey, T. Day, R. Annabhimoju, and W. Sherman, "Protein and ligand preparation: Parameters, protocols, and influence on virtual screening enrichments," *J. Comput. Aided. Mol. Des.*, vol. 27, no. 3, pp. 221–234, 2013, doi: 10.1007/s10822-013-9644-8.

[255] J. Huang *et al.*, "CHARMM36m: An improved force field for folded and intrinsically disordered proteins," *Nat. Methods*, vol. 14, no. 1, pp. 71–73, Dec. 2016, doi: 10.1038/nmeth.4067.

[256] B. Hess, H. Bekker, H. J. C. H. J. C. Berendsen, and J. G. E. M. J. G. E. M. Fraaije, "LINCS: A Linear Constraint Solver for molecular simulations," *J. Comput. Chem.*, vol. 18, no. 12, pp. 1463–1472, 1997, doi: 10.1002/(SICI)1096-987X(199709)18:12<1463::AID-JCC4>3.0.CO;2-H.

[257] H. GrubmüLler, H. Heller, A. Windemuth, and K. Schulten, "Generalized

verlet algorithm for efficient molecular dynamics simulations with long-range interactions," *Mol. Simul.*, vol. 6, no. 1–3, pp. 121–142, 1991, doi: 10.1080/08927029108022142.

[258] T. Darden, D. York, and L. Pedersen, "Particle mesh Ewald: An N·log(N) method for Ewald sums in large systems," *J. Chem. Phys.*, vol. 98, no. 12, pp. 10089–10092, 1993, doi: 10.1063/1.464397.

[259] M. W. M. W. Mahoney and W. L. Jorgensen, "A five-site model for liquid water and the reproduction of the density anomaly by rigid, nonpolarizable potential functions," *J. Chem. Phys.*, vol. 112, no. 20, pp. 8910–8922, 2000, doi: 10.1063/1.481505.

[260] X. Daura, K. Gademann, B. Jaun, D. Seebach, W. F. W. F. Van Gunsteren, and A. E. A. E. Mark, "Peptide folding: When simulation meets experiment," *Angew. Chemie - Int. Ed.*, vol. 38, no. 1–2, pp. 236–240, 1999, doi: 10.1002/(sici)1521-3773(19990115)38:1/2<236::aid-anie236>3.0.co;2-m.

[261] G. G. G. G. Maisuradze, A. Liwo, and H. A. H. A. Scheraga, "Relation between free energy landscapes of proteins and dynamics," *J. Chem. Theory Comput.*, vol. 6, no. 2, pp. 583–595, 2010, doi: 10.1021/ct9005745.

[262] F. U. Seifert, K. Lammens, and K.-P. Hopfner, "Structure of the catalytic domain of Mre11 from Chaetomium thermophilum," *Acta Crystallogr. Sect. FStructural Biol. Commun.*, vol. 71, pp. 752–757, 2015, doi: 10.1107/S2053230X15007566.

[263] J. Pei and N. V. Grishin, "AL2CO: Calculation of positional conservation in a protein sequence alignment," *Bioinformatics*, vol. 17, no. 8, pp. 700–712, 2001, doi: 10.1093/bioinformatics/17.8.700.

[264] J. Wang, P. Cieplak, and P. A. Kollman, "How Well Does a Restrained Electrostatic Potential (RESP) Model Perform in Calculating Conformational Energies of Organic and Biological Molecules?," *J. Comput. Chem.*, vol. 21, no. 12, pp. 1049–1074, 2000, doi: 10.1002/1096-987X(200009)21:12<1049::AID-JCC3>3.0.CO;2-F.